DEVELOPMENT OF SLED RANGE TEST FACILITY FOR STORE SEPARATION MODEL

A THESIS SUBMITTED TO
THE GRADUATE SCHOOL OF NATURAL AND APPLIED SCIENCES
OF
MIDDLE EAST TECHNICAL UNIVERSITY

BY

ALAETTİN ARDA ÖZYÜKSEL

IN PARTIAL FULFILLMENT OF THE REQUIREMENTS
FOR
THE DEGREE OF MASTER OF SCIENCE
IN
MECHANICAL ENGINEERING

JUNE 2007

Approval of the Graduate School of Natural and Applied Sciences

_____

Prof. Dr. Canan ÖZGEN

Director

I certify that this thesis satisfies all the requirements as a thesis for the degree of Master of Science.

_____

Prof. Dr. S. Kemal İDER

Head of Department

This is to certify that we have read this thesis and that in our opinion it is fully adequate, in scope and quality, as a thesis for the degree of Master of Science.

_____	_____
Dr. Gökmen MAHMUTYAZICIOĞLU	Prof. Dr. Tuna BALKAN
Co - Supervisor	Supervisor

Examining Committee Members

Prof. Dr. Metin AKKÖK	(METU, ME)	_____
Prof. Dr. Tuna BALKAN	(METU, ME)	_____
Asst. Prof. Dr. Yiğit YAZICIOĞLU	(METU, ME)	_____
Asst. Prof. Dr. İlhan KONUKSEVEN	(METU, ME)	_____
Dr. Gökmen MAHMUTYAZICIOĞLU	(TÜBİTAK-SAGE)	_____

I hereby declare that all information in this document has been obtained and presented in accordance with academic rules and ethical conduct. I also declare that, as required by these rules and conduct, I have fully cited and referenced all material and results that are not original to this work.

Name, Last name: Alaettin Arda ÖZYÜKSEL

Signature :

ABSTRACT

DEVELOPMENT OF SLED RANGE TEST FACILITY
FOR STORE SEPARATION MODEL

ÖZYÜKSEL, Alaettin Arda
M.S., Department of Mechanical Engineering
Supervisor: Prof. Dr. Tuna BALKAN
Co-Supervisor: Dr. Gökmen MAHMUTYAZICIOĞLU

June 2007, 142 pages

The aim of this thesis is to develop a test facility in order to validate the safe separation of a store model from the aircraft model with the analysis of the acquired data. Different alternatives are considered in the conceptual design and a facility is selected which contains the rail constructed 5 meters above the ground. 300 meter test range is used to accelerate the aircraft model, attached to the carriage with solid rocket engines. The concept is to accelerate the carriage within the first 100 meters, to perform the separation of the model at the desired velocity when the rocket engine is burned out, and in the last 100 meters, to decelerate the carriage in order to recover the models. After the parts of the carriage are designed with respect to the requirements of the separation and completing the similitude study of scaled models with the ratio of 1/8, separation tests are performed. These tests are

constrained with 0.9 Mach due to the store and test aircraft limitations. Doppler radar is issued to measure the velocity and photogrammetry method is used to validate and analyze the separation and to obtain the vertical trajectory of the store model. Measured trajectory of the store model is compared with the trajectory of the full scale store.

Keywords: Store Separation, Similitude, Photogrammetry

ÖZ

MODEL YÜK AYRILMA TESTLERİ İÇİN
RAYLI DENEME ALTYAPISI GELİŞTİRİLMESİ

ÖZYÜKSEL, Alaettin Arda
Yüksek Lisans, Makina Mühendisliği Bölümü
Tez Yöneticisi: Prof. Dr. Tuna BALKAN
Ortak Tez Yöneticisi: Dr. Gökmen MAHMUTYAZICIOĞLU

Haziran 2007, 142 sayfa

Bu tez çalışmasının amacı, yük modelinin uçak modelinden güvenli bir şekilde ayrılmasının, toplanan verilerin analizi ile doğrulanması amacı ile bir test altyapısı geliştirmektir. Kavramsal tasarım aşamasında farklı alternatifler üzerinde çalışılmış ve yerden 5 metre yükseklikte raya sahip olan altyapı seçilmiş ve inşa edilmiştir. Uçak modelinin bağlı olduğu test düzeneğinin, katı roket motorları yardımı ile hızlandırma amacı için 300 metre uzunluğundaki test alanı kullanılmıştır. Yapılmak istenen, ilk 100 metrelik bölümde aracı hızlandırmak ve roket motoru sustuğu anda istenilen ayrılma hızına ulaşıp yük modeli ayrılmasını gerçekleştirmek ve son 100 metre içerisinde modelleri kurtarmak için aracı yavaşlatmaktır. Ayrılma koşullarına göre test düzeneğinin tasarımı ve 1/8 oranında ölçeklenmiş modellerin benzeşim çalışmalarının tamamlanmasından sonra, ayrılma testleri gerçekleştirilmiştir.

Test uçağının limitlerinden dolayı ayrılma testleri en yüksek 0.9 Mach değeriyle sınırlandırılmıştır. Doppler radar kullanılarak hız ölçümleri gerçekleştirilmiştir, ayrıca ayrılmanın analizi ve doğrulanması için fotogrametri metodu kullanılmıştır. Yük modelinin ölçülen ayrılma verileri, tam ölçekli yük ayrılma verileri ile karşılaştırılmıştır.

Anahtar kelimeler: Yük Ayrılması, Benzeşim, Fotogrametri

Dedicated to Türkiye,

to my family, to my girlfriend,

and also to all heavy metal brothers and sisters

ACKNOWLEDGEMENT

I would like to express my special thanks to my supervisor Prof. Dr. Tuna BALKAN for his guidance, support, tolerance. I would like to state my sincere gratitude to my co-supervisor Dr. Gökmen MAHMUTYAZICIOĞLU for his motivation, supervision and patience.

The support provided by TÜBİTAK-SAGE is greatly acknowledged. I would like to thank to Koray DAYANÇ and Vedat EKÜTEKİN for their support and advices. I would like to express very special thanks to Sevsay AYTAR ORTAÇ for her support, supervision, encouragement and for her effort in this thesis. I would like to thank to my brothers İ. Murat KARBANCIOĞLU, K. Efe KAFDAĞLI, Ümit KUTLUAY, K. Kürşat KARAİL and Selçuk ATAÇ for being the best test team members whom I am proud and honored to be their friend, colleague, and teammates for all these tests and the hard working days.

I would like to express my thanks to Ali İhsan "*MacGyver*" AKBAŞ who helped without a doubt in every chaotic situation with all his kindness and understanding and for being a great technician.

I would like to express my special gratitude to Erdinç N. YILDIZ, Alper AKMEŞE, Burcu DÖNMEZ, for their discussions, instructions and suggestions.

Finally, I would like to send my thanks to my family who supported, cared and trusted me at each challenging stage of my life. I would like to thank to my girlfriend for her great patience and support and motivation.

TABLE OF CONTENTS

LIST OF TABLES

LIST OF FIGURES

LIST OF SYMBOLS

a	Linear acceleration
c	Distance from the neutral axis of the beam to the surface
C	Width of bearing
C_D, C_L	Drag and Lift coefficient
C_E	Extended dynamic load rating
C_r, C_{0r}	Load ratings
d	Bore of bearing
D	Outer diameter of bearing
D_1, D_2, D_3	Drag forces on the aircraft model, the sting and the main body, respectively
f_1, f_2, f_s	Friction force between rail and the carriage
F	Thrust force
F_E	Real flight condition ejection force
F'_E	Model test condition ejection force
g'	Model flight condition gravitational acceleration
g, g_∞	Real flight condition gravitational acceleration
I_X, I_Y, I_Z	Moment of inertia about x, y, z axis
I'_X, I'_Y, I'_Z	Model moment of inertia about x, y, z axis
l	Reference length
k	Spring stiffness

L	Lift force
L_{10}	Life of the bearing
m'	Model mass
m	Store mass
M'_{∞}	Model flight Mach number
M_{∞}	Real flight Mach number
M_{CG}	Moment on the center of gravity of carriage
n	Scale factor
N	Operation speed of bearing
N_1, N_2	Reaction force on the front and rear bearings, respectively
P	Equivalent radial load on bearing
Re'_{∞}	Model flight Reynolds number
Re_{∞}	Real flight condition Reynolds number
S	Wet area
t'	Model flight condition time
t	Real flight condition time
T'_{∞}	Model test condition temperature
T_{∞}	Real flight condition temperature
T	Kinetic energy
Q'_{∞}	Model test condition dynamic pressure
Q_{∞}	Real flight condition dynamic pressure
V, V'_{∞}	Model test condition velocity
V_{∞}	Real flight condition velocity
x_1, x_2	Linear position of masses
y	Vertical position of pylon main body
Z	Model linear position

Z'	Real linear position
ρ'_∞	Model test condition air density
ρ, ρ_∞	Real flight condition air density
μ	Friction coefficient
σ	Stress
θ'	Model angular position
θ	Real angular position
ω_n	Natural frequency

Acronyms

CFD	Computational Fluid Dynamics
CMM	Coordinate Measuring Machine
CNC	Computer Numerical Control
CTS	Captive Trajectory System
DIN	German Institute for Standardization
DOF	Degrees of Freedom
GPS	Global Positioning System
IRIG-B	Inter Range Instrumentation Group – Time Code Format B
Pps	Picture per second
rpm	Revolution per minute
TTL	Through The Lens

CHAPTER 1

INTRODUCTION

1.1. OVERVIEW

Aircrafts are one of the most critical and important platforms among the defense industry. The mission scenarios for the aircrafts increase thoroughly, with the implementation of external stores. This increasing demand through history brings some problems and difficulties that risk the aircraft and also the pilot. In [1], store is described as “any device intended for internal or external carriage and mounted on aircraft suspension and release equipment, whether or not the item is intended to be separated in flight from the aircraft.” Store can be named for bomb, rocket, fuel tank, instrumentation pod, or container.

Store can only be used on an aircraft if it is certified to that particular aircraft which means the specific store/aircraft compatibility must be determined so that the airworthiness qualification of the store is proven. By this way it is ensured that “the store is physically, mechanically, electromechanically, environmentally, structurally and aerodynamically compatible with aircraft systems”, as stated in [1].

It is challenging, time-consuming and expensive process to integrate a store into today's advanced military aircrafts. CFD analysis, wind tunnel tests and flight tests are the traditional methods for this integration process. As presented in [2], these items are the three branches of an integrated approach to store separation analysis. These methods are related and they are also feedbacks for each other, as it is shown in the diagram Figure 1. Illustrations of these tests for same aircraft are given in Figure 2, Figure 3 and Figure 4.

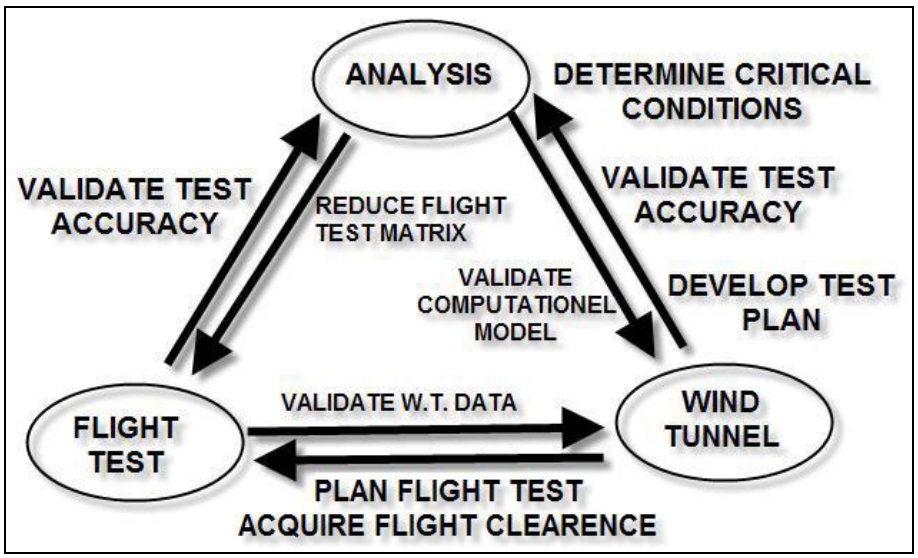

Figure 1 – Integrated Approach to Store Separation

One of the requirements of the certification is the safe separation of the store from the aircraft. The problem is to verify and demonstrate the safe separation right after the release from the aircraft.

Figure 2 – A View of Separation of a Bomb from Aircraft in Flight Test

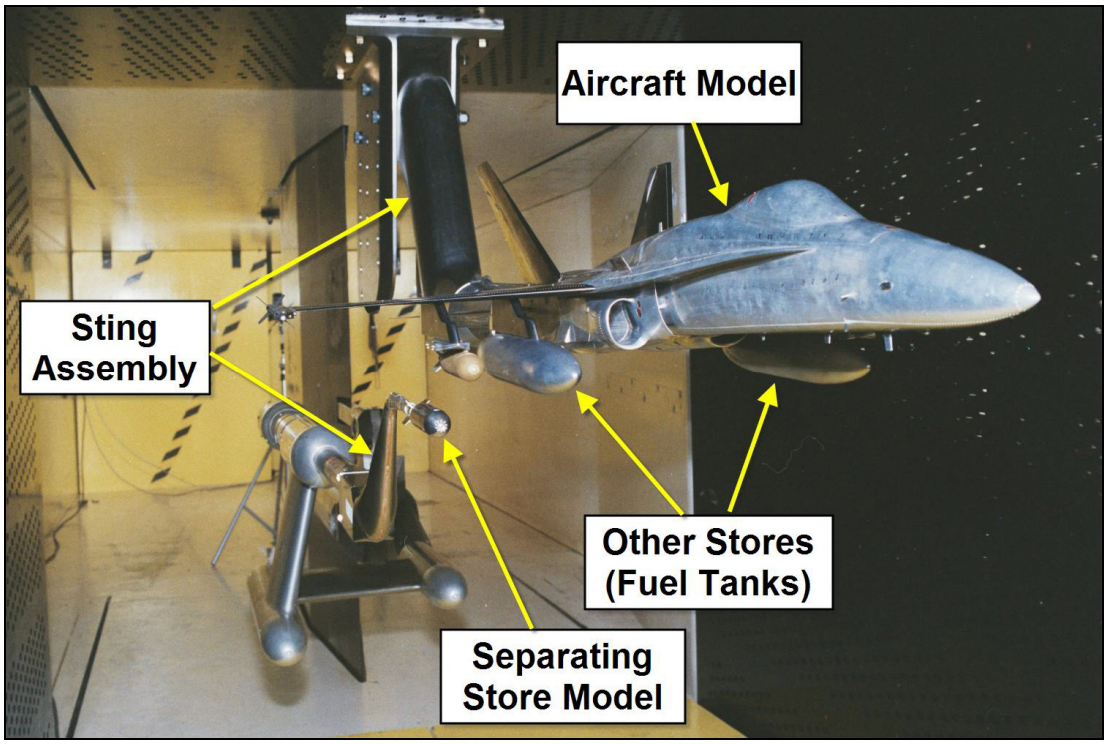

Figure 3 – A View of Typical Wind Tunnel Store Separation Test Setup

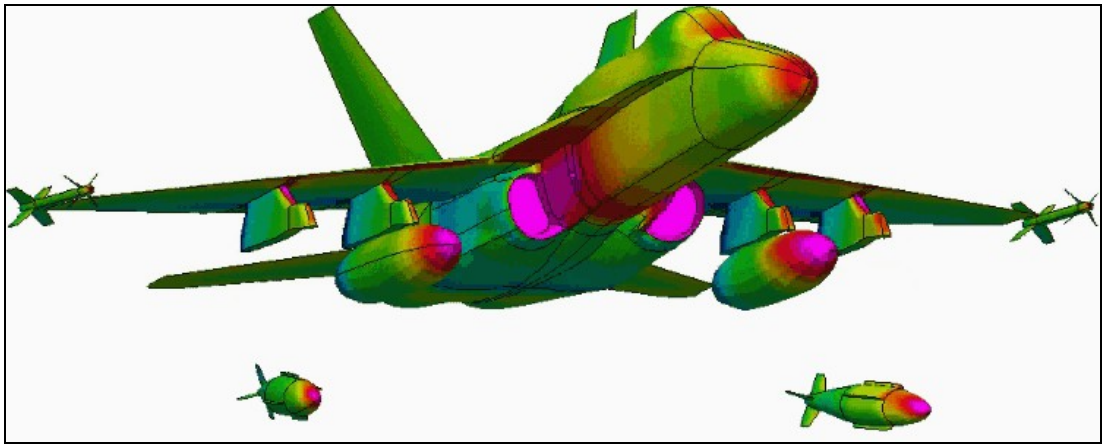

Figure 4 – A View of CFD Separation Analysis

1.2. STORE SEPARATION

When all the physical contact is terminated between a store and an aircraft or between store suspensions equipment, the store is said to be separated from the aircraft, [1]. According to the definition in [1], a separation is said to be safe if store is separated from an aircraft within the design limits of itself and the aircraft and/or other external stores, and without undesirable counter effects on the aircraft, suspension equipment, or the other released and unreleased store.

Safe separation problem is one of the major concerns and the flow field interaction between store and aircraft demands attention to insure acceptable separation, [3].

There are different methods for testing, verifying and analyzing the safe separation and gathering trajectory data. In history, separation tests were conducted in trial and error fashion that the stores dropped from the aircraft

at gradually increasing speeds until the store came close to or sometimes actually hit the aircraft. Sometimes this led to loss of the aircraft which make test more difficult and unwanted procedures even for the pilots, [4]. Examples of these situations are given in Figure 5.

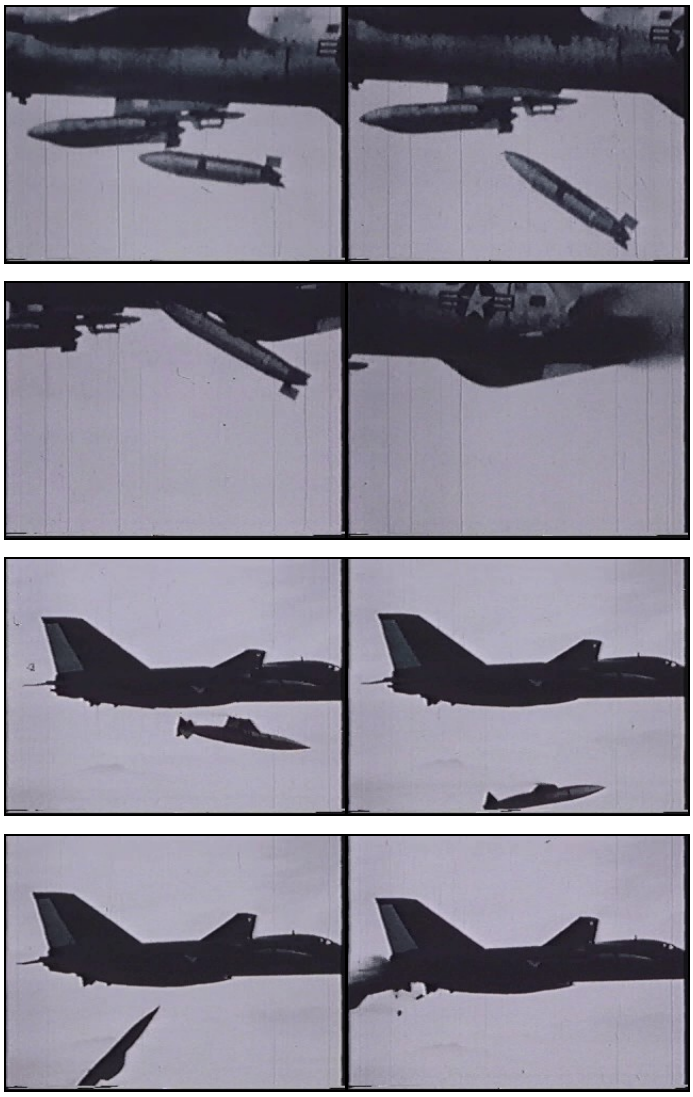

Figure 5 – Captured Images of Two Unsafe Separations

In the search for alternative methods, Captive Trajectory System (CTS) method for store separation wind tunnel testing was developed. In the course of time, the use of the wind tunnel to acquire valid separation data has been well established and represents the most economical means of generating separation data, [3]. A typical wind tunnel setup is shown in Figure 3.

Parallel with this progression, Computational Fluid Dynamics (CFD) had become to the point of supplying a trajectory solution for a store in an aircraft flow field. In the first era of CFD, tools were limited to linear techniques. With the advance of computers in 20th century, CFD is used to predict flight test trajectories for stores and usefully integrated into aircraft/store compatibility programs, [4], [5].

In wind tunnels, there are several methods to simulate experimentally full-scale flight tests to determine store separation characteristics and produce satisfactory correlation with full-scale flight test data, [3]. Basic methods are:

- Captive trajectory testing
- Flow field survey testing
- Dynamically scaled drop-model testing

In the captive trajectory method, scaled models of the aircraft and stores are supported on fixed mounting in a controlled air stream under laboratory conditions. A typical image of the application is illustrated in Figure 3. In the figure, stings, so called the fixed mountings, are also indicated. Sting-attached store model and aircraft model motions are dynamically calculated and the forces on the sting are measured. This combination helps to obtain the desired trajectory data.

In [1], dynamically scaled drop method is explained as a dynamically scaled store model in the flow field of an aircraft model is released or ejected to determine the separation trajectory. The drop models have to be dynamically similar with respect to the full scale store and must be extremely accurately scaled concerning the geometric properties and dynamic mass properties, like mass, center of mass, moments of inertia, [6]. The model release unit is needed for each store. Forced separation is simulated with springs, impulse cartridges or pneumatic system located properly in the pylon or rack in order to contact the store model correctly. The main information is acquired by high speed photography. This data acquisition method is called photogrammetry, which is the process of deriving information about the dynamics of an object through measurements made on images recorded on film or electronic media, [7], [8]. The path during the separation process of the scaled model is photographically recorded for analysis.

1.3. SCOPE OF THE THESIS

In this thesis, the problem to be solved is, to validate and verify the safe store separation of a store from the aircraft at desired velocities. This problem is issued in one of the TUBITAK-SAGE projects and thesis studies are started simultaneously. Once the CFD analysis is completed, the wind tunnel tests are required for the validation of the results. At this point, no similar studies were done about the safe separation of a store before in Türkiye. In order to accomplish that mission and solve the problem, the use of a wind tunnel is needed and Türkiye has only one wind tunnel, named “Ankara Wind Tunnel”, which is one of the facilities of TUBITAK-SAGE. The limitations about this wind tunnel are the allowable speed within the tunnel, the size of the tunnel and additionally there is no captive trajectory instrumentation in the tunnel.

According to the national security issues, the suitable wind tunnels in other countries could not be used. Besides, the cost of these tests for making them in a foreign country is excessive. Alternatively, building a new wind tunnel that satisfies the requirements of tests needs a very long period that can not be finished within the project schedule and the planned studies. Since the foreign facility usage is not possible, it is decided to design and build a brand new high speed test track in order to minimize the risk of not performing the wind tunnel tests. The aim of this thesis is to design the facility in order to validate safe store separation, which will be unique in Türkiye and in the world, perform the required tests in that facility, and analyze these results in order to obtain trajectory of the store and to validate the safe separation of that particular store.

In Chapter 2, the design of the facility is explained in details. In the conceptual design part of this chapter, the functional analyses and evaluation of the alternatives for facility are given. After the simulation of the setup motion is explained, the detailed information about the mechanical design of the carriage is presented. The similitude study is performed and each scaled part of the setup is explained. The last sections include the acceleration systems and related deceleration studies.

In Chapter 3, data acquisition systems are introduced. Case study is explained and the results are given

In Chapter 4, a brief summary and evaluations of the study are performed. Discussions and some concluding remarks are also made in this chapter.

CHAPTER 2

FACILITY DEVELOPMENT

2.1. CONCEPTUAL DESIGN

The separation test will be performed in order to verify and to document the safe separation of the store model from the test aircraft model. In the beginning of the conceptual design, the functional requirements of store separation are stated. These requirements are for the design of the rail, sled and aircraft/store interface and rocket engines.

In the conceptual design, the functional analyses are done for store separation, the test aircraft model, and store model and separation system. According to these analyses, functional alternatives for the facility are developed. The decision for the test setup is concluded according to the functional alternatives that are considered among manufacturability, usability and reliability.

Separation tests are planned to be performed at maximum velocity of 0.9 Mach, which is the primary requirement for the conceptual design. Other requirements are given in the following sections.

2.1.1. Functional Requirements of Store Separation

The analysis is made by considering the requirements of the test procedure before, during and after the tests. The requirements for each step are as follows:

- Launch
- The first movement and acceleration of the aircraft model
- Fulfilling the requirements of the separation
    - Aircraft model velocity
    - Aircraft model angular position
    - Separation configurations
- Separation
- Monitoring and recording the separation and the free fall of the store model
- Deceleration of the aircraft model
- Recovering the aircraft model safely

2.1.2. Functional Analysis of Subsystems

Functional Analysis of Aircraft Model

This analysis is made for deciding the general criteria's of the aircraft model that will be used in the tests.

- Stably carrying the store model
- Gathering the store model to the desired conditions for the separation

- Carrying the measurement systems
- Carrying the separation system
- Decelerating after the separation
- Withstanding the launch, flight, separation and deceleration forces

Functional Analysis of Store Model

The only possible function for the store model is carrying the measurement systems

Functional Analysis of Separation System

Similarly, the possible functions for the separation system are given below.

- Keeping the store model and the aircraft together until the separation moment
- Applying the scaled forces of the original separation
- Withstanding the launch, flight and separation forces

2.1.3. Test Setup Alternatives

According to the functional analysis, some possible alternative test setups, that fulfill the requirements, are described in the following sections. These alternatives will be evaluated for choosing the best.

Alternative 1

Aircraft model with rocket engine is launched from a fixed and inclined platform. A sample illustration is shown in Figure 6.

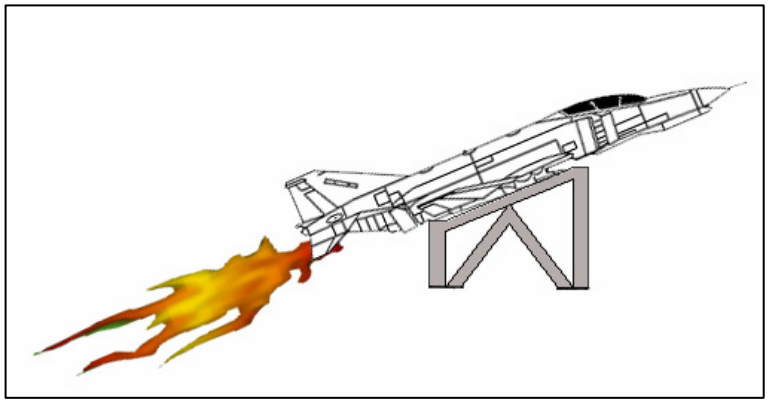

Figure 6 – Model Aircraft with Rocket Engine

Advantages:

- No need to a facility cost

Disadvantages:

- Placement problem of rocket engine
- The problem of withstanding to the structural forces during launch
- Displacement of the center of gravity
- Stability problem of the aircraft model
- Difficulty of the separation mechanism design
- Monitoring difficulties of separation

- The need of the rocket engine design
- The possibility of not reaching to the required velocity for separation
- Difficulty of repeatability in order to make controllable tests
- Increasing cost if the aircraft model cannot be recovered

Alternative 2

A carriage with rocket engine accelerates on a rail or parallel two rails and the aircraft model separates from the carriage at the end of the rail. A sample illustration is shown in Figure 7.

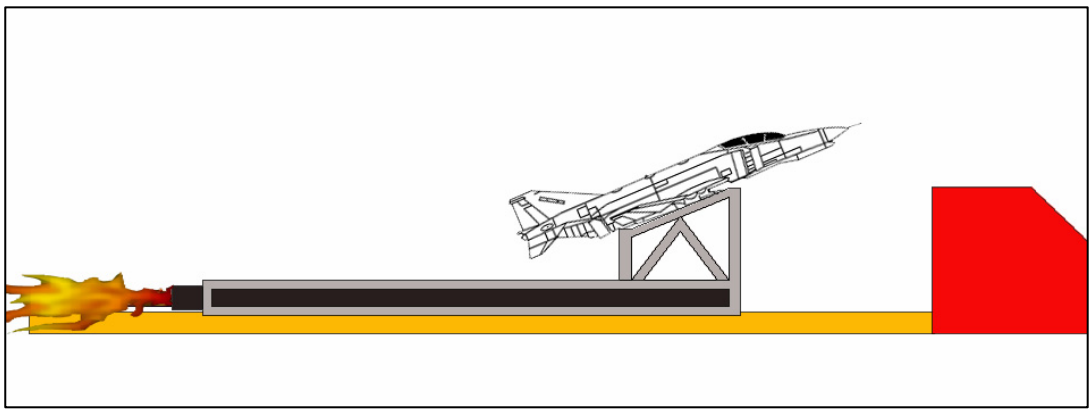

Figure 7 – The Carriage on a Rail with a Rocket Engine

Advantages:

- Multipurpose usage of facility rather than separation tests

Disadvantages:

- Stability problem of the aircraft model due to not having control surfaces.
- Separation position estimation problem
- The need to design of separation mechanism
- Difficulty of repeatability in order to make controllable tests
- Increasing cost if the model aircraft cannot be recovered
- The need to design of rail and carriage
- The cost problem due to the corrosive effects of the rocket engine chemicals

Alternative 3

Carriage with rocket engine, which aircraft model is attached, accelerates on steel rope. Sample illustrations are shown in Figure 8 and Figure 9.

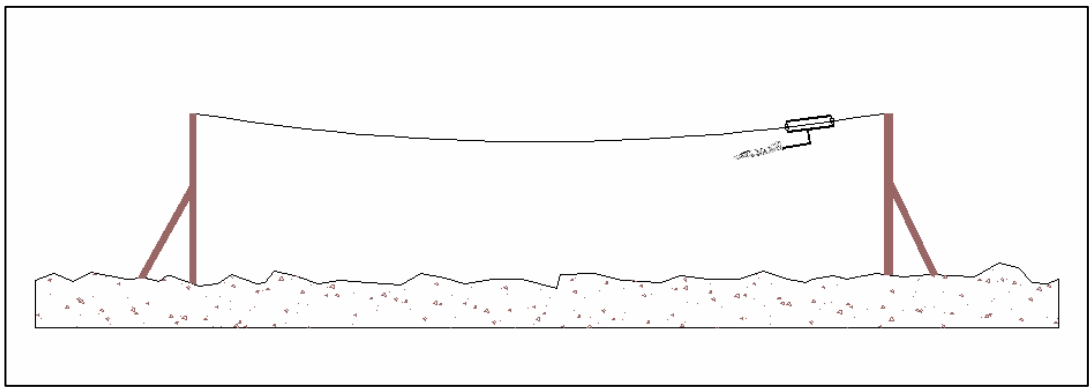

Figure 8 – Carriage Moving on a Steel Rope

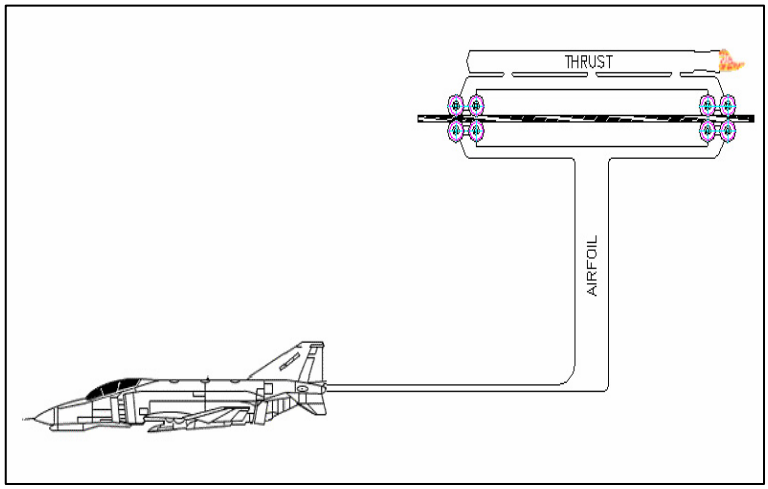

Figure 9 – Carriage with Rocket Engine

Advantages:

- Low cost for facility

Disadvantages:

- The need to design of the carriage
- The need to design of the deceleration mechanism
- Stiffness and vibration problem
- Dependency on weather
- Stiffness problem of towers
- Elongation problem of steel ropes
- Heat problem due to friction
- High cost for the maintenance
- Difficulty to make the ropes parallel

Alternative 4

The idea is to use a radio-controlled aircraft model, which can be obtained off-the shelf. However, there is no radio controlled aircraft model that can fly up to the velocity where the separation happens.

Alternative 5

A carriage and aircraft model assembly that accelerates on the rail, which is hung at a certain height. A sample illustration is shown in Figure 10.

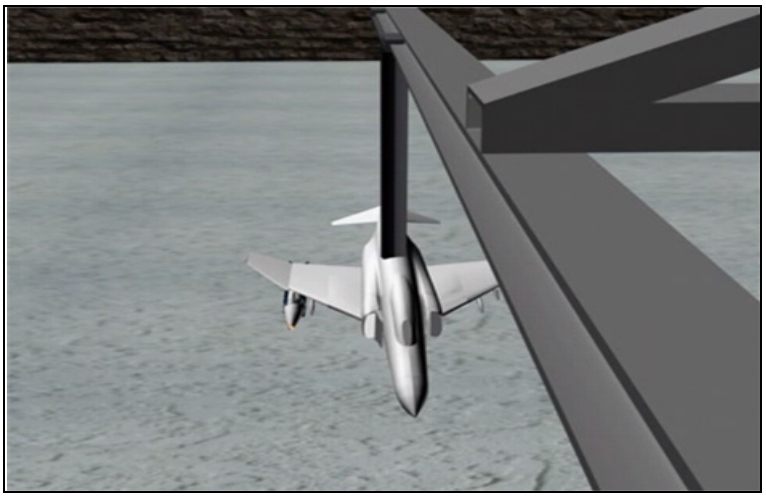

Figure 10 – Rail and Carriage with Rocket Engine

Advantages:

- Multipurpose usage of facility rather than separation tests
- Reusability for different tests

Disadvantages:

- High cost facility
- The need to design of the deceleration mechanism
- The need to design of the carriage
- High cost for the maintenance
- The cost problem due to the corrosive effect of the rocket engine chemicals

Alternative 6

The aircraft model will be launched parallel at a certain altitude. A sample illustration is shown in Figure 11.

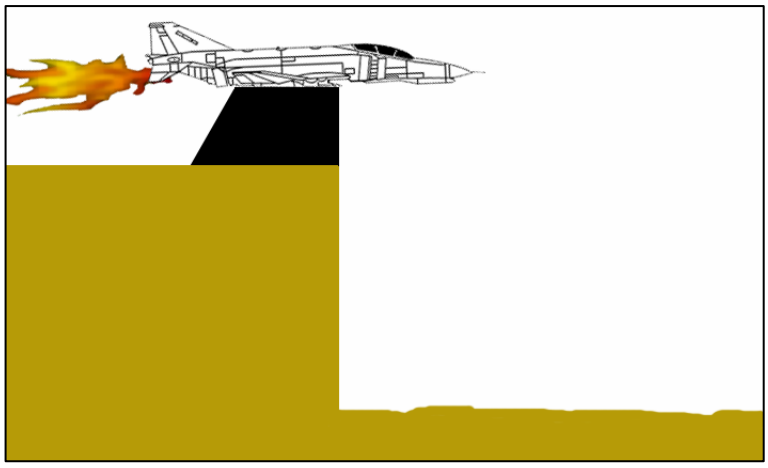

Figure 11 – Parallel Launching

Advantages:

- Low cost facility
- Multipurpose usage

Disadvantages:

- Placement problem of rocket engine
- The problem of withstanding to the structural forces during launch
- Displacement of the center of gravity problem
- Stability problem of the aircraft model
- Difficulty of the separation mechanism design
- Monitoring problem
- The need of the rocket engine design
- The possibility of not reaching to the required velocity for separation
- Difficulty of repeatability in order to make controllable tests
- Increasing cost if the aircraft model cannot be recovered.

Alternative 7

Fixed armed carriage will accelerate on a rail and at the terminal part of the rail; the aircraft model separates from the store model. A sample illustration is shown in Figure 12.

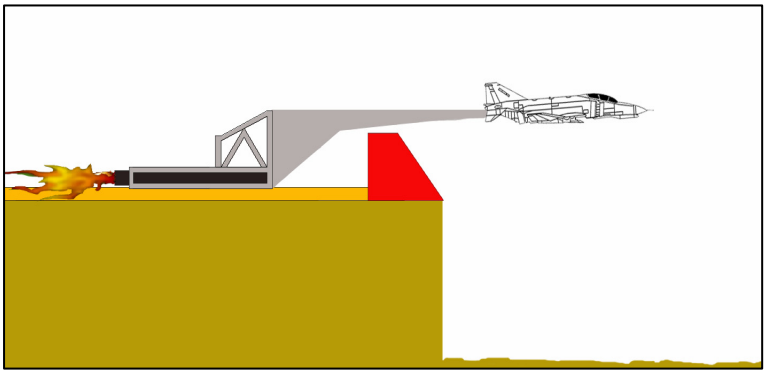

Figure 12 – Carriage with a Fixed Arm in the Front

Advantages:

- Average cost facility
- Multipurpose usage

Disadvantages:

- Difficulty of repeatability in order to make controllable tests
- The need to design of the carriage
- The need to design of the deceleration mechanism
- High cost for the maintenance

Alternative 8

Carriage with a fixed arm, which, holds that aircraft model at a certain height, will accelerate on a rail, is shown in Figure 13.

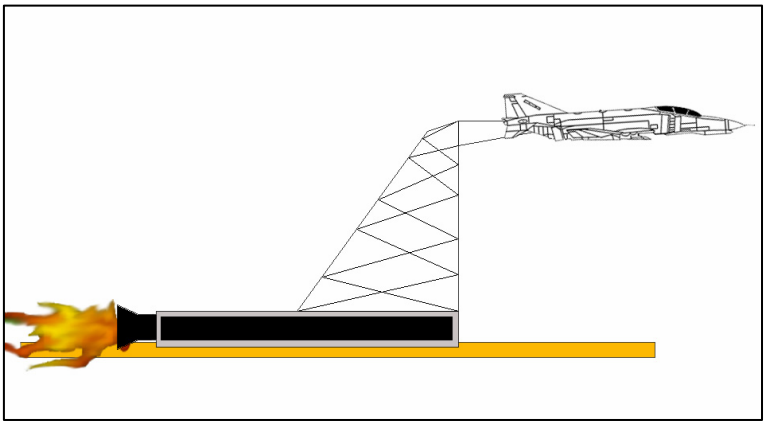

Figure 13 – Carriage with a Fixed Arm at the Top

Advantages:

- Average cost facility
- Multipurpose usage

Disadvantages:

- The need to design of the carriage
- The cost problem due to the corrosive effect of the rocket engine chemicals
- The need to design of the deceleration mechanism
- Stiffness and vibration problem

2.1.4. Evaluation of the Alternatives

There are eight different alternatives for the test facility and the best choice must be made among them. Among all the alternatives, besides the

advantages that are listed above for each of them, the requirements of the separation are the driving factor in the evaluation. These requirements are similitude inputs for the separation process some of which are the separation velocity and the aerodynamics of the store.

In the evaluation procedure, first the requirement about the ground effect on the test setup is analyzed so that the similitude of the aerodynamics can be performed. For the tests at high speeds, the ground effect can not be neglected. In order to decide the necessary and sufficient flight altitude of the aircraft model, CFD analysis is performed. It is observed that aircraft model should fly at least 3 meter above from the ground so that the flow around the aircraft model is disturbed less than 5%. A sample capture of the analysis is shown in Figure 14.

Another source for the distortion of the airflow can be the rail itself. The wall effect of the rail can affect the aerodynamics. So in order to make it negligible, the distance of the store model from the rail is arranged. This can be performed with the usage of a sting. Detailed explanation for the sting is given in section 2.2.2.

The alternatives 1, 2 and 6 are eliminated because of the evaluations according to the repeatability and excessive design necessity. Since there is no radio controlled model aircraft in the market that can satisfy the requirements, the alternative 4 is automatically eliminated.

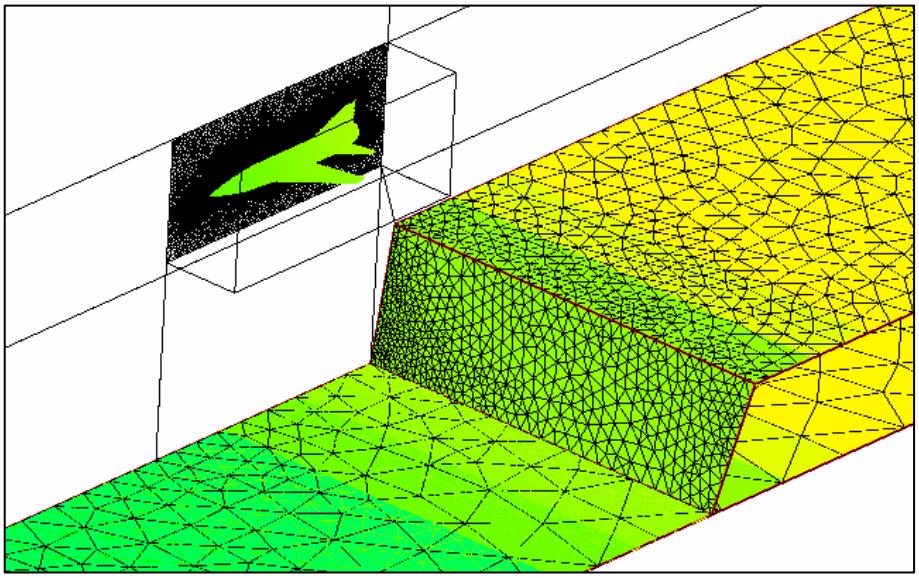

Figure 14 – A View of CFD Analysis Model

The acceptable distance for the safe separation of the store model from the aircraft model is its own length, [1]. The length of the store model is 0.484 m which is represented in the results of the similitude studies in the Chapter 2.3.3. The store model should fly at least 0.3 seconds to free fall through this particular distance. In this calculation, it is assumed that there is no lift acting on the store model. Another assumption is made for the Alternative 7 with fixed arm in front of the body is that its length should be 5 meters at most in order to withstand the structural and launch stresses. The carriage that travels at 150 m/s needs 0.033 seconds to go 5 meters. In this period the store model free falls approximately 6 mm and this is not sufficient to demonstrate that the separation is acceptable. So this alternative is eliminated. The eliminations are summarized within Table 1. The cross marks are placed for the corresponding reasons. The alternatives that are not eliminated are indicated in shaded areas.

Table 1 – Test Alternatives Elimination Chart

	Similitude Application Constraints (Ground Effect)	Repeatability, Excessive Design	Availability
1		X	
2		X	
3			
4			X
5			
6		X	
7	X		
8			

An effectiveness evaluation is made for the alternatives 3, 5 and 8, which are not eliminated. These alternatives are graded according to the manufacturability, ease of use, multi-purpose usage, repeatability, maintenance, work safety, cost and reliability. Grades are given in Table 2. Alternative 3 is given low grades for multi-purpose usage, repeatability and reliability. The other two choices have close points and as a conclusion, alternative 5 is chosen as the facility and test setup configuration.

According to the result of the feasibility studies, the area shown in the Figure 16 is settled. Due to the restrictions about the territory of TUBITAK-SAGE, the facility area is fitted within to an area of 300 meters in length and 20 meters in width. The height of the rail is 5 meters from the ground, which is selected according to the CFD results.

Table 2 – Grading Chart for Alternatives 3, 5 and 8

	Alternative 3	Alternative 5	Alternative 8
Manufacturability	5	3	3
Ease of use	3	4	3
Repeatability	2	4	4
Maintenance	5	3	3
Multi-Purpose	1	5	4
Work safety	3	4	4
Cost	5	3	3
Reliability	2	4	4
TOTAL	**26**	**30**	**28**

Rail is chosen to be IPB100 Profile DIN 1025. Wide flanges of the IPB profile instead standard I profile, support the carriage and provide more space for design. At the both end of each profile, which is 6 meters long, there is a support, which is shown in Figure 15. The dimensions in the figure are given in millimeters.

The construction is completed in summer season and due to the high summer temperature, the profiles are readily elongated. At lower temperatures, like in winter, the shrinkage results in gaps in the junctions of the profiles. These gaps are filled with suitable pieces of the same profile.

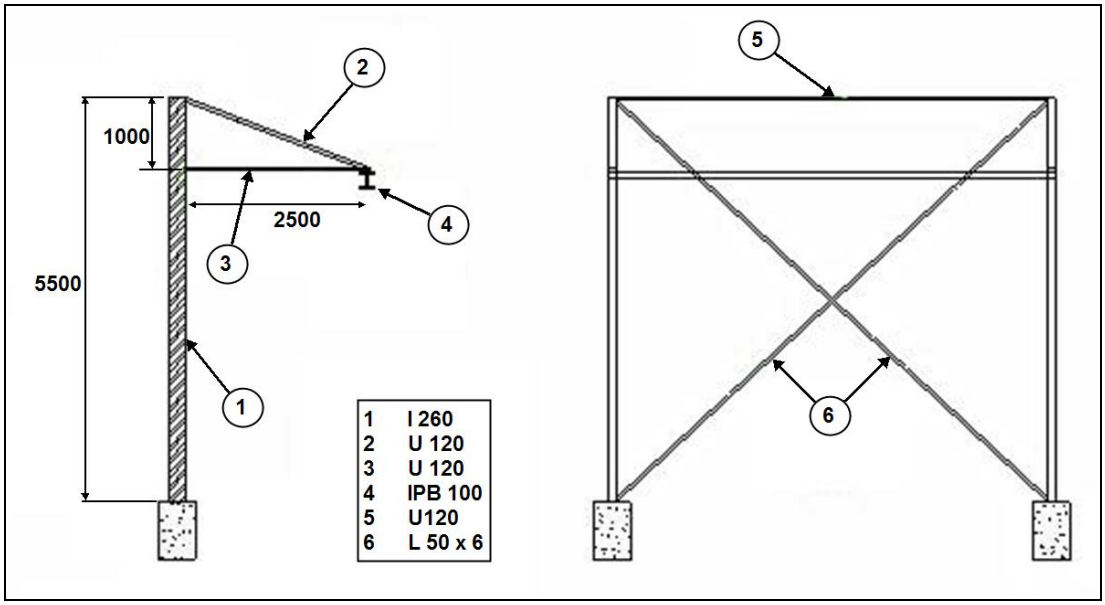

Figure 15 – Rail and Rail Support Construction Layout

Figure 16 – A View of Constructed Sled Range

2.2. TEST AIRCRAFT MODEL CARRIAGE DESIGN

After completing the conceptual design for the facility, it is decided that the setup should has a rail at 5 meter above from the ground. Beneath this rail, the aircraft model with the store model should be carried to the desired velocities. For this purpose, a carriage should be designed and this carriage must handle all the requirements in order to accomplish the tests. It should be capable of carrying the store model attached aircraft model through 300-meter range.

In this 300-meter range, the carriage should accelerate up to the separation velocity. It is foreseen that, this velocity should be reached within the first 100-150 meters of the range. After achieving this velocity, the separation mechanism should be triggered and the separation of the store model takes place. The carriage and the aircraft model should move together with the separated store model until proving the safe separation. This is required for keeping the airflow around the store model as possibly similar as the original separation condition. Consequently, carriage should decelerate and stop at the end of the rail. While accomplishing these tasks it should carry the separation mechanism, the store model, trigger systems and the rocket engines as additional masses.

According to the functions that are specified above, the design requirements are established. First, the carriage must withstand the launch acceleration with all the additional masses. It should also withstand the deceleration.

In the conceptual design, the carriage is thought to be like Figure 18. Bearings will be used at the contact points of the carriage with the rail. At these contact points, bearings will be used from both upside and downside of

the rail. In the middle of the carriage main body, the sting will be mounted. The first conceptual design of the carriage and the main parts are shown in Figure 17. The carriage is composed of main body, bearing assembly, sting, rocket engines and the aircraft model.

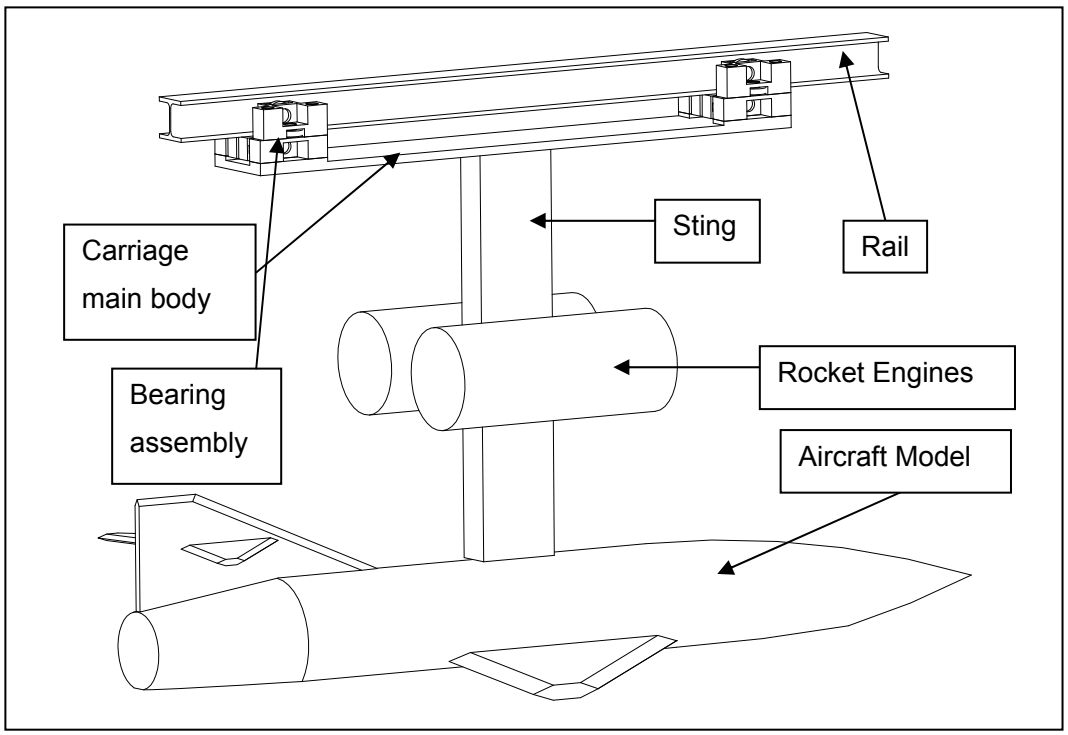

Figure 17 – Conceptual Design of the Carriage

2.2.1. Dynamic Model of the Aircraft Model Carriage

During the carriage design, a mathematical model is built in order to simulate the setup dynamically, [15]. The aim of the dynamic modeling study is to analyze the system behavior before the actual test. The results of the analysis are used in the designing the tests. Simulation results will allow

deciding which rocket engine should be used, and how many rocket engines should be used in order to achieve the desired velocity. Also according to the position information, it can be predicted at which position burnout occurs. By this way, the time and the place for the separation mechanism activation will be decided. Same information is also used for the placement of the cameras that will monitor the separation. Because of the ease of altering the parameters and visualization of the outputs, MATLAB® Simulink is chosen for the modeling tool

In the modeling, the aerodynamic coefficients and the friction coefficient are assumed to be constant. Another assumption about the rocket engines is the constant mass flow rate. For the aerodynamic forces, it is assumed that only the drag and the lift forces are acting on the body and the details of this model is represented in the following paragraphs.

The free body diagram of the test setup is given in the Figure 18. In this diagram, the geometric parameters and inertial, aerodynamic and thrust forces are shown. The weight of the carriage is given as “mg”. The reaction forces on the front and rear bearings are represented with N_1 and N_2, respectively. D_1, D_2 and D_3 are the drag forces on the aircraft model, the sting and the main body, respectively. The thrust force of the rocket engine is given by F and the lift force on the aircraft body represented by L. The front and rear friction forces, on the contacts between rail and the carriage are given with f_1 and f_2. According to the free body diagram and the given coordinate system, the equations of motion are written and solved simultaneously by the simulation tool.

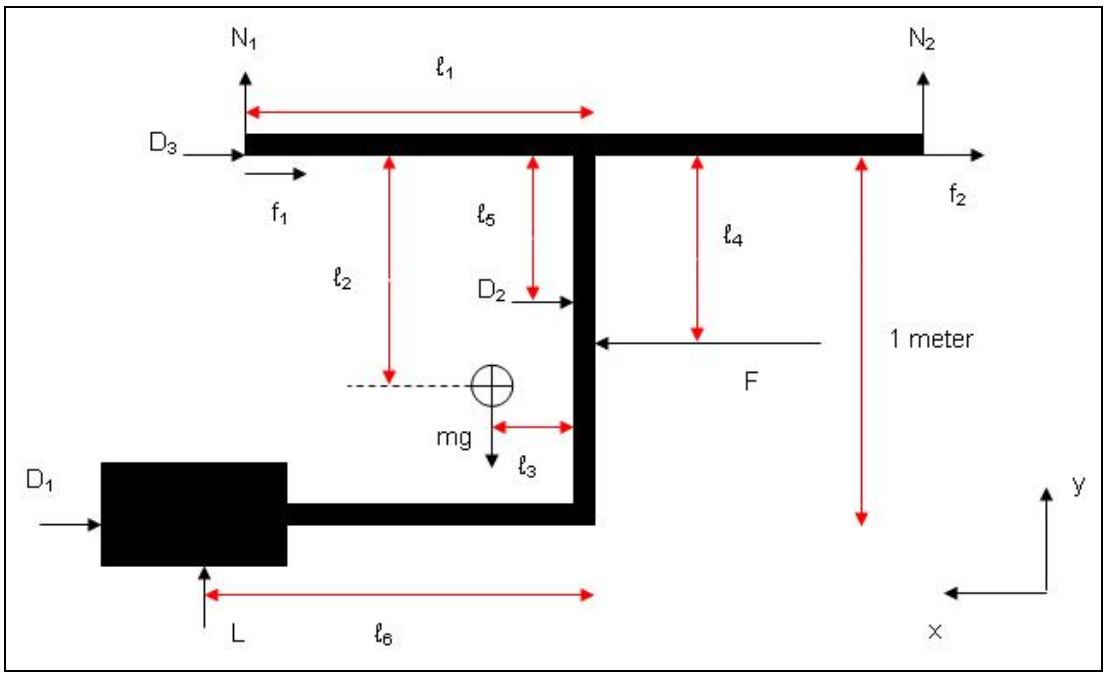

Figure 18 – Free Body Diagram of the Setup

$$\sum F_x = m \cdot a$$

$$F - D_1 - D_2 - D_3 - f_1 - f_2 = m \cdot a \tag{1}$$

$$\sum F_y = 0$$

$$N_1 + N_2 + L - mg = 0 \tag{2}$$

$$\sum M_{CG} = 0$$

$$\begin{aligned} -F(\ell_2 - \ell_4) + N_1(\ell_1 - \ell_3) - N_2(\ell_1 + \ell_3) + (f_1 + f_2) \cdot \ell_2 \\ + D_3 \cdot \ell_2 + D_2 \cdot (\ell_2 - \ell_5) - D_1 \cdot (1 - \ell_2) + L(\ell_6 - \ell_3) = 0 \end{aligned} \tag{3}$$

For the friction forces on the body, the following equation is used.

$$f_{1,2} = N_{1,2} \cdot \mu \tag{4}$$

The block diagrams of the dynamic model are shown at Appendix A. The necessary dimensions shown in Figure 18 of the carriage are defined as the geometrical inputs of the model and given in Table 3.

Table 3 – Dimension Descriptions of the MATLAB® Simulink Model

ℓ_1	half distance between the reaction forces
ℓ_2	vertical distance between center of gravity, and the carriage main body
ℓ_3	horizontal distance of center of gravity from the sting
ℓ_4	vertical distance of thrust vector from the carriage main body
ℓ_5	vertical distance of resultant drag force on the sting from the carriage main body
ℓ_6	horizontal distance of aircraft models center of gravity from the sting

The inputs about the thrust on the carriage are the thrust data itself, which is read from a text file. These data files are prepared as a database for each type of the rocket engine as a result of static firing tests. They include the time and the thrust information at the time. The results of these tests are used directly in this simulation. The other inputs are the number of the rocket engines, the mass of the rocket engine and the rocket engines mass consumption rate. Therefore, in the simulation, the mass consumption is calculated and variable mass is used.

The mass of the setup and aerodynamic data are also other inputs for the simulation. These data are given in modular manner. The setup is divided into three parts. These parts are the aircraft model, the sting and the main body of the carriage. On the coordinate system the drag force and the lift force are the components on x and y-axes, respectively. The equations of the aerodynamic forces are given in Equations (5) and (6).

$$D = \frac{1}{2}\rho V^2 S C_D \tag{5}$$

$$L = \frac{1}{2}\rho V^2 S C_L \tag{6}$$

For each part of the setup, air density, the wet area, S, drag coefficient C_D, lift coefficient C_L are input parameters. V is the velocity of the carriage along the rail. The outputs of the simulation are obtained graphically for the carriage dynamics and given in Chapter 3.

There is an additional MATLAB® Simulink block in the model for the moment calculations for different sting cross-sections. The investigated cross-section is defined by the length from the main body and the block gives the moment curve. This output will be used in the design of the required parts of the carriage.

2.2.2. Mechanical Design of Carriage Subsystems

The mechanical design of the carriage is made according to the results of the conceptual design. The primary requirement for the carriage is to withstand the launch acceleration. The deceleration is not specified as a requirement

because the acceleration from the thrust will be at least as high as the deceleration.

The general shape and the components of the carriage are decided in conceptual design phase. It is concluded that the main body of the carriage will be supported by the bearing assemblies in order to hold the rail. All the other components will be fixed to the main body.

The strength analysis is made for each of the individual part on the carriage. As seen in the Figure 17, the parts are the main body, the sting and the bearing assembly. The bearing assembly is composed of bearings, shafts, and supports for these shafts and bolts.

Design point for the mass of the test setup is decided as 100 kg without rocket engine. The acceleration will be supplied by the thrust of the rocket engine named R4. The detailed information about this engine is given in section 2.4.

Mechanical Design of the Sting

As mentioned before, the sting should support the aerodynamic surfaces during the test. It is mounted to the middle point of the main body. The common usage for an aerodynamic testing is to hold the model from the back in order not to disturb the flow around. A typical application is shown in Figure 19.

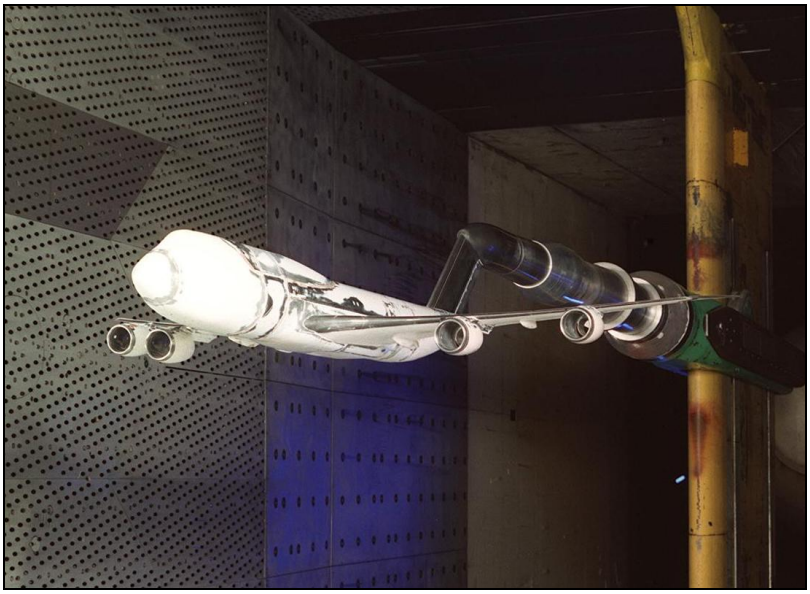

Figure 19 – A View of Sting Usage in a Wind Tunnel (Holding From Back)

Because of the manufacturing and the structural difficulties, it is decided to support the aircraft model from the middle. Since the store is under the wing, the support is decided to be connected at the top of the aircraft. In the literature, this kind of usage of stings is very common and one of them can be seen in Figure 20. By using this kind of support, the disturbance effect of the sting to the aerodynamic flow can be neglected. Since the flow field above the aircraft model is mainly affected, it can be assumed that the flow field beneath the aircraft is not disturbed. The conceptual samples of the L-shaped and straight stings are shown in Figure 21 and Figure 22.

In this section, the design of the sting is performed by choosing the profile and proper dimensions. The stress calculations are performed according to the results of the MATLAB® Simulink model, which gives the corresponding moments in desired cross-sections.

Figure 20 – A View of Sting Usage in a Wind Tunnel(Holding From Middle)

Figure 21 – Conceptual L-Shaped Sting

Figure 22 – Conceptual Straight Sting

The moments on the critical cross-section of the sting is shown in the following figure. This particular moment on the interface cross-section is found from the MATLAB® Simulink model. The moment in this particular cross-section turns out to be approximately 93000 N.m. The maximum value of this moment is approximately 160710 N.m. Right-hand side graph is showing the time interval of 0.025 – 0.07s where the maximum moment of this cross-section can be seen.

The stress due to bending moment is can be calculated as,

$$\sigma = \frac{M \cdot c}{I} \tag{7}$$

Where M is the moment on the particular cross-section, I is the second moment of area of the profile and c is the distance from the neutral axis of the beam to the surface.

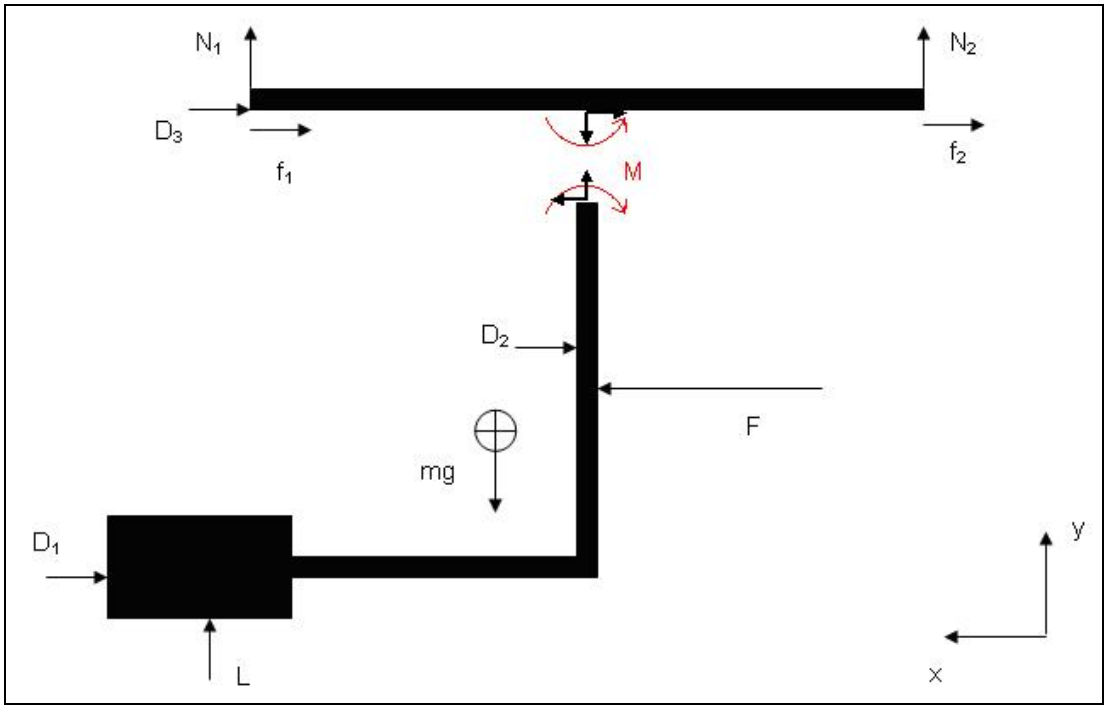

Figure 23 – Free Body Diagrams for the Sting Design

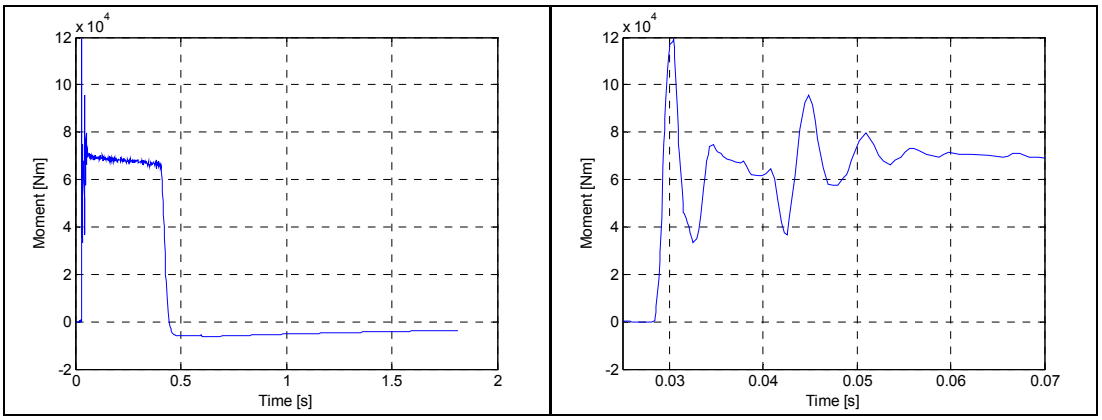

Figure 24 – Graph of Bending Moment of the Interface Surface between Sting and Main body

In the first analyses, aluminum Bosch profile is considered, [19]. A sample cross-section among these profiles is given in Figure 25. These profiles have the benefit of having relatively large inertia to mass ratio than the standard steel profiles. The attachment of the sting has to be supplied by two bolts and it is concluded that the allowable stress is not enough to withstand the required launch accelerations. In order to improve the cross section stress capacity, welding to a steel carriage for fixing the sting is not possible since the material is aluminum. Similarly, it is not possible to support and strengthen up this profile because of the welding difficulties.

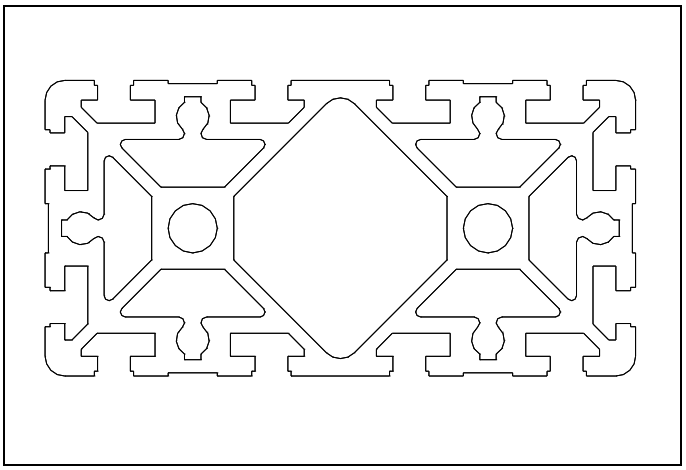

Figure 25 – Cross-section of 90 x 180 Bosch Profile

After these analyses, and observing the application difficulties, it is decided to consider a standard DIN1025 I profile. I-200 profile is chosen for the analyses, because of the large inertia and comparable mass value. The inertial values for this profile are given in Table 4 and profile is given in the following figure.

The advantage of the I-200 profile is being made of steel so it is suitable for welding which is used to fix the sting profile to the main body. In the analysis of this profile first the beam cross-section and then the welding cross-section is observed.

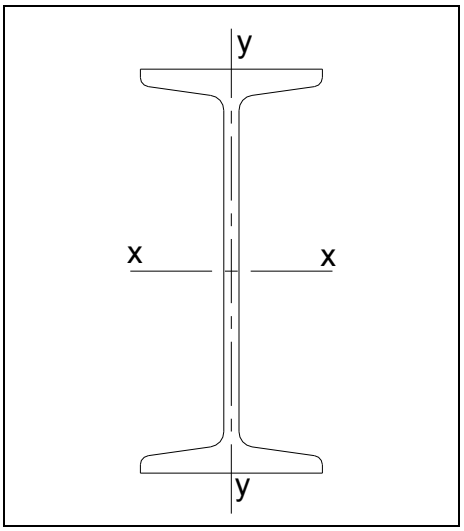

Figure 26 – Cross-section of I-200 Profile

The c value of the profile in the Equation (7) is 100 mm, which is the half length in the y direction. Using the inertia information, which is given in Table 4, the result for the stress is calculated as 751 MPa. Since the material of this profile has the yield strength of 275 MPa, the single beam is not able to withstand the applied moment.

In the analyses of the weld, first the type of the welding electrode (metal) and then the geometry must be determined. The properties of the welding metal are given in Table 5, [16]. It is assumed that this welding metal will be applied

in a 10 mm thickness. The drawing of welding on the periphery of the I-200 profile is shown in Figure 27 where dimensions are given in millimeters.

Table 4 – DIN1025 I-200 Profile Properties

Designation	I profile DIN1025-U St44-2 I-200
Cross-sectional Area	33.4 cm^2
Weight	26.2 kg/m
Moment of Area (I_x)	2140 cm^4
Section Modulus	214 cm^3
Ultimate Tensile Strength	440 N/mm^2
Yield Strength	275 N/mm^2

Table 5 – Properties of Welding Metal

Classification	TS 563 EN 499 : E42 3 B 42 H10
	AWS A5.1 : E 7018
Yield Strength	460 N/mm^2
Ultimate Tensile Strength	530 N/mm^2

The inertia of this cross-section is approximately calculated as width of the weld multiplied with the peripheral of the I-200 cross-section. It is drawn and calculated with the AutoCAD® Mechanical Desktop. The results are given in the table below.

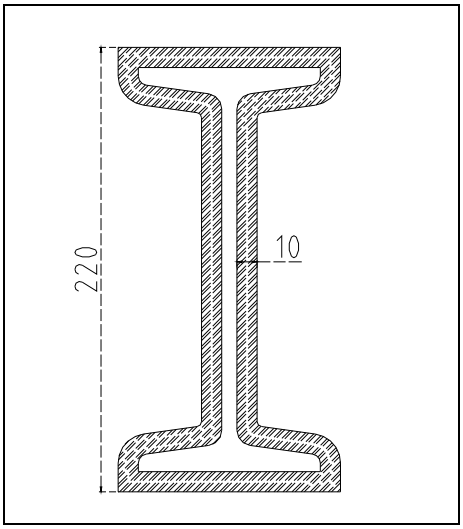

Figure 27 – Cross-section of Welding Around I-200 Profile

Table 6 – Geometrical Properties of the Weld

The area of the welding [cm^2]	74.87
The Moment of Area of the welding [cm^4]	4682
Applied Stress [MPa]	378

It is observed that calculated stress value is less than the yield strength of the welding metal, which is given in Figure 27. In the design procedure of this test setup, a safety factor of two is selected because of the dynamic effects and compensating the unpredictable factors and casualties. In the design analyses, all the calculations are performed as if they are only static loadings. After this safety factor is issued, the allowable stress for the welding is changed from 460 MPa to half of it, 230 MPa. Therefore, the calculated stress for the welding, which is 378 MPa, is not less than the allowable stress

of 230 MPa. A method to solve this problem is to issue a flange that will be placed in front of the sting in order to increase the inertia of that particular cross-section. For the cross-section, presented in Figure 28 where dimensions are given in millimeters, the flange has a 180x10 mm^2 cross-section area where it has interface with the main body. The inertia of this area is calculated with the same way and found as 15844 cm^4. Since the area is not symmetric, the c values are different for compression and tension sections. For the tension side the distance of the neutral axis to the surface is 176.54 mm and for the compression side, it is 223.5 mm. Therefore, the stress on the compression side will be larger. According to these values and using the Equation (7), the stress turns out to be 226 MPa. The result is less than the allowable stress, 230 MPa and is acceptable.

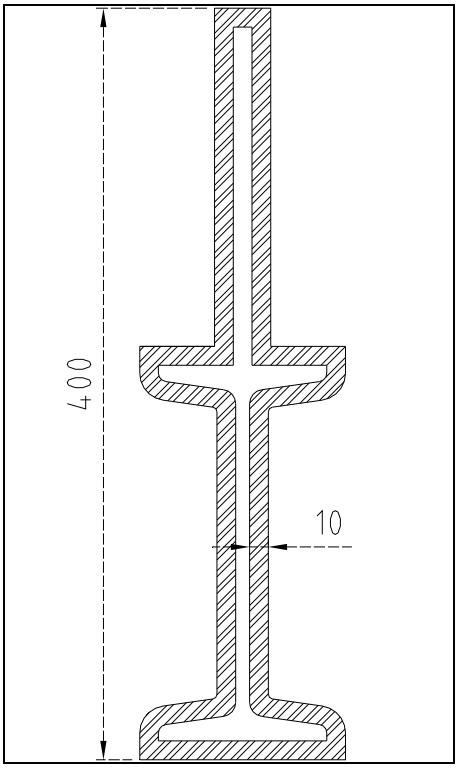

Figure 28 – Cross-section of Welding Around I-200 Profile and Flange

The vertical length of the flange among the sting is found by making iterations on the dynamic simulation model. It is known that the allowable stress is 137.5 MPa, which is the half of the yield strength of I-200 profile. The maximum moment at which the allowable stress would not be exceeded, is calculated as 29425 N.m.

In the dynamic model, as mentioned before, the moment calculation can be performed for a particular cross-section of the sting. The corresponding vertical length of the cross-section at which the moment is equal to 29425 N.m is found as 367 mm from the main body. The 3D model of the 1 meter long I-200 profile sting and the 180x367x10 mm right-triangular cross-sectional flange can be seen in Figure 29 where dimensions are given in millimeters.

Mechanical Design of the Main Body

The primary objective for the main body is to support the sting and aerodynamic surfaces. The main body of the carriage is designed by choosing its profile and dimensions. The length is decided to be 2 meters. The profile is selected to be U profile. In this selection, the placement of the bearing assemblies is considered. The results of the simulation are used for the design analyses. In the analyses, simply supported beam is used with the proper moments and forces. It is concluded that U120 profile is suitable and can withstand the launch stresses.

Mechanical Design of the Bearing Assembly

The main body that will move along the rail needs to be supported so that the acceleration gives minimum corrosive damage to both rail and the setup. Since one of the primary requirements of the tests is the repeatability, in order to make controllable tests and because of the high cost of the maintenance, the movement of the test setup should not give permanent damage to the rail. If the supports are working in only slip condition, the rail will be corroded in each test gradually. The use of bearing is decided to employ roll motion.

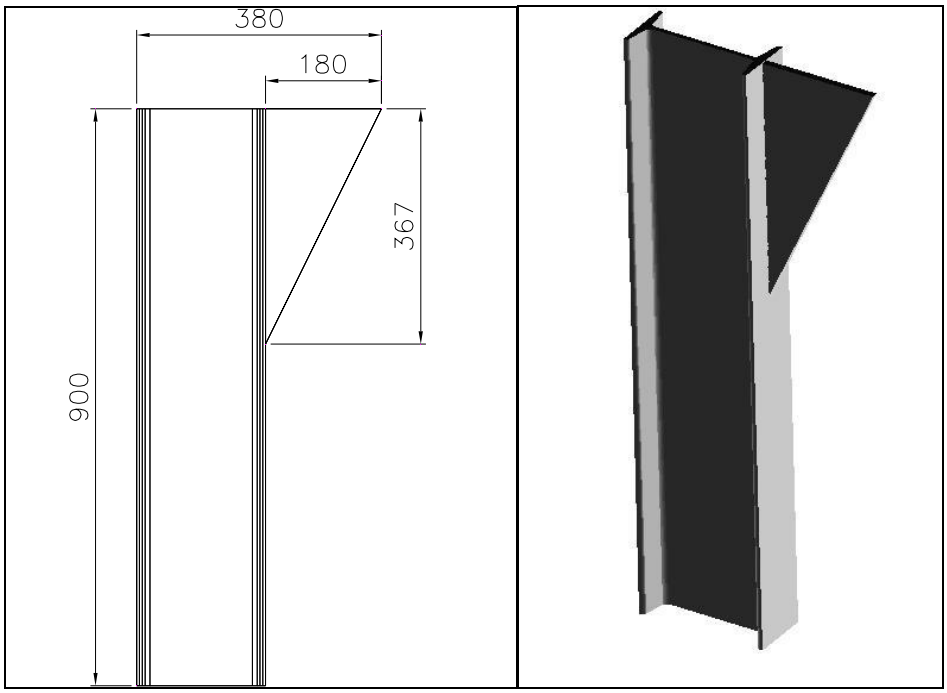

Figure 29 – Dimensions and 3D Model of the Sting and Flange

For the support of the bearings, lower flange of the IPB100 profile of the rail is used. While the rocket engines are fired, in order to maintain the contact of the bearings and the rail, it is necessary to use eight bearings, with equally place both on top and beneath the rail. So the contact to the rail is granted and the contact will not be lost during the launch sequence. These eight bearings bring a placement problem of the setup to the rail. In order to make the placement easy, the position of the lower ones should be adjustable such that after placing the carriage to the rail, the lower bearings can be fixed afterwards. Besides, this adjustability is also used for applying a preload to the bearings. This preload is used in order not to lose contact while deflections happen at the shafts of the bearings.

For these requirements, there is a need of double bearing usage at each four corner of the main body. There will be a support for the bearings and a shaft for each bearing.

The forces acting on the bearings are obtained from the dynamic model as previous analysis. The simulation is run with the same parameters and the normal (reaction) forces on the bearings, N_1 and N_2 that are shown in Figure 18 are obtained. The graphical representation of the reaction force N_1 is given in Figure 30. Since rear reaction forces are smaller than the front ones, design criteria are decided according to the front reaction force. As it can be observed from the graph, the maximum force is approximately 11000 N. The first part of the assembly to be analyzed is the support of the bearing, solid model is given Figure 31.

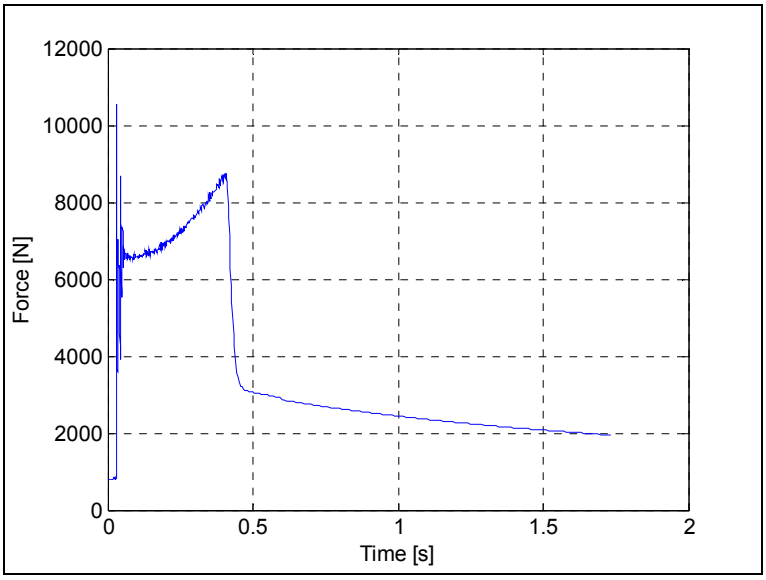

Figure 30 – Reaction Force on the Front Bearings

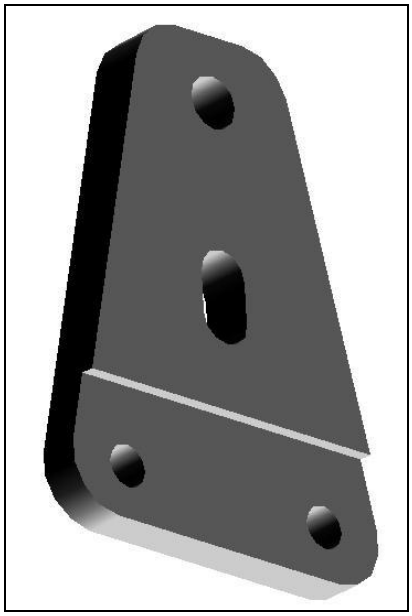

Figure 31 – Solid Model of the Bearing Support

The two holes are used to fix the support to the main body with M16 bolts. The cross-section that passes through the center of these holes is to be analyzed first, after that, the bolts are analyzed; corresponding cross-sections are shown in Figure 32. The material of this part has 290 MPa yield strength, [17], and with the safety factor, the acceptable strength is going to be 145 MPa.

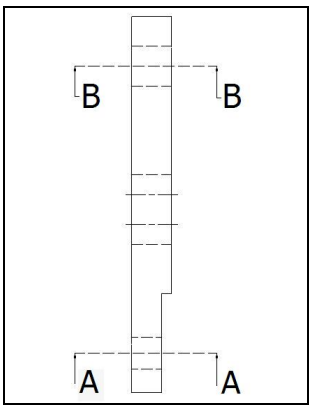

Figure 32 – Bearing Support Cross-Sections

Table 7 – Properties of the Cross-Sections of Bearing Support

Area of the cross-section A-A, [cm^2]	16.2
Moment of Area of cross-section A-A [cm^4]	3.04
Area of the cross-section B-B, [cm^2]	11
Moment of Area of cross-section B-B [cm^4]	2.1

The reaction force is assumed to be applied from the midpoint of the bearing contact line with the rail. The distance between the reaction force and the

neutral axis of the cross-section is 32 mm. According to the data given in Table 7, the stress due to bending turns out to be 43.3 MPa in A-A, and 63.7 MPa in B-B. These stresses are less than the allowable stress therefore they are all acceptable.

At the cross-section A-A, two M16 bolts and at the cross-section B-B M20 bolts are used. For the M16 bolt, the area is approximately 2 cm^2 and the inertia is 0.32 cm^4. Since two bolts are used, the inertia is doubled and the stress becomes 218 MPa. In the upper section B-B, M20 bolts are used to fix the bearing shafts whose solid model is given in Figure 33. The calculations are performed at the cross-section where the bearing shaft interfaces the support. The cross-sectional area of the M20 bolt is approximately 3.14 cm^2 and the inertia is 0.78 cm^4. The stress on the bolt is 223 MPa. As mentioned before the yield strength of 8.8 quality bolt is 640 MPa and with the safety factor, this value is halved to 320 MPa that concludes the stress values at the bolts are acceptable.

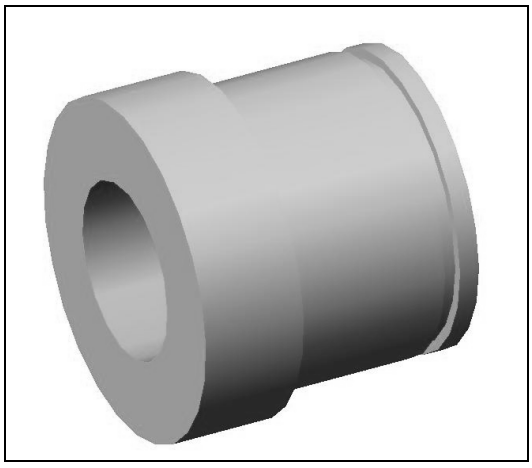

Figure 33 – Solid Model of Vertical Bearing Shaft

Until the rocket engines burn-out, there occurs a misalignment in the trust vector. The vertical misalignment can be compensated by the bearings used on the support but for the horizontal misalignment, there should be a part that restricts the undesired horizontal movement. In order to avoid this phenomenon, four bearings that are placed horizontally, just touching the far edge of the lower flange of the IPB100 rail profile. So that the carriage is kept on the rail and the only contact to the rail is the bearings, not the support. For the analyses of the horizontal bearing, the misalignment of the thrust vector is assumed to be 5° in order to be in the safe region.

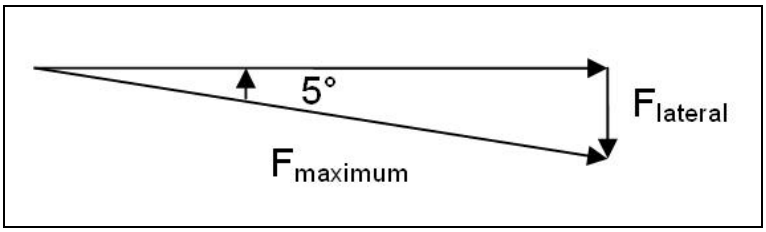

Figure 34 – Thrust Misalignment

As it can be seen from Figure 34, lateral force can be found with the following equation.

$$F_{lateral} = F_{maximum} \cdot \sin(\alpha) \tag{8}$$

Where the maximum thrust for the R4 rocket engine is 18222 N and α is the angle of misalignment so that the lateral force is calculated as 1588 N and moment is found as 159 N.m. The diameter of the shaft is taken as 20 mm so the stress on this particular cross-section is 202 MPa, which is less than the

allowable stress. The solid model of the horizontal bearing shaft is given below.

After completing the design of support and the shafts, the work left is the selection of the bearings. This selection is performed for the vertically placed bearings that are attached to the support and horizontally placed bearings that are attached to its own shaft as mentioned before.

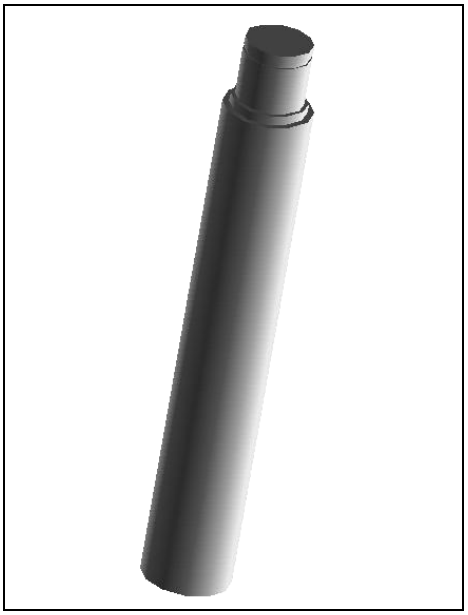

Figure 35 – Horizontal Bearing Shaft Solid Model

The bearings are selected among FAFNIR Ball Bearings, [20]. For the vertically placed bearings, the applied radial load on bearing is taken as the maximum value of the thrust. The lateral forces on these bearings are directly applied by the horizontal bearings. Therefore, the only loading will be the radial loading for vertically placed bearings.

This selection is made according to the loadings and the geometric constraints that bearings are placed between the flanges of the IPB100 profile. From the catalogue, 206W is selected, among the Light 200W series. The properties of this bearing are given in Table 8 and the corresponding parameters are shown in Figure 36.

Table 8 – Properties of 206W FAFNIR Radial Ball Bearing

Bore, d (mm)	30
Outside Diameter, D (mm)	62
Width, C, (mm)	16
Weight (kg)	0.213
Extended Dynamic Load Rating, (N)	31000

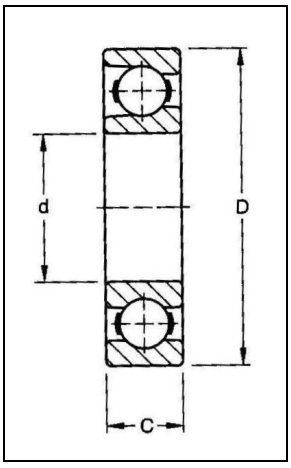

Figure 36 – Parameters of a Radial Ball Bearing

The life calculation of the bearing is performed with the following equation, [20].

$$L_{10} = \frac{166667}{N}\left[\frac{C_E}{P}\right]^3 \tag{9}$$

Generally, life is expressed as the number of hours that 90% of a group of identical bearings will exceed under a given set of conditions, and is referred to as the L_{10}. In the Equation (9), C_E represents Extended Dynamic Load Rating in newtons and P is for Equivalent Radial Load on Bearing in newtons. The operation speed, in rpm is represented with N. The velocity profile according to the design criteria is given Figure 37 as obtained from the dynamic model.

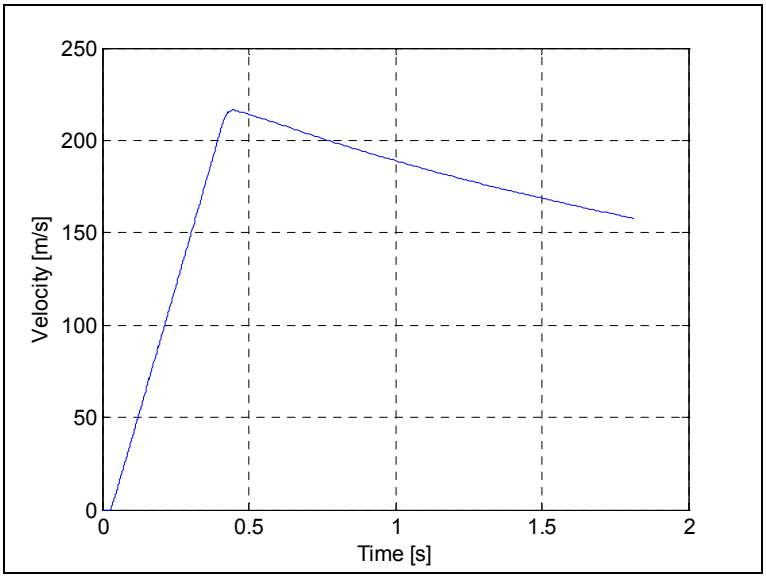

Figure 37 – Velocity Profile

At the maximum velocity of the carriage, the bearing has an angular velocity of 7420 rad/s. By using these values, the life of the bearing turns out to be 1.16 hours, which is sufficient to perform a whole test safely.

The horizontal bearings have the lateral force of the carriage as mentioned above as the applied radial loading. The axial load for the horizontal bearing is acting on the vertically placed bearings so that there will be no axial load for horizontal bearings. According to the load ratings, this bearing is selected from the standard bearing catalog, [21], as 6202 radial ball bearing, Table 9. The manufactured assembly is demonstrated in the Figure 38.

Table 9 – Properties of 6202 Standard Radial Ball Bearing

Bore, d (mm)		15
Outside Diameter, D (mm)		35
Width, C, (mm)		11
Load Ratings (kN)	C_r	7.65
	C_{0r}	3.75
Speed Limit (R.P.M)	Grease	20000
	Oil	24000

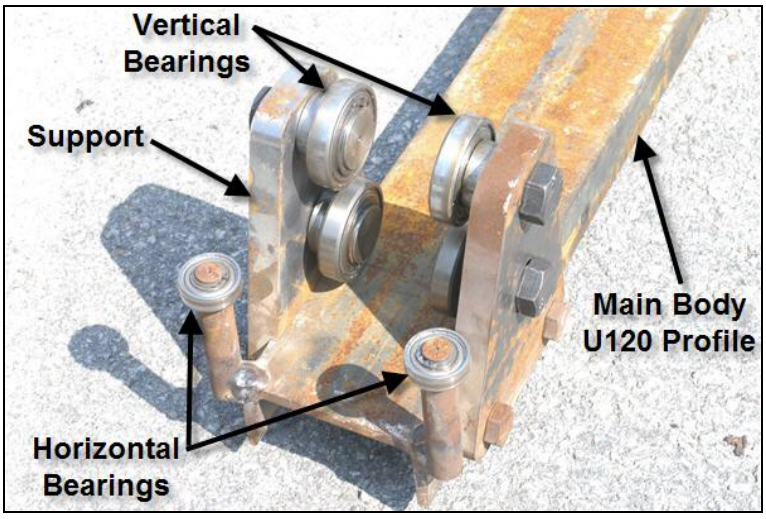

Figure 38 – A View of Components of the Bearing Assembly

2.3. DESIGN OF AIRCRAFT/WING/STORE/PYLON MODELS WITH SIMILITUDE

In this section, the similitude analysis carried out during design phase is presented and the design and development of the aircraft model, wing, store model and the pylon model are explained in details.

2.3.1. Principles of Similitude

This section includes the calculations performed with the different similitude methods, which are used, for the store model and the ejection condition in order to match with the real store separation test of the full-scaled aircraft and the selection of the suitable method. The similitude methods are examined for the free fall tests and the calculations are made for the separation conditions.

In the free fall tests, for the store and the separation conditions, there is a need to fulfill two criteria. One of them is that the aerodynamic forces and moments acting on the store model. These forces and moments should be a scaled version of the real flight conditions. The second one is that according to these forces and moments, the flight characteristics and so the dynamic characteristics should represent the real flight conditions.

Aerodynamic scaling can be defined as the reduction of the linear dimensions according to the store model and aircraft model, [22]. The prerequisite of the force and moment scaling is to achieve the flow similarity between the real flight conditions and test conditions. This flow similarity can be accomplished by assuring that the effects of the compressibility and the

viscosity are the same. Compressibility is related with the Mach number which can be defined by the expression $\frac{V_\infty}{a_\infty}$, while viscosity is related with Reynolds number. Accordingly, if the Reynolds and Mach numbers are selected suitably according to the full scale test conditions with respect to the flow, aerodynamic coefficients obtained from the scaled tests reflect the characteristics of the full scaled flight aerodynamics. Even in the wind tunnel tests, while the Mach number is fulfilled, it may not be possible to achieve the desired Reynolds Number. Additionally the aerodynamic properties of the store model are not dependent on Reynolds number as much as Mach number. Therefore, these problems against the Reynolds number are usually acceptable. In general, the scaling of the aerodynamic forces and moments are applicable when the conditions given in Table 10, are satisfied:

Table 10 – Conditions for Scaling

Model Dimensions	Model store = $\frac{1}{n}$ Real store
Mach Number	$M'_\infty = M_\infty$
Reynolds Number	$Re'_\infty = Re_\infty$

In the similitude studies, some assumptions should be considered and the assumptions made in this particular study are the followings:

- While making the calculations of the mass, moment of inertia and ejection forces for the test conditions and the real flight conditions, the air density is assumed to be equal.

- In the calculations of the ejection force, for the test conditions and the real flight conditions, temperature is assumed to be equal.

The reason for these assumptions is, as the temperature changes in test, the ejection force could not be adjusted due to the mechanism used for ejection, which is explained in the section 2.3.4. The aircraft model that is obtained for the store separation tests, has a scale of 1/8, so that the scale is taken as same for the models and similitude calculations. There are three primary methods for scaling. These are Froude scaling, “Heavy” Mach Scaling and “Light” Mach Scaling. All these scaling methods are explained and compared in the following sections.

Froude Scaling

Froude number can be defined by the expression $\frac{V_\infty^2}{l \cdot g_\infty}$. This number is used to satisfy the scaling of inertial and gravitational effects with the addition of the geometric similitude. The value of the Mach number is reduced in order to achieve flight similarity; this leads some errors for the aerodynamic model that should be accepted. This similitude method is valid for the flows whose compressibility effect is small, which means the flow should be low subsonic, [22]. Corresponding equations for the Froude scaling is given in Table 11.

As the physical properties of the store model are appropriate according to these equations, the dynamic motion of the model is related with the real model using the equations given in Table 12.

Table 11 – Froude Scaling Relations [42]

Gravitational Acceleration	$g' = g$
Time	$t' = t\sqrt{\frac{1}{n}}$
Velocity	$V'_\infty = V_\infty \sqrt{\frac{1}{n}}$
Mach Number	$M'_\infty = M_\infty \sqrt{\frac{1}{n}\frac{T'_\infty}{T_\infty}}$
Mass	$m' = m\frac{\rho'_\infty}{\rho_\infty}\left(\frac{1}{n}\right)^3$
Mass Moment of Inertia	$I' = I\frac{\rho'_\infty}{\rho_\infty}\left(\frac{1}{n}\right)^3$
Ejection Force	$F'_E = F_E\frac{\rho'_\infty}{\rho_\infty}\left(\frac{1}{n}\right)^3$

Table 12 – Dynamic Model for Froude Scaling [42]

Linear position	$Z' = Z\frac{1}{n}$
Linear velocity	$\dot{Z}' = \dot{Z}\sqrt{\frac{1}{n}}$
Linear acceleration	$\ddot{Z}' = \ddot{Z}$
Angular position	$\theta' = \theta$
Angular velocity	$\dot{\theta}' = \frac{\dot{\theta}}{\sqrt{1/n}}$
Angular acceleration	$\ddot{\theta}' = \frac{\ddot{\theta}}{1/n}$

The store separation test is planned to be made in the transient and low subsonic region. Therefore, considering the fact about the compressibility effects, it is concluded that the Froude scaling is not suitable.

“Heavy” Mach Scaling

In the Mach number scaling, the compressibility effects of the flow for the model are taken into consideration by using the real flight Mach number and so the scaling of the geometry is done accordingly. Mach scaling can be carried out in two different ways where the former one is the “Heavy” mach scaling.

As compared to Froude Scaling, the heavy-scaled model’s mass will be “n” times larger. This is because the Mach number is matched for the scaling of the aerodynamics rather than the dynamic motion. In other words, the model store must have a density ”n” times larger than the original store density.

With this “heavy” Mach scaling method, on a stationary aircraft, the path of the center of mass of the model will correctly similitude the real store. However, the small scaled models cannot be made heavy enough as to match the inertial properties, so this model cannot be used. Corresponding equations for the “Heavy” Mach scaling is given in Table 13.

The “Heavy” Mach scaling and the Froude Scaling of the physical properties of model give the same result for the dynamic motion. During the ejection process for the real ejection conditions, since the complete similitude of the roll rate and the angle of attack of the model is not achieved, the aerodynamics of the store model have differences. The dynamic relations for this scaling method are given in Table 14. The real model has a mass of

941.2 kg. According to this scaling method, our 1/8 scale store model should have a mass of

$$m' = 941.2\left(\frac{1}{8}\right)^2 = 14.7\,\text{kg}$$

There is no such material that can satisfy the required mass for the store model. Disregarding the inertial properties and the location of the center of mass by without giving any empty space inside the model and if cupper is used with a density of 8.94 g/cm^3, the store model will weigh approximately 7 kg, which is far nearly half of the expected value. Therefore, the "Heavy" Mach scaling method is not applicable to the separation test.

Table 13 – "Heavy" Mach Scaling Relations [42]

Gravitational Acceleration	$g' = g$
Time	$t' = t\sqrt{\frac{1}{n}}$
Mach Number	$M'_\infty = M_\infty$
Velocity	$V'_\infty = V_\infty\sqrt{\frac{T'_\infty}{T_\infty}}$
Mass	$m' = m\frac{Q'_\infty}{Q_\infty}\left(\frac{1}{n}\right)^2$
Mass Moment of Inertia	$I' = I\frac{Q'_\infty}{Q_\infty}\left(\frac{1}{n}\right)^4$
Ejection Force	$F'_E = F_E\frac{Q'_\infty}{Q_\infty}\left(\frac{1}{n}\right)^2$

Table 14 – Dynamic Model for "Heavy" Mach Scaling [42]

Linear position	$Z' = Z\frac{1}{n}$
Linear velocity	$\dot{Z}' = \dot{Z}\sqrt{\frac{1}{n}}$
Linear acceleration	$\ddot{Z}' = \ddot{Z}$
Angular position	$\theta' = \theta$
Angular velocity	$\dot{\theta}' = \frac{\dot{\theta}}{\sqrt{1/n}}$
Angular acceleration	$\ddot{\theta}' = \frac{\ddot{\theta}}{1/n}$

"Light" Mach Scaling

In the Froude scaling and "Heavy" Mach scaling, the gravitational fields both in the model test environment and in the real flight environment are considered to be equal. The gravitational field in the test environment adjustment is not possible yet. However, if it could be realized, both the Mach number for the aerodynamic and the dynamic motion scaling would be satisfied. In the "Light" Mach scaling, the gravitational accelerations in the model test environment and in the real flight environment are not supposed to be equal. As the gravitational accelerations are not equal, the following equations in Table 15 are governed.

If the physical properties of the store model are scaled according the "Light" Mach scaling method the following equations are become valid for the dynamics of the store model and real store.

Table 15 – "Light" Mach Scaling Relations [42]

Gravitational Acceleration	$g' = g\dfrac{\left(V'_\infty / V_\infty\right)^2}{1/n}$
Time	$t' = t\sqrt{\dfrac{1}{n}\left(V'_\infty / V_\infty\right)}$
Mach Number	$M'_\infty = M_\infty$
Velocity	$V'_\infty = V_\infty\sqrt{\dfrac{T'_\infty}{T_\infty}}$
Mass	$m' = m\dfrac{\rho'_\infty}{\rho_\infty}\left(\dfrac{1}{n}\right)^3$
Mass Moment of Inertia	$I' = I\dfrac{\rho'_\infty}{\rho_\infty}\left(\dfrac{1}{n}\right)^5$
Ejection Force	$F'_E = F_E\dfrac{Q'_\infty}{Q_\infty}\left(\dfrac{1}{n}\right)^2$

Table 16 – Dynamic Model for "Light" Mach Scaling [42]

Linear position	$Z' = Z\dfrac{1}{n}$
Linear velocity	$\dot{Z}' = \dot{Z}\sqrt{\dfrac{1}{n}}$
Linear acceleration	$\ddot{Z}' = \ddot{Z}$
Angular position	$\theta' = \theta$
Angular velocity	$\dot{\theta}' = \dfrac{\dot{\theta}}{\sqrt{1/n}}$
Angular acceleration	$\ddot{\theta}' = \dfrac{\ddot{\theta}}{1/n}$

The first approach is making the test without changing the normal gravitational field. The consequence will be the error in the vertical acceleration. One can accept the errors of the incorrect gravitational acceleration in the test results, or apply a correction factor in order to compensate the errors in the acceleration. If the error is just accepted, it must be remembered that the constant error in the vertical acceleration results in linearly growing error in the vertical velocity and quadratically growing error in the vertical position of the store model relative to the aircraft. The correction factor should be applied in order to increase the ejection forces to compensate the lack of gravitational acceleration. Then the sum of the ejection acceleration and gravitational acceleration can model the gravitational acceleration that should be in the test environment.

In the second approach, during the store separation, the aircraft model accelerated upwards at a desired value. This method is used by the British Aerospace (BAE), [28]. For example, for a 1/30 scaled model at the store separation period, the acceleration applied on the aircraft model will be 29g and with the 1g gravitational acceleration acting on the model. Therefore, the separation takes place with the resultant value of 30g. The third approach is to apply a magnetic field on the test environment, which is difficult to achieve and not very cost effective.

After analyzing all three scaling methods, the “Light” Mach Scaling method is selected as the most applicable one. The results of this scaling method are given in the following tables.

Table 17 – Original Store Properties

Mass, [kg]		941.2
Mass Moment of Inertia, [kg.mm^2]	I_X	26539161
	I_Y	587473500
	I_Z	587705249

Table 18 – Store Model Properties

Mass, [kg]	$m' = 941.2\left(\frac{1}{8}\right)^3 = 1.8$
Mass Moment of Inertia, [kg.mm^2]	$I'_X = I_X\left(\frac{1}{8}\right)^5 = 26539161\left(\frac{1}{8}\right)^5 = 810$ $I'_Y = I_Y\left(\frac{1}{8}\right)^5 = 587473500\left(\frac{1}{8}\right)^5 = 17928$ $I'_Z = I_Z\left(\frac{1}{8}\right)^5 = 587705250\left(\frac{1}{8}\right)^5 = 17935$
Ejection Force, [N]	$F'_E = F_E\left(\frac{1}{8}\right)^2$
Time, [s]	$t' = t\sqrt{\frac{1}{8}}$
Mach Number	$M'_\infty = M_\infty$
Gravitational Acceleration	$g' = g$

Ejection Force

The release mechanism on the pylons is actuated by pyrotechnics. After the locks are opened, store needs to be pushed away from the aircraft in order to make sure that the safe separation of the store occurs. This is accomplished with two pistons that hit and push the store between the suspension lugs. These pistons are actuated with the gas generated by the explosion of the pyrotechnics. The piston initial positions are set in order to touch the store so the impact is minimized and energy transfer is maximized.

According to the working principle of the mechanism, there are two pyrotechnics used on the pylon. Considering the weight of the store, the suitable and pre-tested pyrotechnics is selected. Between the pyrotechnics and the piston, an appropriate orifice is used to arrange the pressure exposed on to the piston.

In the application of the chosen scaling model to the ejection force, first the one that is used on the full scale store must be determined. The pyrotechnics and the orifices of the full scale store are tested and the results of the tests are given in Figure 39 to Figure 42. After selecting the ejection forces, similitude is applied according to the maximum values. These tests are performed with two different orifices. The sample orifices are numbered with 3 and 4.

The maximum force values of the ejection force tests are given in the Table 19. According to these results, for the store separation test, tests no.5 and no.7 are come out to be suitable to simulate the real ejection forces.

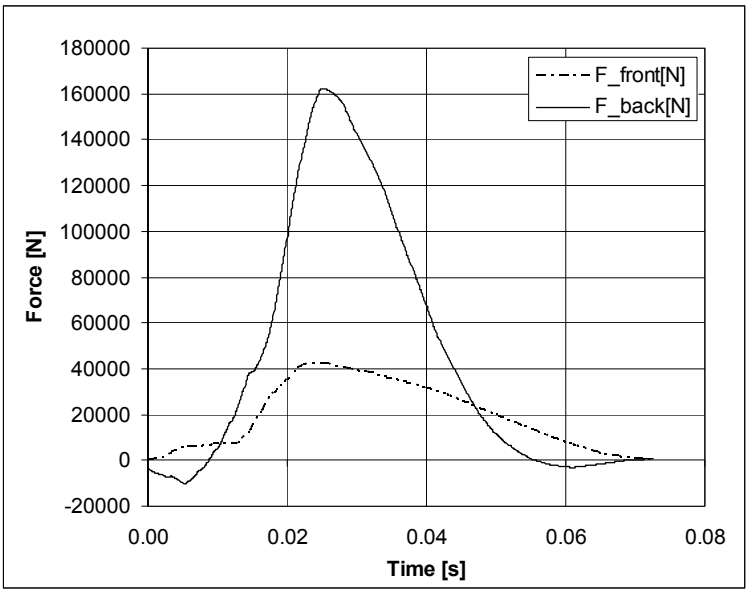

Figure 39 – Ejection Force Test No.2 (3-3)

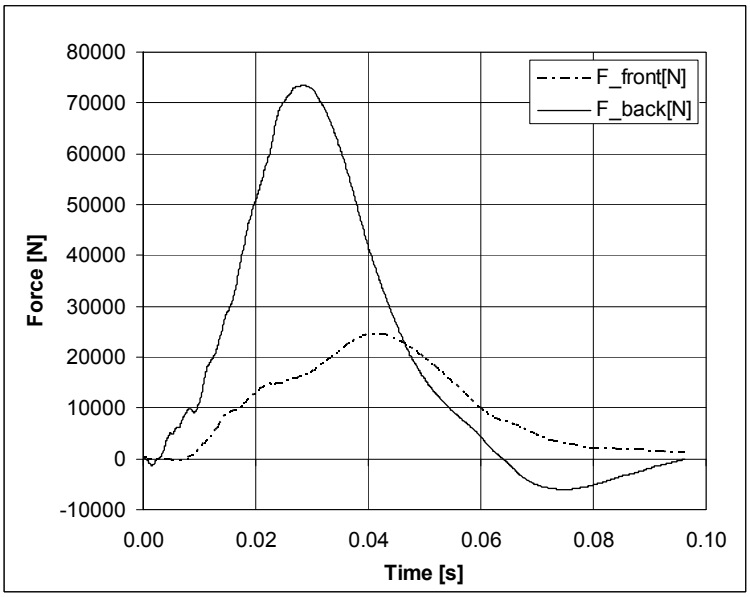

Figure 40 – Ejection Force Test No.5 (3-3)

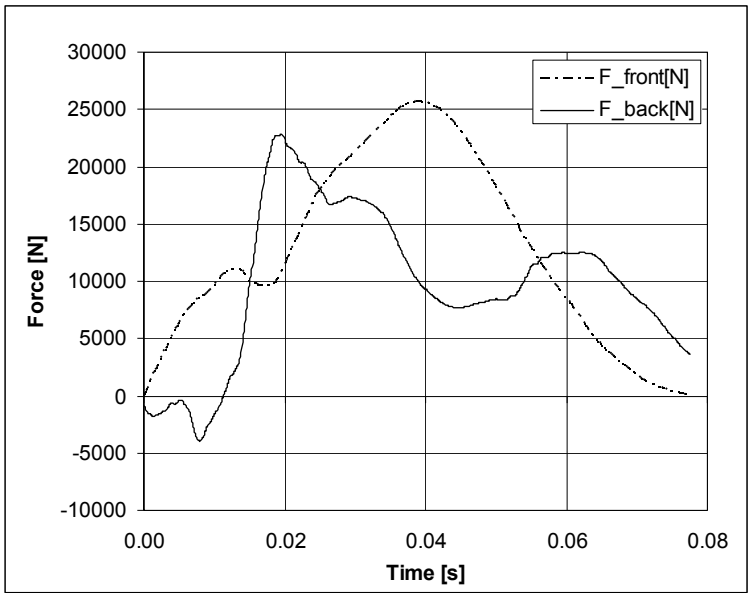

Figure 41 – Ejection Force Test No.4 (4-4)

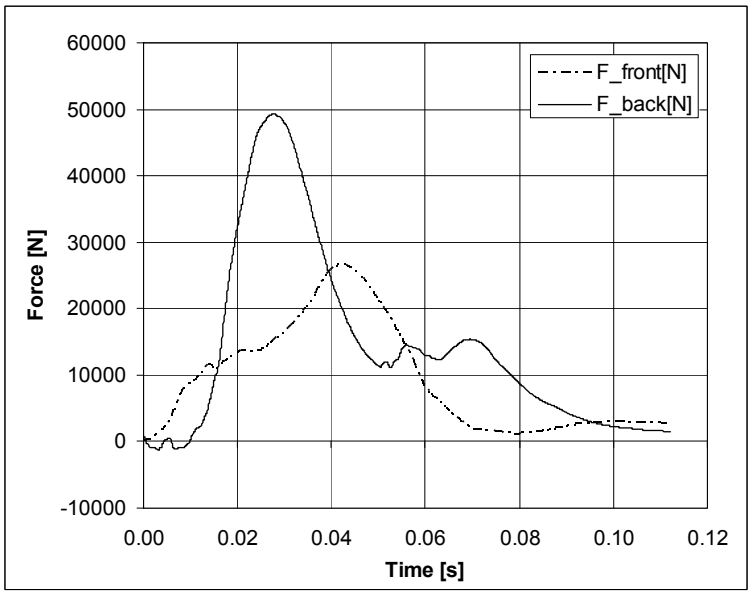

Figure 42 - Ejection Force Test No.7 (4-4)

Table 19 – Maximum Values for the Orifices 3-3 and 4-4

Test No.	Orifice	Front (N)	Back (N)
2	3-3	42265	162410
5	3-3	24570	73480
4	4-4	25685	22806
7	4-4	26595	49402

The results of the test no.5 and no.7 are applied to similitude for both force and time point of view and they are scaled according to the “Light” Mach Scaling method. The similitude results are given in Figure 43 and Figure 44. The application duration for both full and scaled piston ejection forces are given in Table 20.

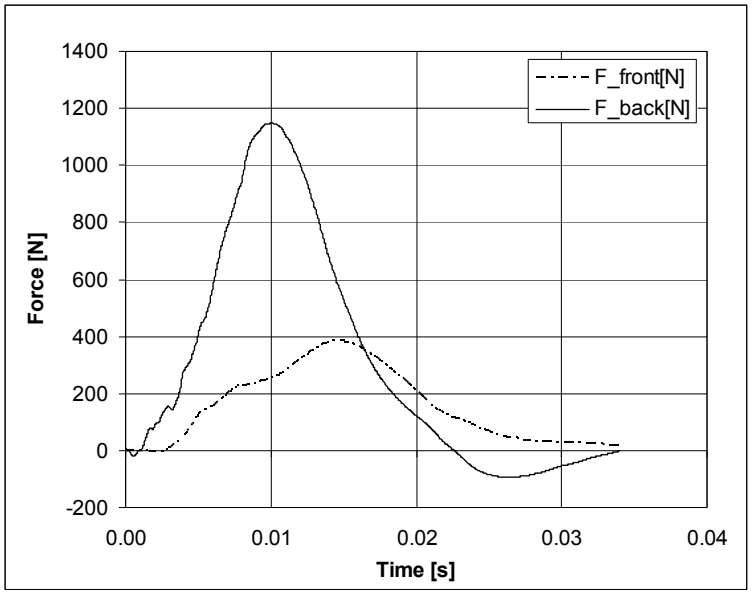

Figure 43 – Scaled Results of Test No.5 (3-3)

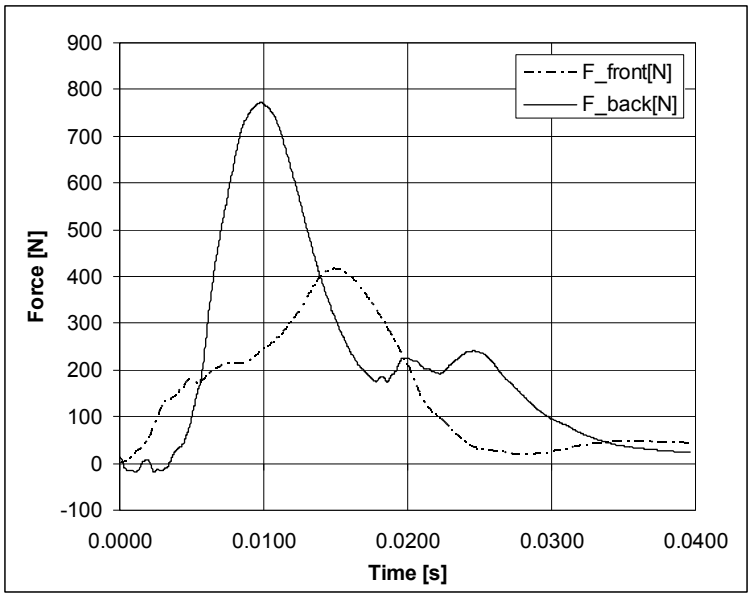

Figure 44 – Scaled Results of Test No.7 (4-4)

Table 20 – Application durations of the Ejection Forces

Test and Orifice no.	Time, [s]	Scaled time, [s]
Test No.5 (3-3)	0.0962	0.0340
Test No.7 (4-4)	0.1121	0.0396

In the store separation tests, the similitude must be applied in both to the force and to the time for the ejection process. However, mechanically, this is difficult to realize. It is a good assumption that reducing these two variables into one by applying the similitude to the impact, which is calculated with, force and time. The impacts are obtained by simply numerically calculating the area under the force-time graphs. With the help of MATLAB® Curve Fitting Toolbox, the data are curve fitted and the area under this curve is

calculated by numerical integration. The results for the impacts are given in Table 21.

Table 21 – Impulse Results of the Scaled Ejection Forces

Piston	Impulse [N.s]	Average Impulse [N.s]
Back Piston Test No.5 (3-3)	11.04	7.89
Front Piston Test No.5 (3-3)	4.73	
Back Piston Test No.7 (4-4)	8.87	7.34
Front Piston Test No. 7 (4-4)	5.82	

2.3.2. Aircraft Model

The aircraft used in the certification tests is a scaled model of test aircraft. In the market, the available largest scale for test aircraft is 1/8. This model is supplied with a radio controlled turbojet engine but as explained in the 2.1.3, it is not possible to reach the desired velocities with this engine.

Occupied model is obtained as a shell without the jet motor and it is made of composite material. Besides, of being light, it is not capable to withstand the launch acceleration. In order to withstand the launch accelerations it must not only be light but also strong enough. As to obtain a model with these properties, application of the composite materials is suitable with extra strengthening.

The dimensions of model aircraft should be verified that it is at 1/8 scale of the original aircraft. Model is measured in Coordinate Measuring Machine, CMM and shown that it has the correct dimensions.

To duplicate a model that can handle the launch requirements from the readily bought model is the final decision about model aircraft. The external geometry is duplicated but the inner structure is built up according to give enough strength for the tests. In this stage, there appeared a need of composite material production skill, which is not included within the capabilities of TUBITAK-SAGE. By working together with another company, which is specialized in the composite material manufacturing, it is concluded that it is possible to build a model having required strength for the tests. In the assembly process of the new composite model aircraft, the sting also assembled to the composite with a metal plate embedded in the model aircraft. The picture of the composite model aircraft is shown in Figure 45. A sketch of the aircraft model with basic dimensions is given in Figure 46. The dimensions on this figure are in millimeters.

Figure 45 – A View of Composite Test Aircraft Model with Sting

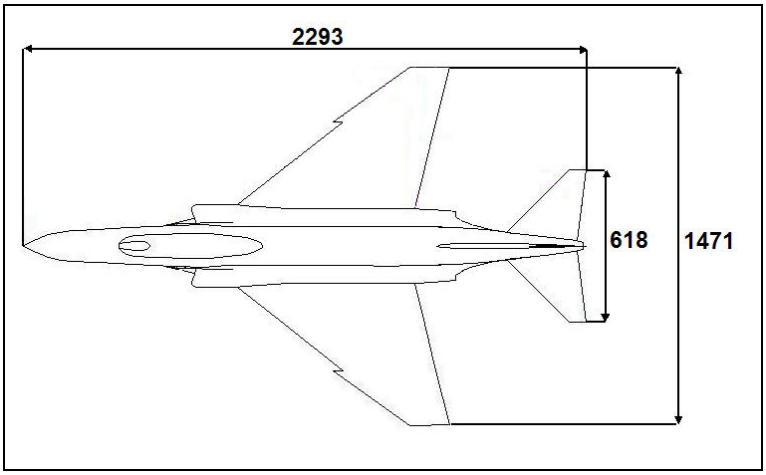

Figure 46 – Sketch of Aircraft Model

2.3.3. Store Model

The store model properties are calculated in the similitude section and given in Table 18. The store model has constrains for mass, moment of inertial and center of mass location. These three constraints must be satisfied. The solid model of store model is shown in Figure 47. Additional to the inertial properties, the center of mass is also need to be scaled properly with respect to the original store. The distance of the center of mass from the nose is 1623 mm for the original store. Therefore, for the store model this value is 203 mm according to the scaling factor.

In order to satisfy the requirements for center of gravity and inertial properties at the same time, store model is made of steel and aluminum parts that have drilled holes along the longitudinal axis. This problem is solved by using the code in [26].

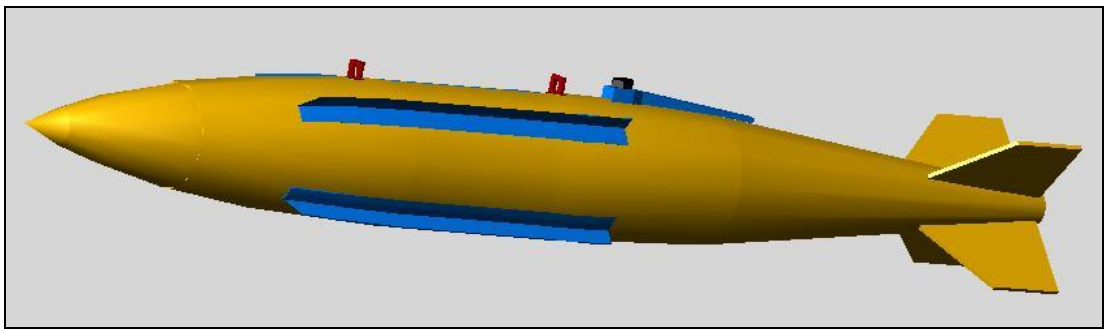

Figure 47 – Solid Model of Store Model

2.3.4. Pylon Model

The aircrafts issue the pylons to carry the external stores under their wings and body. In test aircraft, there are nine pylon places under the wings and the body. These places are shown in the Figure 48 with their numbers. The numbers are given as ascending order from left to right when looked through the bottom of the aircraft.

In general, the functions of the pylons of the aircrafts are first, to carry the store safely to the desired location or to carry it for whole flight duration, which is so called the captive flight. If the pilot wanted to separate the store for any reason, like to drop the munition to a target or like to make a jettison, which means to drop the store in the case of emergency, the pylon must release the store safely with the command of the pilot, which is usually the firing signal to that particular pylon. Each store is certified to a certain pylon and the store that is used in this particular test is certified to the pylons number 1 and 9 whose locations are shown in Figure 48. The pylon on the test aircraft is shown in Figure 49.

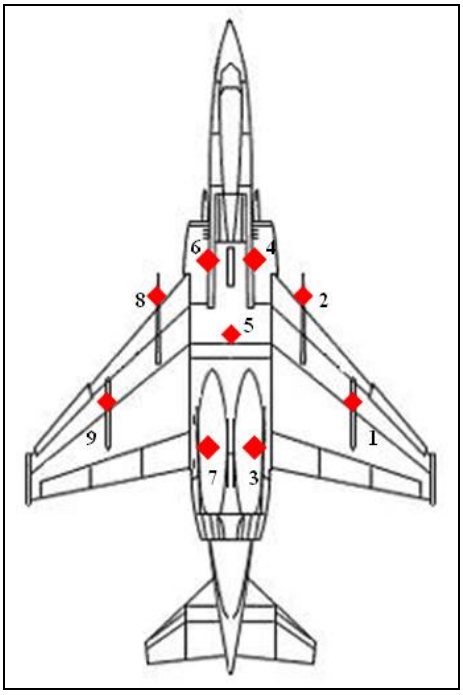

Figure 48 – Pylon Places and Numbers

In the Figure 50, the store can be seen just before being fixed to the pylon and as mentioned before, the store is fixed to the pylon from its suspension lugs. In the same figure, the suspension lugs and the sway braces are indicated. When the suspension lugs are inserted their particular places, pylon locks, which are activated with one mechanism, enter into the lugs simultaneously when the operator turns an inserted key. After the locking operation, the store needs to be fixed with the help of sway braces. This must be done to make sure that the store will not move and will not be affected by any vibrations coming from the body and also when exposed to the excitations of the aerodynamic flow, aircraft will not be affected by the vibration coming from the store. There are four sway braces on a pylon and they are fixed to a predefined state, which defines the force exerted on to the

store. The sway braces are pressing on to the store and pushing away the store whiles the lugs holding it, so the fixing is done.

Figure 49 – A View of Pylon of the Test Aircraft

Pylon Model Design

In the design of the scaled model of the test aircraft pylon, the design criteria are the main functions of the original pylon. The three main functions of the pylon model which are first to lock the store model and carry it safely, second, it can be triggered at a predefined location on the range and third is to eject the store model at desired conditions. The sway braces are also considered in the model. Additional to the original pylon, the pylon model should withstand to the launch accelerations of separation tests.

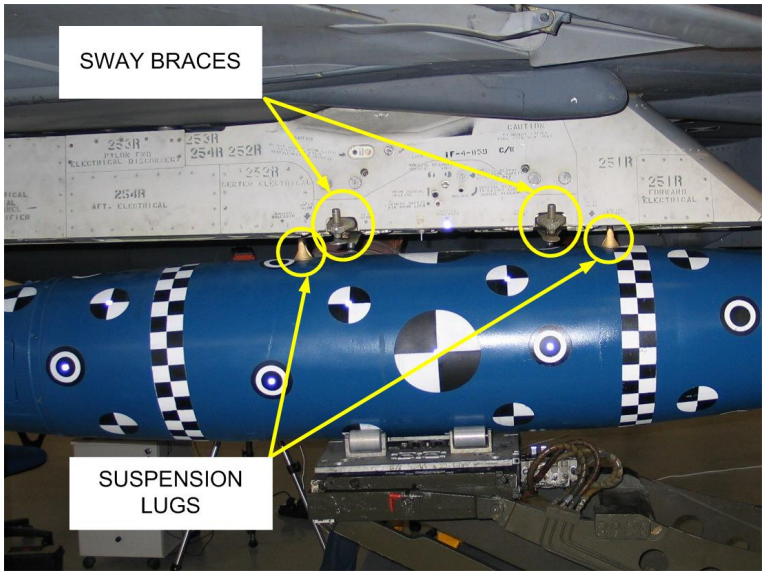

Figure 50 – A View of Store and Pylon

Besides of the functional requirements for the pylon, there are also the geometric constraints that are the results of the similitude application According to the scale ratio of the aircraft model, it must have the same ratio. In Figure 51, the shell for the scaled model is shown.

All dimensions are equally scaled down for the store model. The outer dimensions are the most critical because of the aerodynamics and the flow around the pylon model. Other than the outer dimensions, the ones, which are defining the position of the store model with respect to the pylon, are also critical. These are the places where the suspension lugs are fitted and are locked and they are shown in Figure 51. On the other hand, working principle of the pylon is completely different from the original one. There must be a mechanism or mechanisms that can handle all that mentioned functions. The primary constraint for these mechanisms is the geometry.

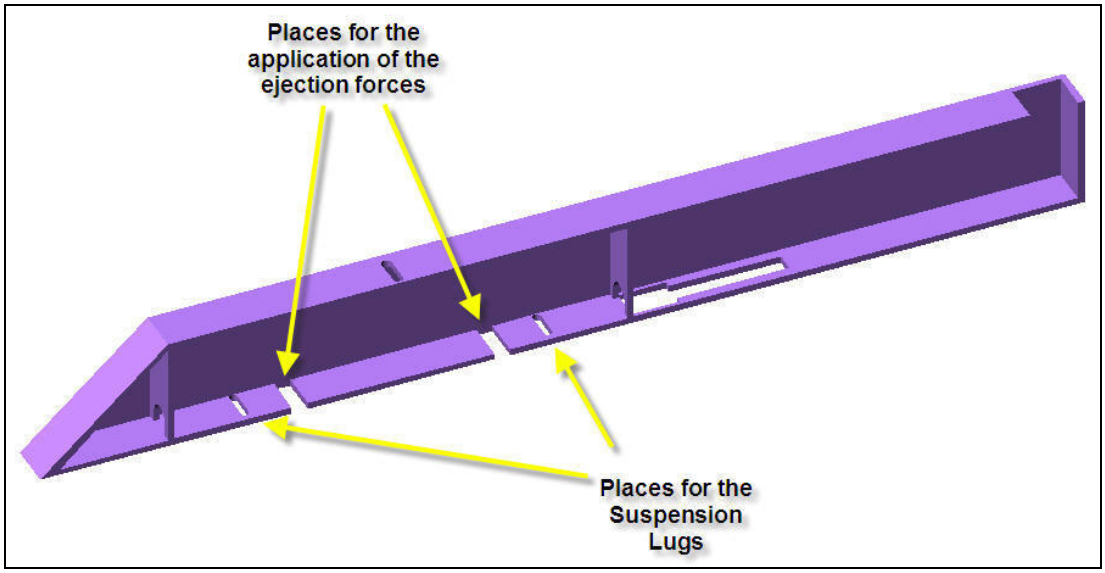

Figure 51 – A View of Shell of the Pylon Model

The thickness, length and width of the model are scaled according to the similitude. However, because of the ease of manufacturing issues, the aft section and the front surface are made flat. The width of the aft section is kept constant and the front surface of the pylon has edges and is not rounded. In the Figure 49 and Figure 50, these surfaces can be observed.

Description of Ejection and Locking Mechanism

There must be a model of the original locking mechanism inside the pylon in order to constraint the motion of the store model. In the conceptual design, it is thought that, a pin can pass through the suspension lugs. By this way with the help of the pin and the model pylon body, the motion of the store model will be constrained except the rotation along the pin axis and this motion will be constrained with the help of the sway braces. The main requirement for this mechanism is synchronization of the pins with each other in order to

release both suspension lugs at the same time. It is critical because at high speeds a small time gap between the openings of the locks can cause failure of the separation.

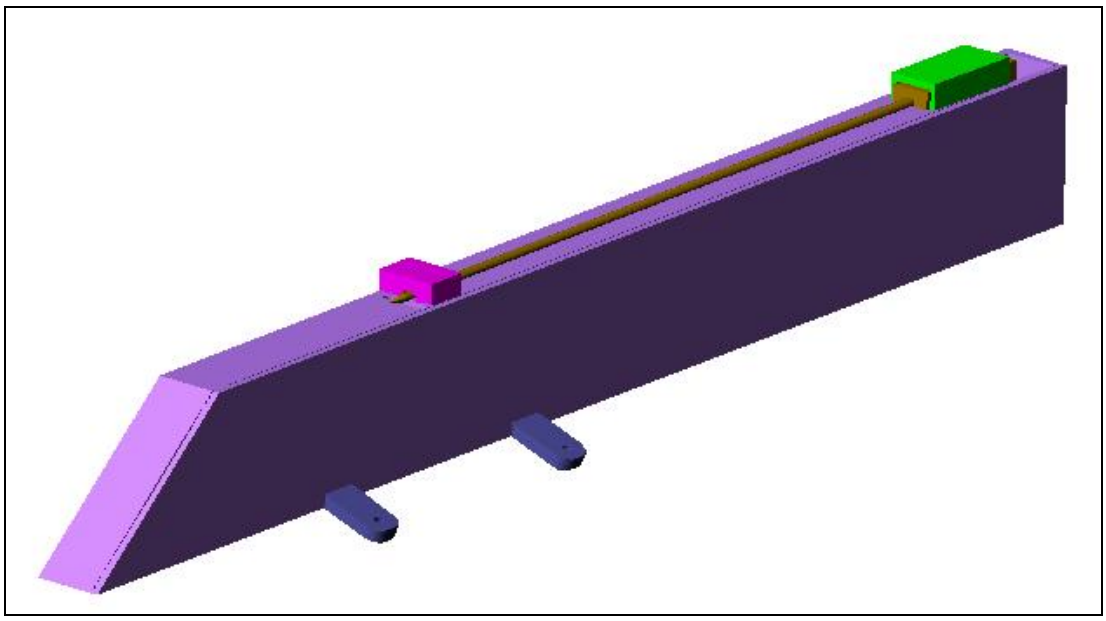

Figure 52 – A View of Solid Model of Pylon Model

Besides the locking mechanism, an ejection mechanism is required to apply the ejection forces, which are calculated in the similitude study. The primary requirement for this mechanism is the geometry. It is supposed to work within the allowed regions, which is defined as the inside of the pylon model. Then the ejection forces must be applied right after the pins are cleared off the suspension lugs, otherwise the consequence would be a self-locked mechanism.

The last mechanism required within the pylon model is an activation system. The activation must be performed at a predetermined location, which is

calculated with the simulation model in the chapter 2.2.1. There should be a trigger system to activate the mechanism.

For each mechanism, first, the requirements are determined and then the conceptual designs are completed. For the locking mechanism, since the synchronization is important, the pins are better opened with same mechanism. In the case of two different mechanisms, the actuation systems should be identical and in manufacturing point of view, it is practically not possible to actuate at the same time and with the same applied force, if there is a significant small time gap. Similarly the timing between opening the locks and ejecting the store model is critical. The ejection force must be applied right after the locks are opened and again there occurs a critical synchronization problem.

After considering different mechanism alternatives, it is concluded that if it is possible to make a single mechanism, which can handle the requirements of both locking and ejection mechanism at the same time, and also unlocks the pins, then this mechanism should be used in the pylon model. Due to very strict geometrical constrains multi-functional mechanism is the best solution.

It is decided to use two vertical sliders as the locking mechanism. With the mechanism that is shown in the Figure 53, the two pins are the bodies moving horizontal and the problem of synchronization between pins is no longer an issue.

This kind of mechanism also has the advantage of compensating the synchronization problem between the locking and ejection mechanism, if the ejection can be performed with this particular system.

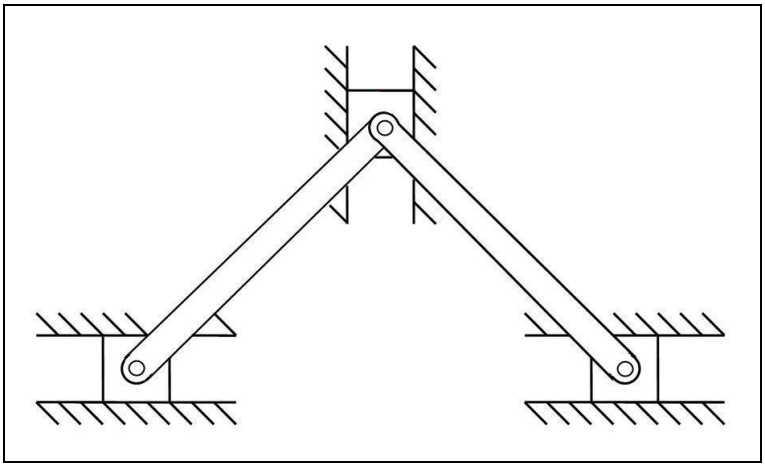

Figure 53 – Two Vertical Slider Mechanisms

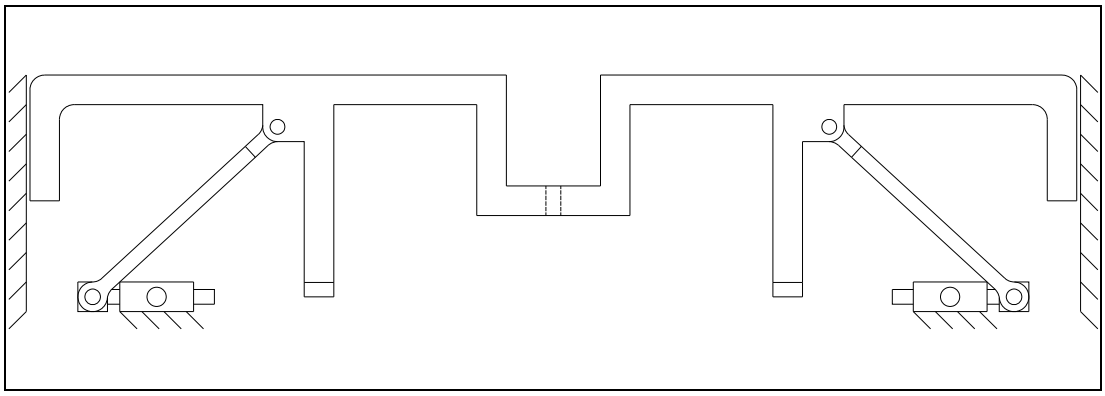

Figure 54 – 2D Scheme of the mechanism

It is decided to add the ejection pusher to the vertical moving body, which is so called main body. The pushers are the scaled models of the pistons on the real pylon. It is possible to push the store model away from the pylon model, right after the locks of the suspension lugs are opened, by adjusting the length of the pushers. By using a single mechanism, the locking, releasing and ejecting procedures are accomplished. The advantages of

single mechanism are; first, there is no synchronization problem and second highly reliability mechanism is obtained. After completing design, the conclusion for the mechanism is shown in Figure 55. The technical drawings of the parts of the mechanism are given in Appendix C.

As it can be seen from above figure, a compression spring is used to actuate the system so the external force is provided with this spring. The usage of the springs for separation at high velocities is discussed in [12]. In the next step, an appropriate spring should be selected so that the required impulse, which is calculated in the section of similitude study about the ejection force, can be exerted to the store model.

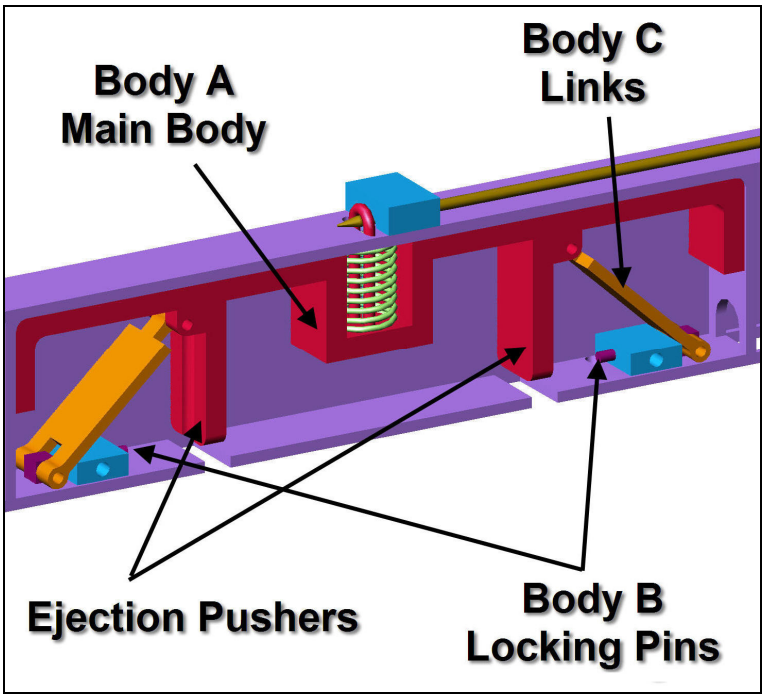

Figure 55 – A View of Mechanism and the Bodies

The motion of body A, which is indicated in the Figure 55, is analyzed. The average impulse that will be applied to the store model is approximately 7.6 N.s.

As explained in the section 2.3.1, the first approach for the error compensation in “Light” Mach scaling, is to apply a correction factor in order to increase the ejection forces so as to compensate the lack of gravitational acceleration and the sum of the ejection acceleration and gravitational acceleration can model the gravitational acceleration that should be in the test environment. Since the scale is 1/8 because of the readily bought aircraft model from the market, the gravitational field should be “8g” so an extra “7g” is needed.

The place, where spring is working within the pylon model, is shown in Figure 55. The corresponding dimensions are also given in Appendix C. According to the similitude study results, an appropriate spring is selected. The stiffness of the spring is 9500 N.m.

Description of Trigger Mechanism

Besides ejection mechanism, a trigger mechanism is needed for ejection process. At the predetermined location on the sled range, the ejection mechanism should be triggered and this is also critical like the synchronization problem of the lock and ejection mechanism. Another reason for a precise trigger timing of the store model is to make a correct placement for the imaging system in the test area. The details for these imaging systems are given in the Chapter 3.1.

The aim of the trigger system is to release the spring at this particular location. The trigger mechanism is composed of a pyrotechnic system and a slider mechanism. The ejection mechanism is locked with a pin inserted into a U shape piece that is placed inside of the spring and is fixed on the main body. This pin holds the mechanism at the starting position until the separation location is reached. Pin is attached to a slider joint so when the pyrotechnic is fired, the pin goes back relative to the main body and clears off the spring. In Figure 57, the components are shown.,

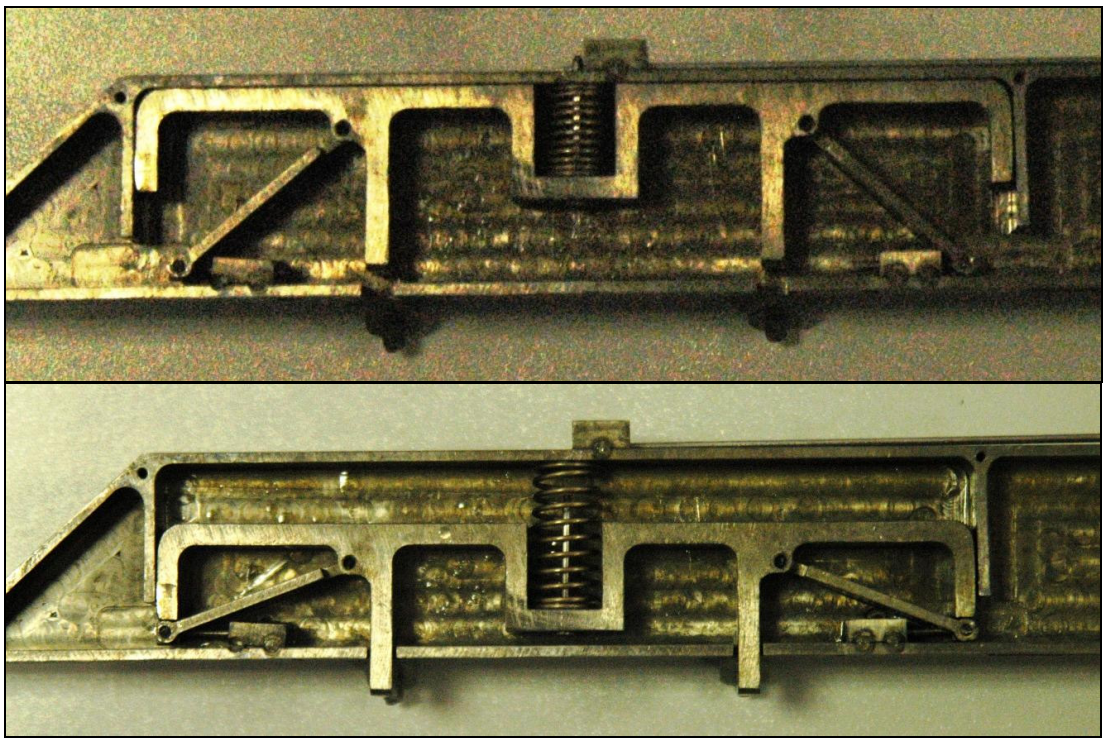

Figure 56 – Pylon Model Mechanism at the Initial and Final Positions

The second important point for this mechanism is how the pyrotechnic is fired. When the power is supplied to the pyrotechnic system, the primary igniter burns first, so a chain reaction series begin. The aim of using this

igniter is to ignite the black powder in order to accelerate the metal piece. As the power applied, the metal piece leaves the system at a certain velocity. The mentioned parts of the pyrotechnic system are shown in Figure 58.

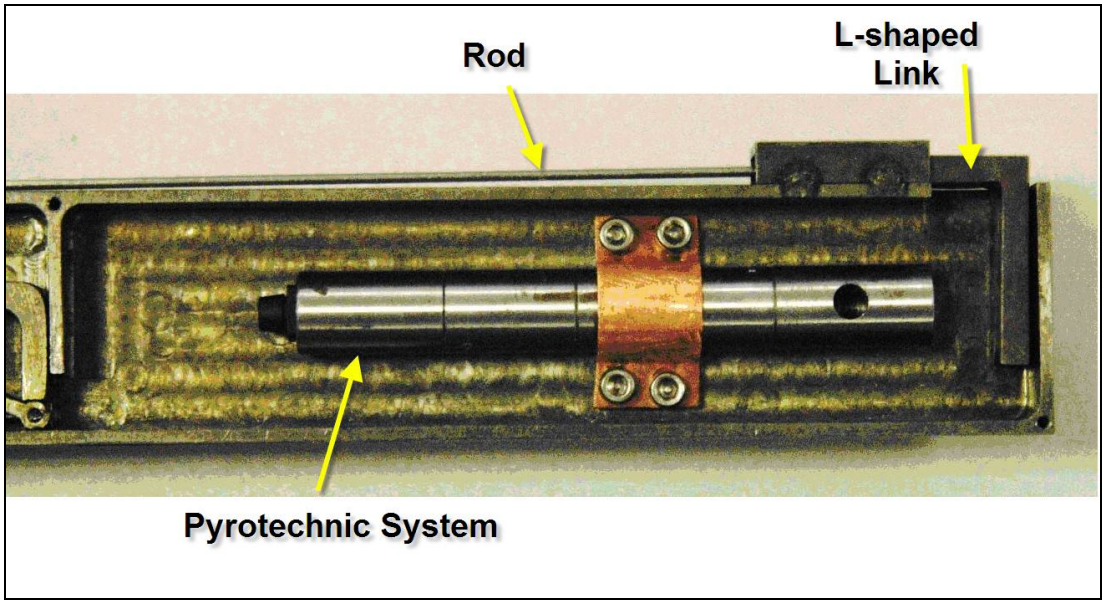

Figure 57 – Trigger Mechanism Components

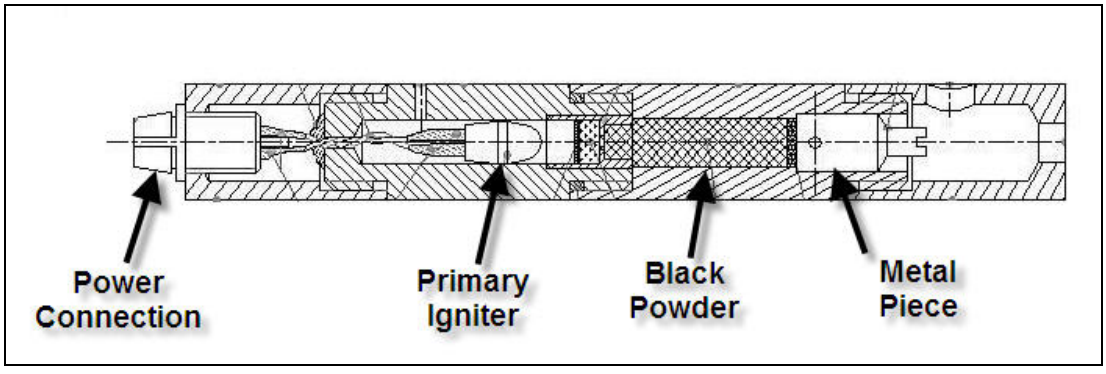

Figure 58 – Pyrotechnic System Components

The pyrotechnic system completes its duty with this high velocity metal piece, which hits to the L-shaped connected to the rod. The slider connection that houses the L-shaped link causes this part to move backwards with respect to the pylon, so the rod gets out from the U-shaped part of the main body.

The power to ignite this system at the desired location is accomplished by an electronic card whose design is beyond the scope of this thesis. A wire is connected to this card at both ends and when this wire is cut, the required voltage difference is applied to the pyrotechnic system. Wire is placed through the shafts of horizontal bearings and in order to cut the wire, a metal sheet is welded to the rail where the triggering of the separation process is decided to locate.

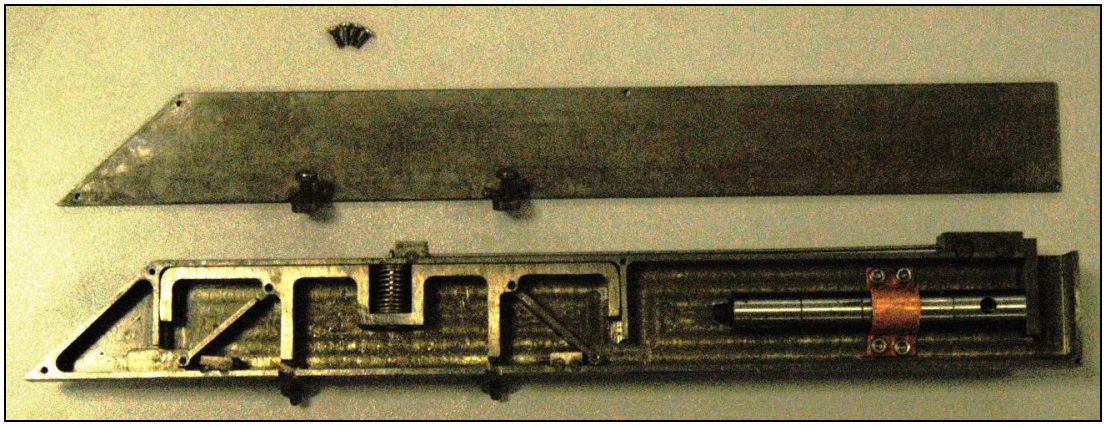

Figure 59 – A View of Pylon Model

2.3.5. Wing Model

Some tests are performed using wing model besides of aircraft model. In the literature, within some applications, the wing model is used instead of aircraft model, [5]. As explained in the section 2.3.2, the aircraft model is used and it works well for the low subsonic velocities but when the test velocity is increased, the model aircraft start fluttering and catastrophic failure is unavoidable.

It is concluded that the aircraft body needs be rigid enough to avoid the flutter effects. The mass of the wing is increased and this failure possibility can be minimized when the wings are made from solid metal. It is decided to use only a single bulk wing model and just accepting the aerodynamic flow error coming from the absence of the aircraft model body, which is negligible, [5]. On the other hand, the reliability of the test will increase because obtaining the results without having a flutter failure is approximately guarantied. The wing is manufactured from aluminum 7075 T6 in the CNC machine and shown in Figure 61.

The mounting to the carriage is performed with the help of bolts. In the assembly of the wing model and the vehicle, the important part is the position of the wing model with respect to the ground. In the full scale aircraft, the root profile of the wing has a 1° angle of attack position with respect to the horizontal so the same angle is kept while placing the wing model. The assembly of the pylon model to the wing is also performed with bolts and the placement is made with the scaled dimensions of the original store placement.

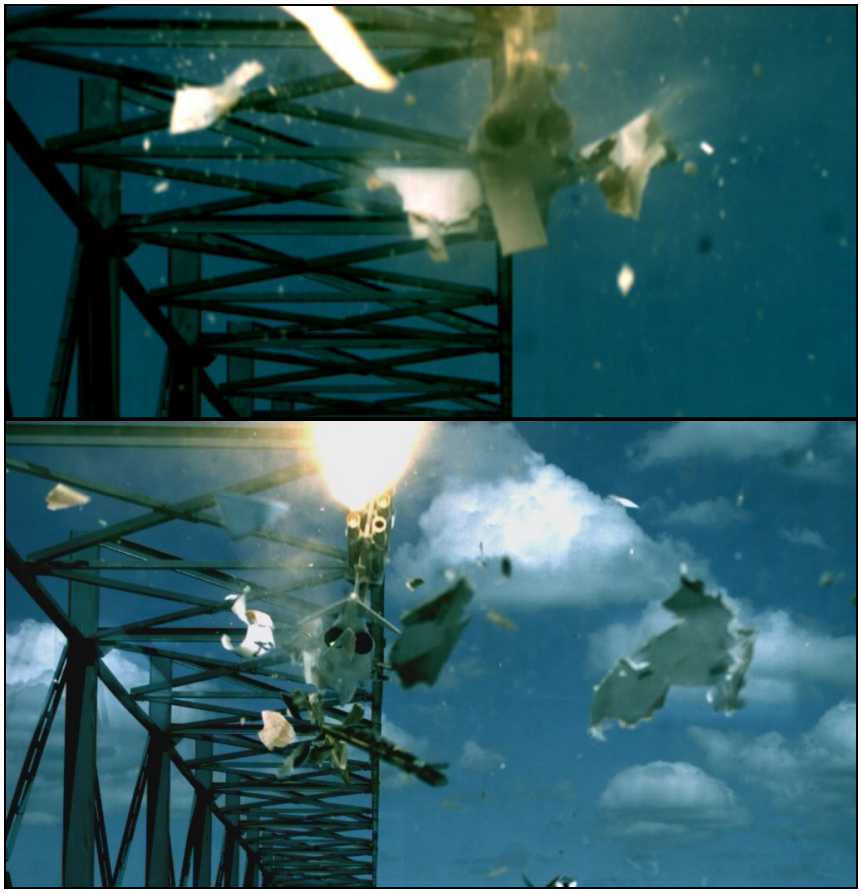

Figure 60 – A View of Failure of the Composite Aircraft Model

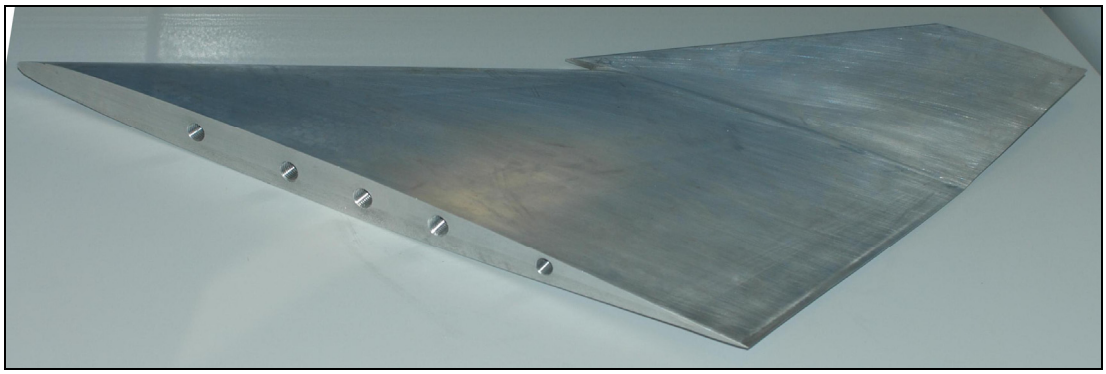

Figure 61 – A View of 1/8 Scaled Aircraft Wing

2.4. CARRIAGE ACCELERATION SYSTEM

The test vehicle must reach the required separation velocity within a predetermined location so the vehicle is required to be accelerated up to the separation velocity just to complete its acceleration before the separation location.

The acceleration of the test vehicle can be performed with different methods. Some of these alternatives for acceleration process are solid propellant rocket engine, liquid propellant rocket engine, a rail with magnetic field like high speed trains and a catapult that exerts stored potential energy.
In application point of view, the most feasible ones among the acceleration methods are solid propellant rocket engine and liquid propellant rocket engine. Other methods requires large amount of initial costs, on the other hand rocket systems are much cheaper.

Analyses and studies are completed for the liquid propellant rocket engines and according to the test requirements, a system is designed and constructed, [39]. The system works with fuel and burner, which are stored in pressure vessels under a certain pressure. Both of them enter to the burning chamber and exit from the nozzle of this chamber.

This system has advantages like, fuel and burner mass flow rates can be controlled with the help of the servo valves during the burning process, which gives the chance to modify the thrust. If there is another nozzle in the opposite or in any directions, the flow can be converted into the desired nozzle and this can be used as a deceleration system. Except these advantages, the necessary pressure value for the fuel can be provided with very thick walled pressure vessels so the weight problem is induced. These

vessels weigh more than the vehicle itself. With this weight, the simulations are performed and concluded that it is not possible to achieve the desired acceleration values with liquid rocket engines.

As the other choices are eliminated, the best solution turns out to be the solid propellant rocket engine. Solid rockets are easy to use in practice and after fixing them, application of voltage is enough for the tests. However, it is a problem that the process is open loop and cannot be controlled. After activating the solid rocket, it is not possible to stop the reaction within the rocket and additionally it is hard to design a new rocket engine to satisfy the requirements, which needs too much time and investment.

2.4.1. Thrust Analysis

The primary requirement of the acceleration system is to complete the acceleration within the first 150 meters of the 300 meters range. After the burning process is finished, there is no acceleration acting on the setup except the acceleration due the friction, which is neglected. This condition is required because original store is released from the test aircraft at a constant velocity.

The available rocket engines and their thrust data are analyzed by using the dynamic simulation tool, which is explained in details in Chapter 2.2.1. The velocity results are checked if they can reach the desired velocity and then if it is satisfied, the position will be checked whether the maximum velocity is reached within the first 150 meters. The available rocket engines belong to the rockets R1, R2, R3, R4, R5 and R6. The necessary variables of these rocket engines for the simulation are given in Table 22.

Table 22 – Properties of the Rocket Engines

	Mass [kg]	Consumable mass [kg]	Burn time [s]
R1	202	125	6.6
R2	40	20	1.8
R3	80	20	4.5
R4	80	21	0.6
R5	9.6	2.8	1.4
R6	11.2	3	1.2

According to the velocity results R1, R2, R3 and R4 are reaching to the desired velocities but the accelerations are not high enough to reach the maximum velocity within the first half of the rail. The single R5 and R6 thrusts are simulated and the following results are obtained.

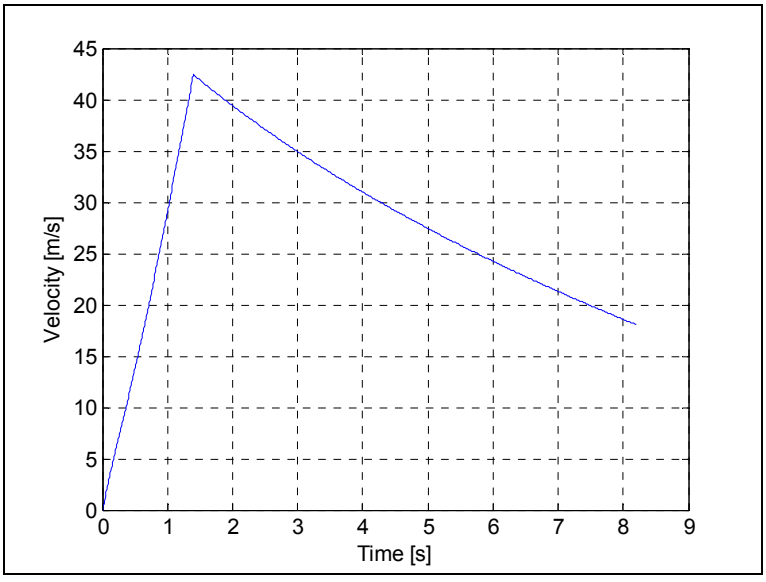

Figure 62 – Velocity vs. Time Plot of Single R5 Rocket Engine

The benefit of the R5 is the multiple usages. They can be mounted to the vehicle in parallel and higher velocities can be obtained. The alternative rocket engine is the R6 with a higher mass and higher thrust value than R5. According to the results, the R5 and R6 are suitable in order to use in the tests. The advantage of these rocket engines are the maximum velocity can be arranged with the number of the rocket engines used.

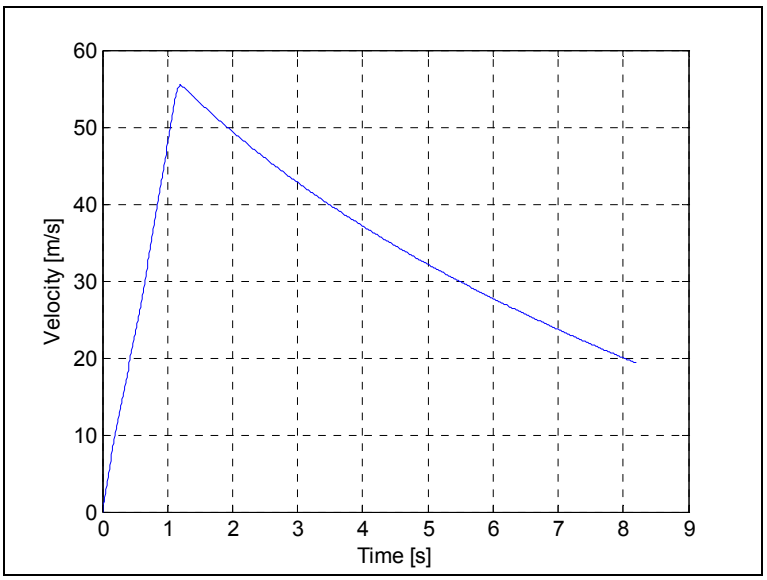

Figure 63 – Velocity vs. Time Plot of Single R6 Rocket Engine

2.5. DECELERATION SYSTEM OF THE CARRIAGE

With a deceleration system, the setup can be recovered and reused after each test, so that the cost would be lowered significantly and consumed time to manufacture a new setup would be saved.

After starting to the test by firing the rocket engines, the setup is accelerated, by the rocket engines burnout, the store is separated and then it is time to decelerate the setup.

Figure 64 – R5 Installed on Conceptual Carriage

The system should be cost effective and easy to apply. There are some methods like the catapult system on the aircraft ship that are used to catch the landing aircrafts, but such systems are very expensive. The alternative methods are listed below, each of them is analyzed, and the expected results are given.

In these analyses, it is considered that the mass of the moving body is 100 kg, and the maximum velocity is 150 m/s while the store is released. The speed of sound is assumed to be 337 m/s at Ankara. After separation of the store model from the aircraft model, approximately 1/3 of the rail is left which

means 100 meters. So within this distance the carriage need to be stopped which means

2.5.1. Energy Dissipation by Plastic Deformation of Metal Pieces

The main idea is to place an array of metal pieces on the rail and let the vehicle hit and plastically deforms these metal pieces in order to dissipate some energy at each impact.
First, the energy to deform a single specimen must be known. The Charpy impact test measures the energy absorbed by the high strain rate fracture of a standard notched specimen. The results of these tests are used to estimate the number of the metal pieces that should placed on the test range. In [40], for low carbon steel at temperatures around 20°C, the value is given as 140 J. Since the pieces will be without a notch, and will be higher than the standard test specimen, an approximation is made and 200 J is taken as impact energy for low carbon steel pieces.

The vehicle at a velocity of 150 m/s and a mass of 100 kg, has a kinetic energy of

$$T = \frac{1}{2} m V^2 = \frac{1}{2} \cdot 100 \cdot 150^2 = 1125000\ J = 1125\ kJ \qquad (10)$$

In order to dissipate this energy 5625 metal pieces are needed.

2.5.2. Mass Addition to the Carriage

After the separation of the store, increasing the mass of the system with additional mass can help to decelerate the system. Simply, the idea is to transfer a portion of the kinetic energy to a vehicle that is placed on the rail. The vehicles are supposed to move together, so that the total kinetic energy of test vehicle is shared.

In the equation given below, the total kinetic energy is calculated. This means 150 m/s will reduce to 106 m/s, right after test vehicle hits and moves together with the stationary vehicle. With the addition of a third stationary vehicle, they will slow down to 75 m/s.

$$\begin{aligned} T_{initial} &= T_{final} \\ \frac{1}{2} m V_i^2 &= \frac{1}{2}(m+m) V_f^2 \\ V_f &= \frac{V_i}{\sqrt{2}} \end{aligned} \tag{11}$$

The primary constraint in this application is the impact forces. To handle the excessive impact forces, the application of a spring between the vehicles is considered. A simple sketch is given in Figure 65. The equations of motion for the two bodies are:

$$\begin{aligned} m_1\ddot{x}_1 + c(\dot{x}_1 - \dot{x}_2) + k(x_1 - x_2) &= 0 \\ m_2\ddot{x}_2 - c(\dot{x}_1 - \dot{x}_2) - k(x_1 - x_2) &= -f_s \end{aligned} \tag{12}$$

The damping is structural and it is not taken into consideration. The parameters m_1, m_2, k, and f_s between carriage and rail are the constants for

this model. The masses, m_1 and m_2 are both 100 kg and the initial conditions are given below.

$$x_1 = 0 \ , \ \dot{x}_1 = 150 m/s$$
$$x_2 = 0 \ , \ \dot{x}_2 = 0 \qquad (13)$$

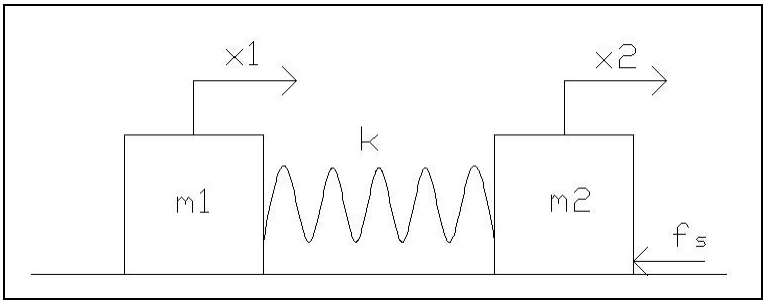

Figure 65 – Two Masses and a Spring System

The friction force is taken as 3000 N as obtained from the simulation. According to these inputs, the equations are solved for different values of spring constant and the results are given in Table 23.

2.5.3. Increasing the Drag of the Carriage

Increasing the drag of the carriage is one of the possible slow-down applications. After the separation occurs, it is planned to increase the drag force and simply to increase the drag coefficient. This can be performed by increasing the wet area across the flow. The most common and practical way is using a parachute.

Table 23 – Simulation Results for Different Spring Constant Values

k [N/m]	Max(x1-x2) [m]	Reaction Force [N]
1000	57.4	57400
5000	25.3	126500
10000	17.8	178000
100000	5.6	560000

In the test aircraft, parachute is utilized when a short range is required for the landing process. These parachutes are investigated and scaled models of these parachutes are obtained. The cone diameter of the scaled parachutes is 1 meter. This value is decided according to the distance between the aircraft model and the rail. The ropes of the parachutes are also extra strengthened. These parachutes are exposed to wind tunnel tests at “Ankara Wind Tunnel”. The parachute is attached to a dynamometer, and then it is exposed to different wind speeds while the forces on the dynamometer are measured. At the result for some certain Mach numbers, the drag coefficient of the parachute is obtained. In the Figure 66 and Figure 67, the setup for the measurement of the drag in “Ankara Wind Tunnel”, is shown.

According to the engagement velocity, the drag coefficient is selected from Table 24. For instance, the velocity of 150 m/s in Ankara corresponds to approximately 0.45 Mach so the drag coefficient of the parachute is interpolated as 0.97.

Figure 66 – A View of Test Setup without Wind

Figure 67 – A View of Test Setup Exposed To Wind

Table 24 – Measured Drag Coefficient Values

Mach Number	Drag Coefficient
0.2	0.93
0.3	0.94
0.4	0.96
0.5	0.98
0.6	1.00

The parachute is placed at 150 m away from the starting point of the range where the store supposed to be separated from the wing before the vehicle reach to that point. The parachute is held in open position on the ground by a structure that holds the peripherals of the parachute with very weak ropes, thus air can quickly fill the parachute. (Figure 68)

The simulation of the system with parachute gives the result of the velocity as in Figure 69. This result is obtained by using three R6 rocket engines. The simulation model is modified that the drag coefficient is increased accordingly when the vehicle reaches to 150^{th} meter. The change of the velocity is also compared in this figure.

This plot can give the idea of the effect of a parachute. According to the results at the contact moment, the velocity will be approximately 130 m/s. and the parachute decrease the speed to nearly 50 m/s. The system without parachute will be at approximately 100 m/s at the end of 300 m. The difference between two cases at the end is approximately 50 m/s.

Figure 68 – A View of Parachute Placement in the Test Area

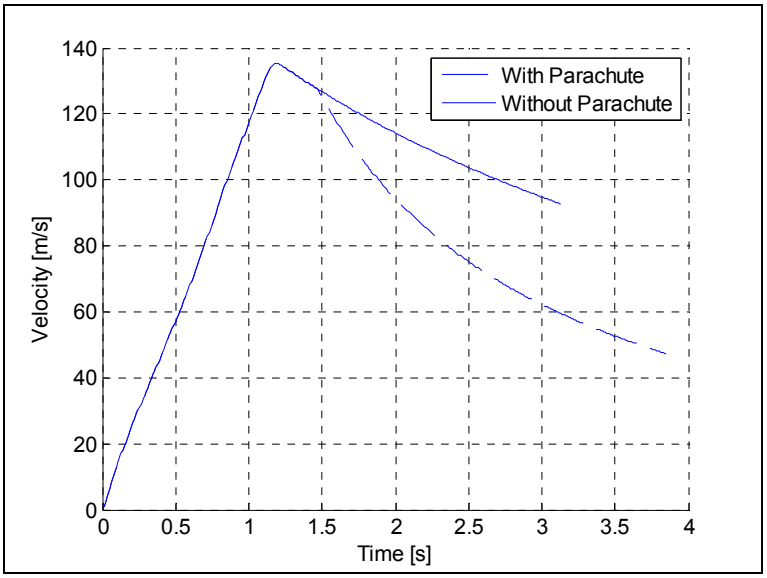

Figure 69 – Velocity Variation With and Without Using Parachute

First, the engagement is performed by a hook at the back of the vehicle that holds the ring where the ropes of the parachute are attached. At the place where the vehicle meets the ring of the parachute, due to the high speed, a serious problem occurs. The parachute ropes cannot withstand the impact forces. In order to get rid of this problem spring effect issued. The elastic and strong bungee jumping rope is connected to the parachute so the impact shock will be reduced between vehicle and parachute.

2.5.4. Deceleration by Brakes

The idea is to use the brake pads and these pads are clamped to the rail surface to generate extra friction between the vehicle and the rail. Pads are placed on the sides of the vehicle and supposed to contact the rails from its flanges. The normal force to generate the friction is supplied with the help of compressed torsion springs. Springs are pre-loaded and metal pieces are inserted so that the clutches have a gap in between that the rail passes through. At the braking point, these metal pieces are hit and removed by stationary notches on the rail so that braking pads presses to the rail flanges. The installed braking system is shown in Figure 70.

2.5.5. Conclusion

Among the methods explained above, the results are discussed and explained. In the first one, using plastic deformation of metal pieces, in order to dissipate 1125 kJ energy, approximately 5625 metal pieces are needed. This alternative has also other problems like fixing and removing the specimens for each test.

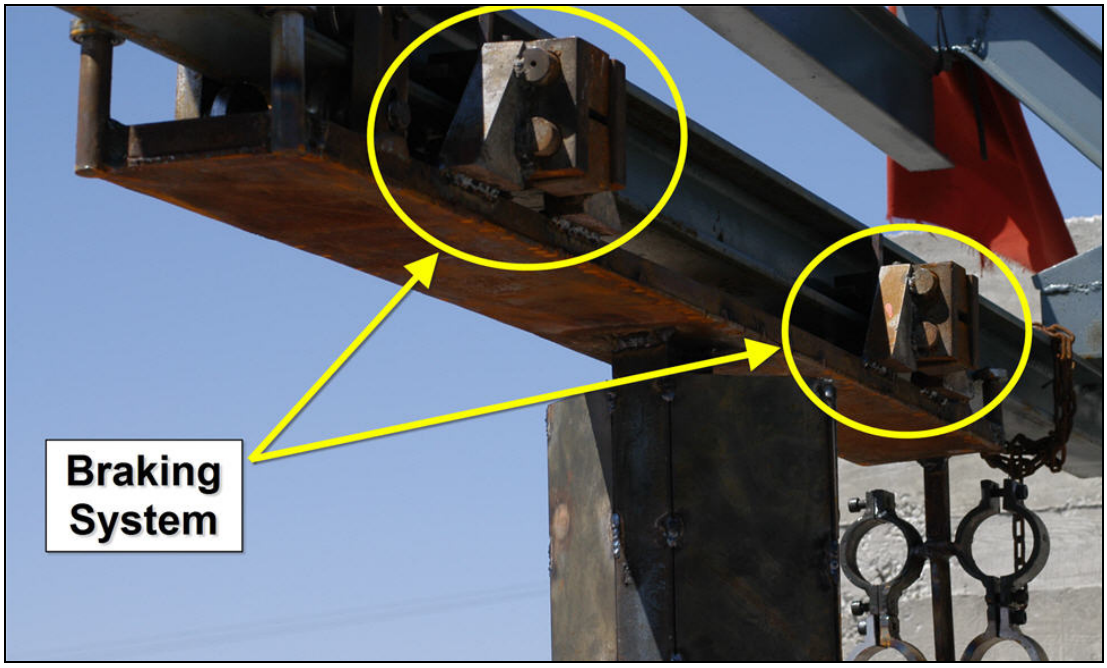

Figure 70 – A View of Installed Braking System

In the second choice, using additional mass, practically the impact forces are excessive to handle by the vehicle. The solution for this problem is to use a spring to store the impact energy. The spring should have low stiffness to compensate the impact forces and also it should be long enough to store that much energy. It turns out to be to use and to support that spring is not possible. In the third method, using parachute, increasing the drag is issued. This method is applied in the tests, and observed when the vehicle holds the ring of the elastic rope attached to the parachute, the parachute could not resist the aerodynamic forces, and torn into pieces. The speed of the vehicle is 120-130 m/s in the test. The fourth alternative is also applied in the previous tests. The consumption of the brake pads is too quick so the deceleration could not be observed. As a conclusion, neither of the methods is successful and it is decided not to use a deceleration system.

CHAPTER 3

TEST AND ANALYSIS OF STORE MODEL SEPARATION SYSTEM

Until this point, how the facility is built and the design of the setup are explained in details. After completing the construction of the facility, necessary tests are made to prove the ground and for the acceptance of the facility. Before starting to the separation tests, some conceptual tests are performed in order to observe the facility during a similar test period.

In the conceptual tests, a dummy vehicle is used with a dummy metal, hand-made aircraft model attached (Figure 71). In these test, the rail is observed during the launch sequence whether any unpredicted situation is happened. In addition, the movement and reactions of the vehicle under the thrust of the rocket engine is observed by recording with high speed cameras. Additionally, some of the subsystems are tested and checked. For instance, the results of the simulation are verified with the results of the tests and the placements of data acquisition systems are decided. These tests are also useful to notice and utilize some improvements to the design of the vehicle in order to reduce the time of the preparation of the setup before each test.

Figure 71 – Dummy Test Setup with R5 Rocket Engine

3.1. DATA ACQUISITION FOR SEPARATION ANALYSIS

In the safe store separation tests, the store must move away a certain distance from the aircraft, which is defined as the interference area, [1]. As mentioned in the earlier chapters, this distance is defined as the own length of the store, therefore data must be acquired during this time interval.

The validation of the safe store separation is done with photogrammetry method. It is possible to analyze the motion of the store right after releasing from the aircraft model, by taking pictures of the process. The imaging instruments need to be quick enough to capture the separation process. The vehicle speed at the separation is high that standard cameras can not capture enough pictures within that time interval. For this reason, high speed

digital cameras are obtained. The model of the cameras is Photosonics Phantom V4.2 whose picture and details are given below.

Figure 72 – A View of Photosonics Phantom V4.2 High Speed Camera

Table 25 – Technical Specifications of Phantom V4.2

Sensor Size (pixel)	512 x 512
Pixel Size (micrometer)	22
Min. Shutter Speed (microseconds)	10
Frame Rate At Full Resolution (pps)	2100
Maximum Record Capacity	4096 frames
Internal Memory	1024 MB
Lens Mounts	1’ Mount
Timing	IRIG-B
Trigger Signal	TTL
Synchronization Signal	TTL

When the store model is released and hit the ground, it makes an unpredictable motion so in order to avoid any accidental results during tests; the cameras are placed inside of the safety cabinets, which have bulletproof glass windows in the front.

It is not possible to view all the separation using only single camera, so two of these cameras are placed to the side of the rail and on to the top of crests. The cameras are placed approximately 15 meter away from the rail. The wide angle lenses can cover much more area than others but they are not preferred due to the high distortion in the edges of the view which is a handicap for the analyses. So, the lenses of the cameras are also selected to view the separation in more perpendicular view with less distortion. On the other hand, when this kind of narrow view lenses are used, the separation cannot be fully covered with single camera. As a result, it is decided to use two cameras looking in adjacent rail portions that vehicle travel right after the store model separated.

Locations of the Phantom cameras are decided according to the simulations and the conceptual tests. The placements of the high speed cameras are shown on the cross sectional view of the facility in Figure 73. The other high speed digital camera, Photron Ultima APX, is placed beneath the rails and a similar safety cabinet is used. The illustration and properties are given below.

Additional to these cameras, a black and white high speed camera is placed to view to launch process to obtain some feedback information about launch and a camcorder is placed in order to view the complete rail.

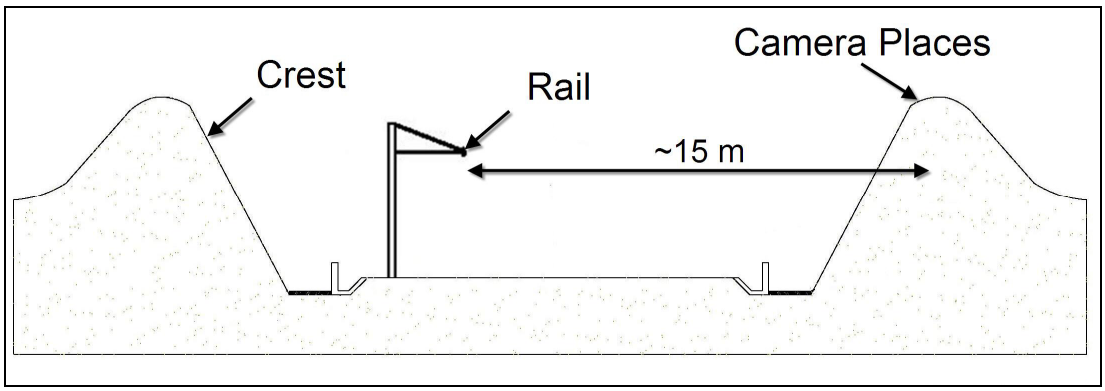

Figure 73 – Placement of the High Speed Cameras

Figure 74 – A View of Photron Ultima APX

In the analysis section of the test results, one of the most critical issues is the timing. After obtaining the images of the separation with several cameras, the problem is to synchronize them accurately. This can be accomplished by triggering all of the cameras from a single source, which is also triggering the rocket engines. By this way, it is guarantied that all cameras can capture the separation and record the same period and the time information is generated

by IRIG-B time code generator so GPS time is printed to the captured images.

The second data to be acquired is the velocity profile, which is measured with 35.497 GHz frequency Doppler radar for the whole motion of the vehicle. A sample view of Doppler radar is given Figure 76. The radar is placed under the launch platform and rail (Figure 75). Its radar beam covers the rail except the beginning part, like 15 to 20 meters. This is sufficient for the acquisition of the velocity profile, but if the initial acceleration data is needed the data can be extrapolated to the beginning of the rail.

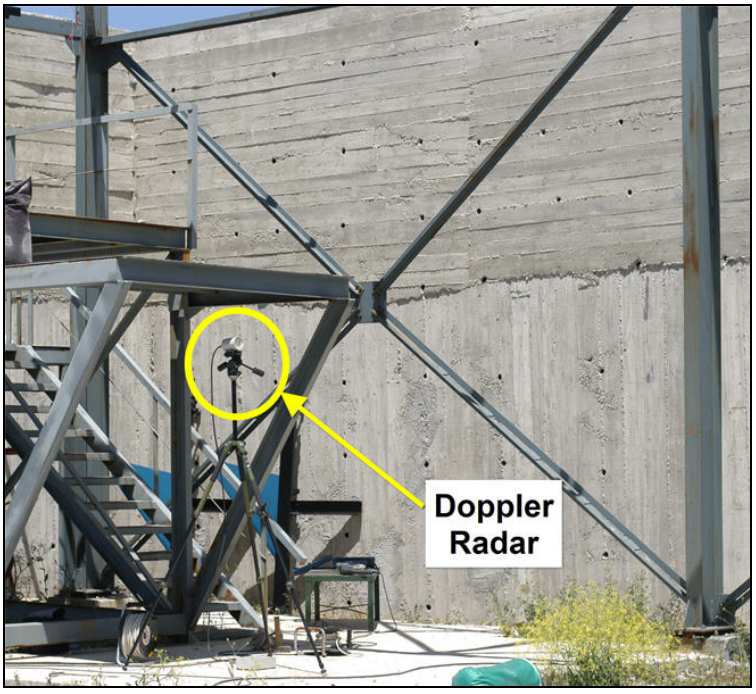

Figure 75 – Placement of Doppler Radar

Table 26 – Technical Specifications of Photron Ultima APX

Sensor Size (pixel)	1024 x 1024
Pixel Size (micrometer)	17
Min. Shutter Speed (microseconds)	4
Frame Rate At Full Resolution (pps)	2000
Maximum Record Capacity	2048 frames
Internal Memory	2.6 GB
Timing	IRIG-B
Trigger Signal	TTL

Figure 76 – A View of Doppler Radar

3.2. CASE STUDY FOR SEPARATION ANALYSIS

After completing the separation tests for a project of TUBITAK-SAGE, the case studies for this thesis are completed. The tests that are made in this thesis study are performed with using the wing model instead of aircraft model.

The first thing to do is to plan the case studies. After deciding the number of tests, the setup preparations are completed. There were six R6 rocket engines, to employ in the case studies. Instead of using them in a single but relatively high speed test, these 6 rocket engines are planned to be used in 3 different tests. The disadvantage is relatively lower speed, but on the other hand, making multiple tests reduce the risk of failure of acquiring data.

Preparations of the tests include the manufacturing of the vehicle and wing as explained in the previous sections. The wing model and vehicle assembly is placed on the rails. The necessary adjustments are completed in the bearing assemblies in order to make the vehicle level.

The pylon model is prepared by fixing the spring and trigger system inside and then it is assembled to the wing model. The store model is mounted while the pylon model is fixed on the wing. After closing the pylon model cover, the cabling of the trigger system is done and vehicle becomes ready for the installation of the rocket engines.

Rocket engines are conditioned to 21°C for at least one day. After all the other systems are ready to go, they are placed into the rocket holders on the vehicle and the power source is connected. The power source is placed in the control room and the output current is fed to a firing control panel. The

triggering signal is direct current and the magnitude is adjusted to the maximum available current of the power source, which is 25 amperes.

Parallel to the preparation of the vehicle and the other systems on the rail, the data acquisition systems are prepared in their places. As mentioned before, the critical part is triggering of the cameras and the Doppler radar. Doppler radar has its own acoustic trigger system and it is placed near the rocket engines so that it can receive the acoustic signals during the launch. This means it is working automatically, and do not need any person for trigger the system. On the other hand, the cameras are triggered by a person holding a remote triggering button attached to the cameras. For the safety precautions, the person is hiding behind the crests. The cameras have a property of being triggered in different positions. They can be triggered before, during or afterwards of the separation process. According the adjusted recording duration, the images are kept within the built-in camera memory. For example when record duration is arranged to two seconds and the trigger is arranged to the afterwards position and the trigger button is pressed, the images within two second period before the trigger moment is recorded. Again similarly, if the trigger position is selected as middle position, the images during one second before and one second after will be recorded. By this way, the cameras can be set up to the middle trigger position and when the person hears the launch of the rocket engines, presses the trigger button. So, the risk of late triggering can be compensated.

When all the systems are ready, the test is proceeded to launch sequence and the test is accomplished. The next step is to analyze the acquired data and investigate if the safe separation happened and validated or not.

3.2.1. Doppler Radar Data Analysis

The Doppler radar data is analyzed with TestCenter© Doppler Radar Velocity Measurement Software. This software can present the velocity profile and can calculate the derivations of this data. In the following figures, the velocity, position and acceleration results for a single and double R6 rocket engine test are given. At the same time, the result of the dynamic simulation from the MATLAB® Simulink model is plotted on the same graphs in order to make comparisons.

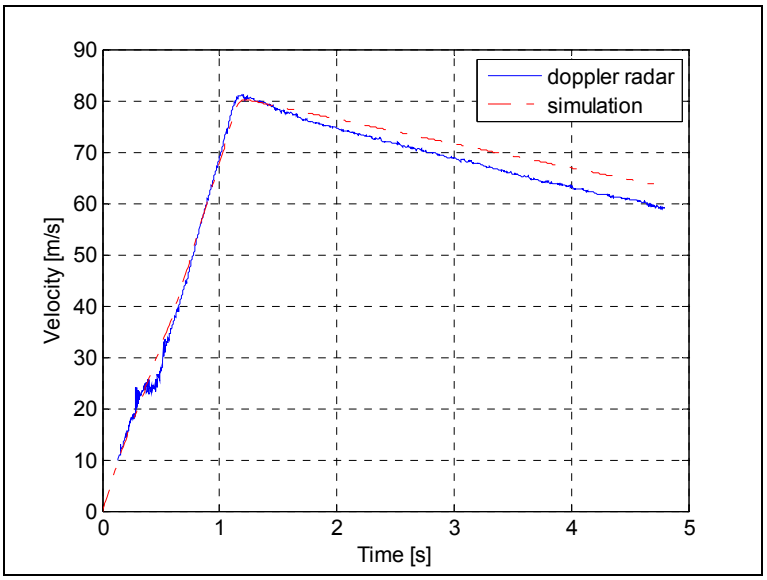

Figure 77 – Velocity with One R6 Rocket

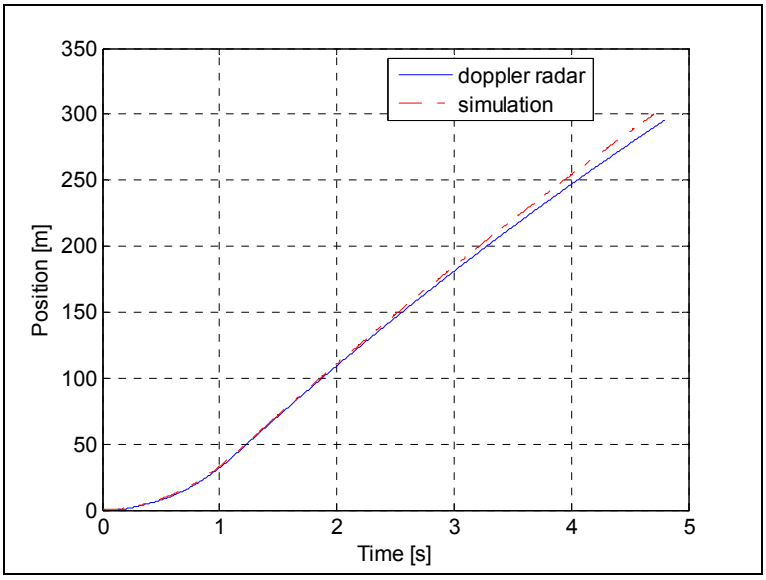

Figure 78 – Position with One R6 Rocket

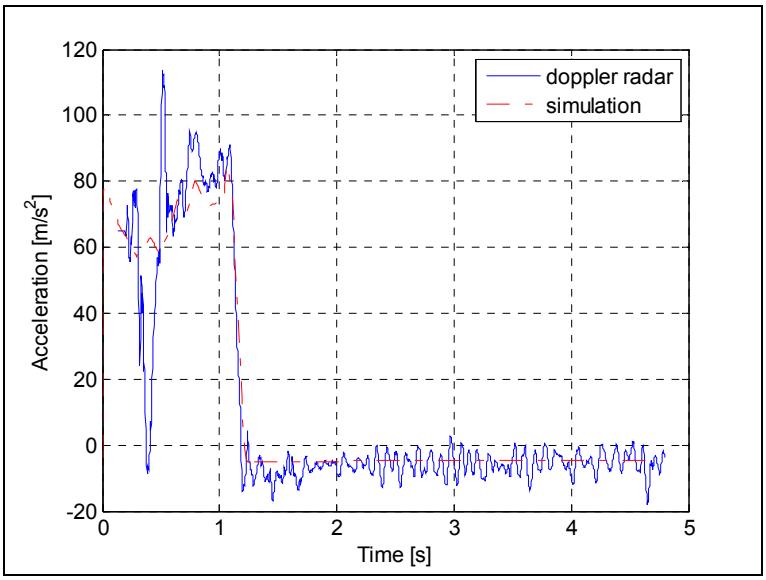

Figure 79 – Acceleration with One R6 Rocket

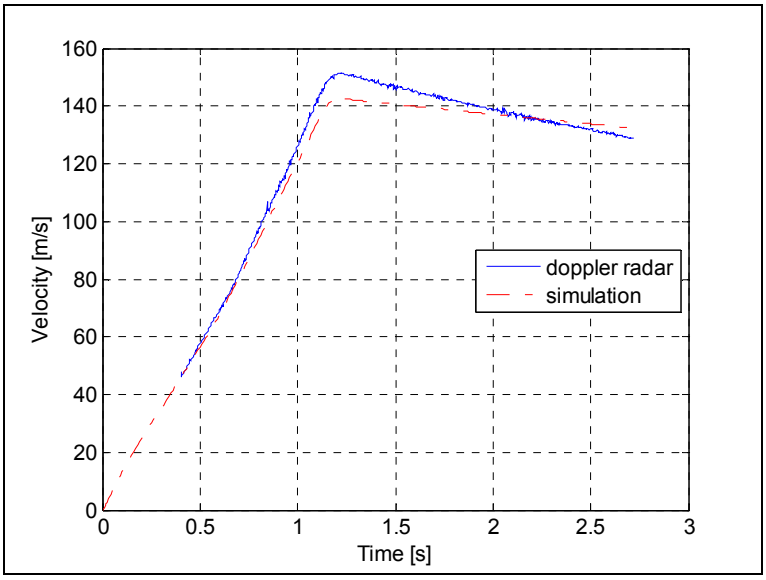

Figure 80 – Velocity with Two R6 Rocket

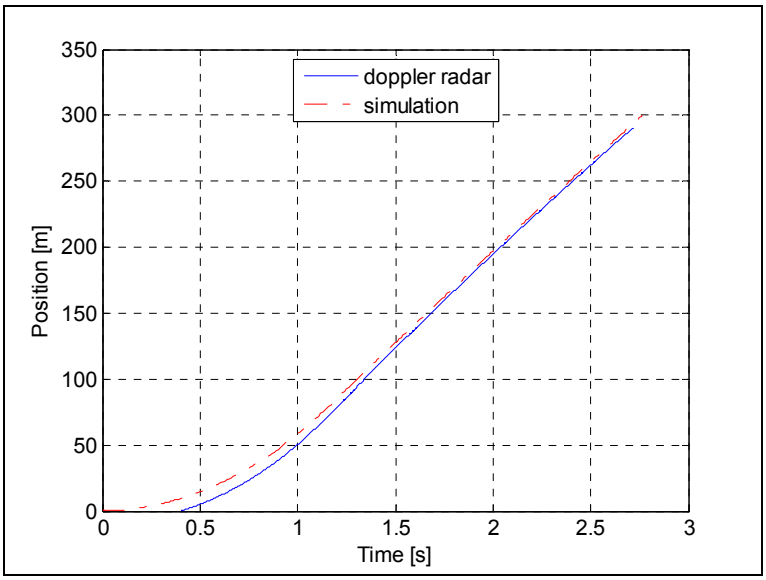

Figure 81 – Position with Two R6 Rocket

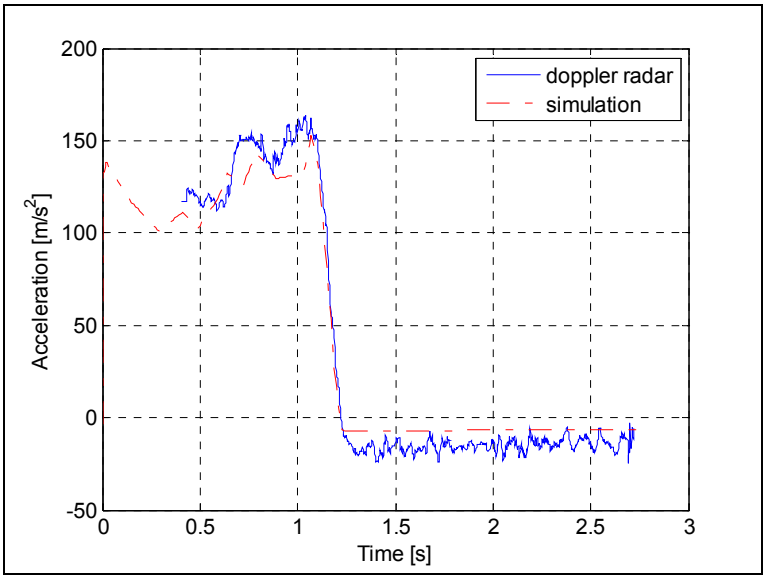

Figure 82 – Acceleration with Two R6 Rocket

3.2.2. Photogrammetric Analysis

In the analysis of motion of the store separation, TrackEye Motion Analysis Software is used, [41]. It is mainly developed and used for the military applications and among the military applications, store separation tests are the main objective. Automotive is another industry area for the usage of this software. Especially it is used for the crash tests and airbag designs. It has the capabilities of using IRIG-B time data and calculating all the motion information within the digital image data by using image processing algorithms.

The software interface is similar to MATLAB® Simulink. The analyses are performed with the dedicated blocks. First step is to prepare the structure for the analyses. In the following figure the block structure, which is used in this case study, is given and the description of each block is shown.

In the first block, the image is loaded to the program, then in the second block target points are placed and tracked in order to analyze the loaded images. The accuracy of the tracked points affects the results directly and these errors in this tracking process are the most significant error source of the analyses. In the third block, the image and the dimensions are scaled according to the input values for the points that have fixed distances in all images. For instance, forward and aft of the vehicle body is tracked in all images and the length of the vehicle is entered as a reference. In the distance analyses block, the distance between the tracked points and a stationary point are evaluated and in the final block, they are listed and exported.

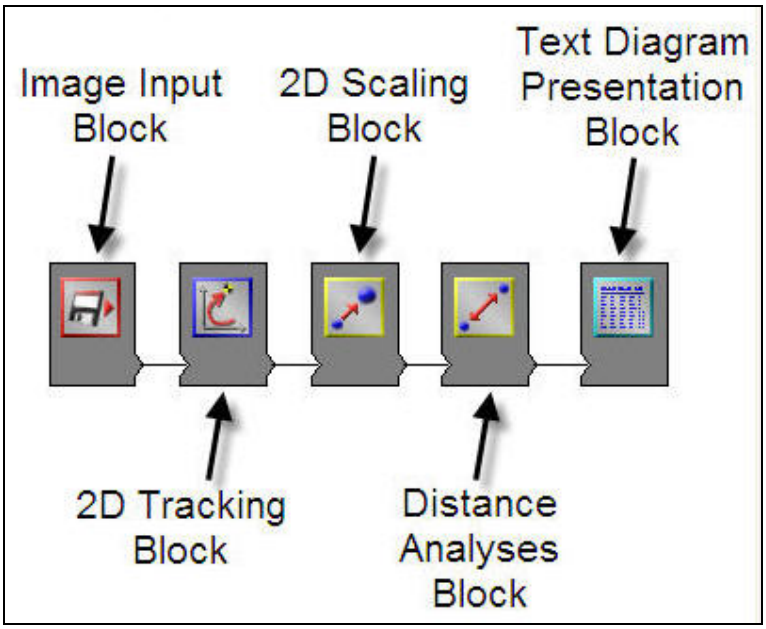

Figure 83 – Analysis Function Blocks of Store Separation

One of the images that is used in the analyses of motion is given in Appendix B. In the image example, the labeled tracked points are can be observed. Some of the images of separation is printed on the same frame by post-process and represented in Appendix B. From this figure, the separation can be observed frame by frame. High speed camera recording settings are given in Table 27.

Table 27 – High Speed Camera Image Recoding Settings

Sample Rate	1000 pps
Exposure Time	150 μs
EDR Exposure	80 μs
Image Width	512 pixels
Image Height	512 pixels

Case study with one R6 is analyzed and in the analyses of the images, the vertical position of the store model is obtained. The tabulated results with respect to time and horizontal position are plotted in the Figure 84, Figure 85, respectively.

The full scale store separation tests are performed in the related project of TUBITAK-SAGE and one of the calculated parameters of the motion of full scale store is the vertical position and it is also calculated with TrackEye software. The full scale flight tests are performed with various speeds and attitudes. In the one that is compared, the separation takes place at 0.31 mach. The one R6 rocket engine test has the nearest mach. The full scale store separation results and the scaled model of this store with similitude are compared in the Figure 86.

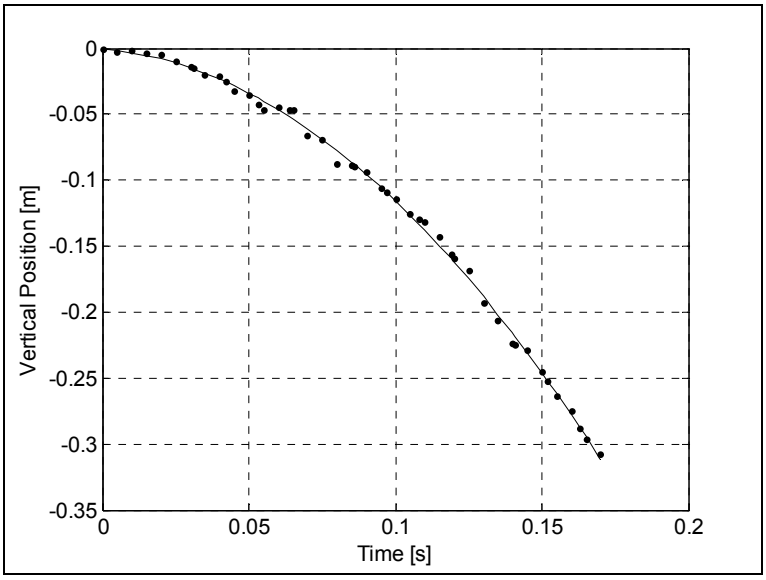

Figure 84 – Graph of Vertical Position of the Store Model vs. Time in One R6 Rocket Test

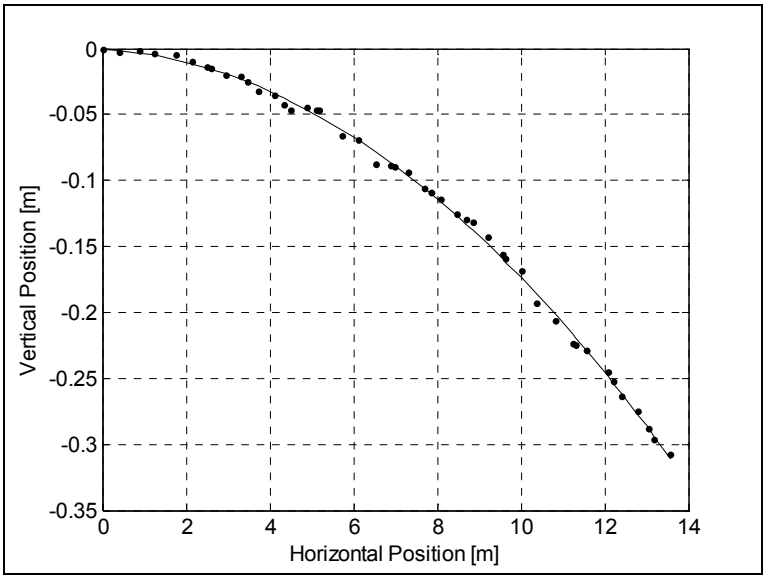

Figure 85 – Graph of Vertical Position vs. Horizontal Position of the Store Model in One R6 Rocket Test

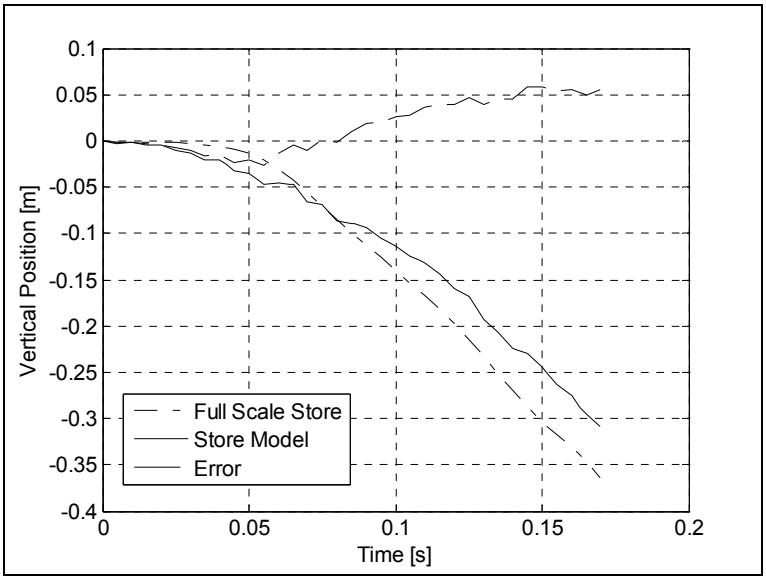

Figure 86 – Vertical Positions of Store Model and Full Scale Store

As it can be observed from the figure that full scale store is separating with a lower velocity than the store model at the beginning. After a while, full scale model catches the store model and moves at a higher velocity than the store model. This difference can be observed also from the error plot within the same figure. The error curve changes sign at a certain point.

The gravitational field modeling is not possible due to the similitude method used for scaling, so the ejection force is arranged. The higher vertical velocity of the store model can be explained with the ejection force arrangement. Since the gravitational field can not be completely modeled, the full scale model is reaching higher velocity.

A couple of error sources can explain the error behavior on the store model. The available measured ejection data are limited in number and so they do not compose a healthy statistical data. By using more ejection data samples,

modeling of the ejection force can be performed more accurately. Additionally, store model geometry has some differences from expected scale model due to manufacturing issues. Especially wings of the store model need to be manufactured thicker than the required value. These differences in the outer dimensions can result in different aerodynamic forces and moments to be acted on the store model.

One of the other error sources is the uncontrollable environmental conditions during test. Test schedule are planned according to the meteorological estimations in order to minimize the effects of the weather, as strong windy days are not selected. However, it is not possible to have a windless weather condition at the facility location and since the wind can not be controlled, the corresponding effects are not considered.

As a result, the store model separates slower than the full scale model but still, separation is safe and the test validates the safe separation. The mentioned errors of the tests are not helping the store model separate easily than the ideal case; on the contrary, the effect of the errors is working against the separation process. For example, the ejection can not be modeled for the complete gravitational field. Therefore, if a real model could be made, the store will be separated easily. This implies that that store model separation is on the safe side according to the validation process.

CHAPTER 4

DISCUSSION AND CONCLUSION

4.1. SUMMARY

In the new era of aircrafts and stores, safe separation process is the one of the most crucial part of the integration issues. Either economical or time consuming, the use of the wind tunnel testing is indispensable. The validation the safe separation, photogrammetric analysis by drop testing is one of the most common methods.

The complications about the wind tunnel blaze to develop a new sled range facility. With the help of similitude studies, scaled model usage is decided in order to reach the separation velocities with less energy. When the aircraft and the store is at the separation velocities, the separation is recorded with digital high speed cameras and the images are to be analyzed for comparing with full scale drop test results.

The development of the facility is started with the simulation of the dynamic system to obtain provisions about the system behavior and the requirements of the necessary subsystem. This simulation is used for the mechanism of the carriage parts, the acceleration system selection, determination of the separation trigger timing and the camera placements.

The aircraft model is reaching to the separation velocities with the help of a sled that moves on the rail. The parts of this sled, the sting, the main body and the bearing assembly, are developed according to the launch acceleration limits.

Since the scaled models are decided to use, a similitude study is accomplished in order to determine the ejection forces and scaling method. In this study, the proper similitude method is chosen, and then this method is applied to all the models used in this test, which are the aircraft, store, pylon and wing models.

The required energy source for this system is investigated and solid rocket engines are decided to be used. The selection for the suitable one is performed with the help of the simulation.

The test is expensive because of the manufacturing of the carriage, the aircraft model, the store model, the pylon model and the wing model and also the cost of rocket engines. In order to decrease the amount of the expendable parts, a study on a deceleration system is completed. Unfortunately, the dissipation of the energy, which raises the velocity to separation level, is not an easy task and the cost to accomplish this process comes out to be much higher than the total of the expandable parts cost, therefore for each test, a new setup is manufactured and used.

Velocity during test is one of the data to be acquired. By using Doppler radar, the velocity profile of the carriage along the rail is tracked within the whole range. The software of the instrumentation is able to give the results of the position, velocity or acceleration and these results are compared with the simulation results.

Besides velocity, the safe separation is validated by photogrammetry method. The digital images that are recorded with high speed cameras are analyzed with TrackEye Motion Analysis Software. Vertical displacement of the store is analyzed and compared with full scale drop test results.

4.2. DISCUSSION AND CONCLUSION

In this thesis study, it is represented that in the designed facility, the safe separation of a store from an aircraft can be demonstrated and validated by applied similitude methods in the tests. Additionally the analyses of the test results are performed in order to make a comparison with the full scale store separation test results by using the images obtained by the digital high speed cameras.

Photogrammetric results show that the validation of safe separation can be performed by using the designed facility and setups. The captured images during the separation process supply the data about the safe separation. Moreover, the motion analyses study gives the vertical trajectory of the store model. These results are also validated with the full scale results of the same store that are obtained in six DOF motion analyses.

The area of the facility is important that the property of the ground is affecting the linearity of the rail especially after a rainy season. Since the rails should be horizontal within a narrow tolerance band, this problem is critical in constructional point of view. It is possible that a vertical offset between two profiles can happen at the conjunction of the profiles of the rail and this may cause serious problems when the carriage passing through. Similarly, due to temperature changes, the elongation and shortening of the profiles can

cause similar problems. According to these problems, precautions must be taken before test. Therefore, there is a need of a platform for working on a rail at five meters above the ground. One is constructed at the beginning of the rail but there comes another problem if an intervention is necessary on another section of the rail. A mobile telescopic platform is useful in these situations.

Other than the constructional issues, some improvements can be done in the dynamic simulation for the future studies. Friction and aerodynamic coefficients and rocket thrust data can be estimated more accurately. In this study the results of this simulation is accurate enough that the placements of the cameras and other issues related with the simulation results are well defined with the current accuracy.

In the tests with aircraft model, up to six rocket engines separation occurred with out any problem, but in the six and eight rocket engine tests, aircraft started to flutter and catastrophic failures happened. The aircraft model is manufactured in order to make it light, but on the other hand the flutter effect can be compensated with a more rigid and massive wings. Therefore, a solid wing model is manufactured and used. In the future tests the aircraft model should be design according to overcome the flutter effects.

Additionally, some investigations and studies must be done the rail that at certain velocities rocket sled can directly cause the rail to resonate. Therefore, these critical velocities for the rocket sled excitation of rail resonance should be determined.

Rocket engines are one of the main problem sources in the tests. R6 and R5 solid rocket engines are used in modular manner, which means the more rocket engine, used, the higher the velocity. Liquid rocket engine can be

more efficient for these tests. In the presence of a liquid rocket engine, tests can be performed in more controllable conditions relative to solid rocket engines. Liquid rocket engine has the ability of working as a retro rocket engine on the same setup so it would be possible to decelerate and recover the test setup, which results an increase the number of the tests and lower cost and less time that spend on the manufacturing of these setups.

In photogrammetry, when a single camera is utilized for recoding the images of the separation, only two-dimensional results can be obtained and the third dimension can not be discerned. It is required that two different cameras at different view angles must be used in order to obtain three-dimensional results and more than two DOF motion analyses.

In the applications, when the motion is recorded with two cameras at the same time, more accurate results can be obtained than a single camera. If these two cameras are viewing from the same side of the store model than the lateral motion become less accurate than the vertical motion.

In the case studies, a camera is placed under the rail to obtain a view angle that is different from the ones on the top of the crest. The cameras on the crest are viewing the separation in tandem vise. The view fields of these cameras are not same but adjacent. Therefore, the motion is planned to be captured with two cameras in different perspectives. Unfortunately, a problem occurred with the camera beneath the rail. The recorded images could not be transferred from the internal memory of the cameras for certain cases and a trigger problem is experienced. While the other two cameras are triggered with out any problem, this camera could not be triggered. This led the results to become two dimensional as explained.

The facility is naturally settled to an open area, which causes the problem of uncontrollable weather conditions. This situation is accepted as an error source to the results. In order to minimize the effects, tests are performed at relatively still air and not at rainy, windy, or extreme weathers.

About the maintenance of the rail for further usage, the corrosion on the flanges of the rail profile should be observed regularly after every test.

This thesis successfully achieves its main objectives by validating the safe separation of store model within a specifically designed facility. Furthermore, by capturing the digital images by high speed photography, the motion analyses of the store model are accomplished and this similitude result is compared and validated with full scale model separation test data.

This thesis is a pioneer study about the store separation certification subject, in the way of becoming a self-sufficient country in the defense industry and technological areas. With out demanding the certification procedures from the foreign countries, it is achieved in Türkiye by using self-developed technologies. The facility is unique in Türkiye and in the world that the other similar ranges have their rails on the ground.

REFERENCES

[1] "**Aircraft/Store Compatibility: System Engineering Data Requirements and Test Procedures**", Military Handbook, MIL-HDBK-1763, 1998

[2] TAVERNA, F., CENKO, A., "**The United States Navy's Integrated Approach To Store Separation Analysis**", RTO MP-16, 1998

[3] BLACK, R. L., "**High-Speed Store Separation – Correlation Between Wind-Tunnel and Flight-Test Data**", 68-361 AAIA 3rd Aerodynamic Testing Conference, 1968

[4] CENKO, A., "**Experience in the Use of Computational Aerodynamics to Predict Store Release Characteristics**" Progress in Aerospace Sciences, 2001

[5] DEMİR, H. Ö., "**Computational Fluid Dynamics Analysis of Store Separation**" Master Thesis, Middle East Technical University, August 2004

[6] VON DER DECKEN, J., ESCH, P., FRITZ, W., "**Theoretical and Experimental Simulation Methods For External Store Separation Trajectory**"

[7] ATKINSON K. B., '**Close Range Photogrammetry and Machine Vision',** Whittles Publishing, 2001

[8] KARBANCIOĞLU, I. M., "**Aerodynamic Parameter Estimation for a Separated Store from an Aircraft**" Master Thesis, Middle East Technical University, September 2006

[9] KIM, H. L., LEE, I., "**Integrated Test and Evaluation Approach to Improve Aircraft Store Separation**" AIAA Atmospheric Flight Mechanics Conference and Exhibition, 2005

[10] CENKO, A., PHILLIPS, K., HOLMES, M., "**Captive Trajectory System Sting Effect On Store Loads**", 32nd Aerospace Sciences Meeting & Exhibit, AIAA 94 – 0195, 1994

[11] SPAHR, H. R., "**Theoretical Store Separation Analyses of a Prototype Store**" AIAA Mechanics and Control of Flight Conference, 1974

[12] BUTLER, G., KING, D., ABATE, G., STEPHENS, M., "**Ballistic Range Test of Store Separation at Supersonic to Hypersonic Speeds**" AIAA-91-0199, 1990

[13] MURMAN, S. M., AFTOSMIS, M. J., BERGER, M. J., "**Simulations of Store Separation from an F/A-18 with a Cartesian Method**" AIAA, Journal of Aircraft, Vol.41, No.4 , 2004

[14] REED, J. F., CURRY, W. H., "**A Comparison Between Transonic Wind-Tunnel and Full-Scale Store Separation Characteristics**" AIAA Journal of Aircraft, Vol.6, No.3 , 1969

[15] ÖZYÜKSEL, A. A. , "**Dynamic Modeling of Sled Range Setup**", TUBITAK-SAGE Report, 2004

[16] ASKAYNAK, KAYNAK TEKNİĞİ WELDING ELECTRODES CO., "**Coated Welding Electrode",** "http://www.askaynak.com.tr", 10.07.2007

[17] SHINGLEY, J. E., MISCHKE, C. R., "**Mechanical Engineering Design**" McGraw Hill, 1989

[18] BEER, F. P., JOHNSTON JR., E. R., "**Mechanics of Materials**", McGraw Hill, 1992

[19] "**Basic Mechanical Elements, Linear Motion and Assembly Technologies**", Rexroth Bosch Group, 2002

[20] "**Torrington Service Catalog**", 2001

[21] "**Motion and Control NSK Rolling Bearings Catalog**", Cat. No. E1101b

[22] WOLOWICZ, C.,H., BOWMAN, J., S., GILBERT, W., J., "**Similitude Requirements and Scaling Relationships as Applied to Model Testing**" NASA Technical Report 1435, 1979

[23] BVM BOB VIOLETT MODELS, "**F-4 Phantom II Assembly and Operation Manual for Single Turbine Power**"

[24] COVERT, E. E., "**Wind-Tunnel Simulation of Store Jettison with the Aid of an Artificial Gravity Generated by Magnetic Field**" AIAA Journal of Aircraft, Vol.4, No.1 , 1969

[25] SCHERBERG, M., RHODE, R. V. "**Mass distribution and Performance of Free Flight Models**" Technical Notes, National Advisory Committee for Aeronautics, 1927

[26] KUTLUAY, U., "**Design Scaling of Aeroballistic Range Models**" Master Thesis, Middle East Technical University, 2004

[27] "**Similitude Relations for Free-Model Wind-Tunnel Studies of Store-Dropping Problem**" Technical note, NACA TN 3907, 1957

[28] BURNS, R. B., "**The Accelerated Light Model Technique of Store Separation as Developed and Used At British Aerospace, Brough.**", 1984

[29] "**Dynamic Similitude Between a Model and a Full-Scale Body For Model Investigation at Full-Scale Mach Number**", Technical Note, NACA TN 2062, 1950

[30] "**A Summary of NASA Data Relative to External-Store Separation Characteristics**", Technical Note, NASA TN D-3582, 1966

[31] HARISH, G., PAVANAKUMAR, M., ANANDHANARAYANAN, K., "**Store Separation Dynamics Using Grid-free Euler Solver**" 24th Applied Aerodynamics Conference, AIAA 2006-3650, 2006

[32] MOYER, S., RİCHHARDSON, P., CENKO, A., SUSI, M., "**Flight Test Incident Via Computational Aerodynamics and Store Separation Analysis**" 33rd Aerospace Sciences Meeting and Exhibit, AIAA 95-0067, 1995

[33] SHORTIS, M. R., SNOW, W., L., "**Videometric Tracking of Wind-Tunnel Aerospace Models At NASA Langley Research Center**" Photogrammetric Record, 15(89): 673-689, 1997

[34] OBERMARK, J., KARLA, K., "**Verification of Simulation Results Using Scale Model Flight Test Trajectories**" Technical Report AMR-AE-04-01, 2004

[35] SKOGLUND, V. J., "**Similitude: Theory and Applications**", Scranton, Pa. International Textbook Co., 1967

[36] MURPHY, G., "**Similitude in Engineering**", Ronald Press Co., 1950

[37] LANGHAAR, H. L., "**Dimensional Analysis and Theory of Models**", New York, Wiley, 1951

[38] SCHURING, D. J., "**Scale Model In Engineering, Fundamentals and Applications**", Pergamon Press, 1977

[39] GÜNDÜZ, E., SÜMER, B., "**Liquid Fuel Rocket Engine Design, Production, Ground Testing Optimization Study**", TUBITAK-SAGE Report, 2005)

[40] ROE, G. J., BRAMFITT, B. L., "**Variability of Charpy Test Results**" Bethlehem Steel Corporation

[41] Image Systems, "**TrackEye Motion Analyses Software**" http://www.imagesystems.se/ImageSystems/TrackEyeproduct.html, 10.07.2007

[42] Keen, K. S., Morgret, C. H., Arterbury, R.L., "**An Analitic Investigation of Accuracy Requirements for Onboard Instrumentation and Film Data for Dynamically Scaled Wind Tunnel Drop Models**" AEDC-TR-96-7, Arnold Engineering Development Center, 1997

APPENDIX A

SIMULATION BLOCK DIAGRAMS

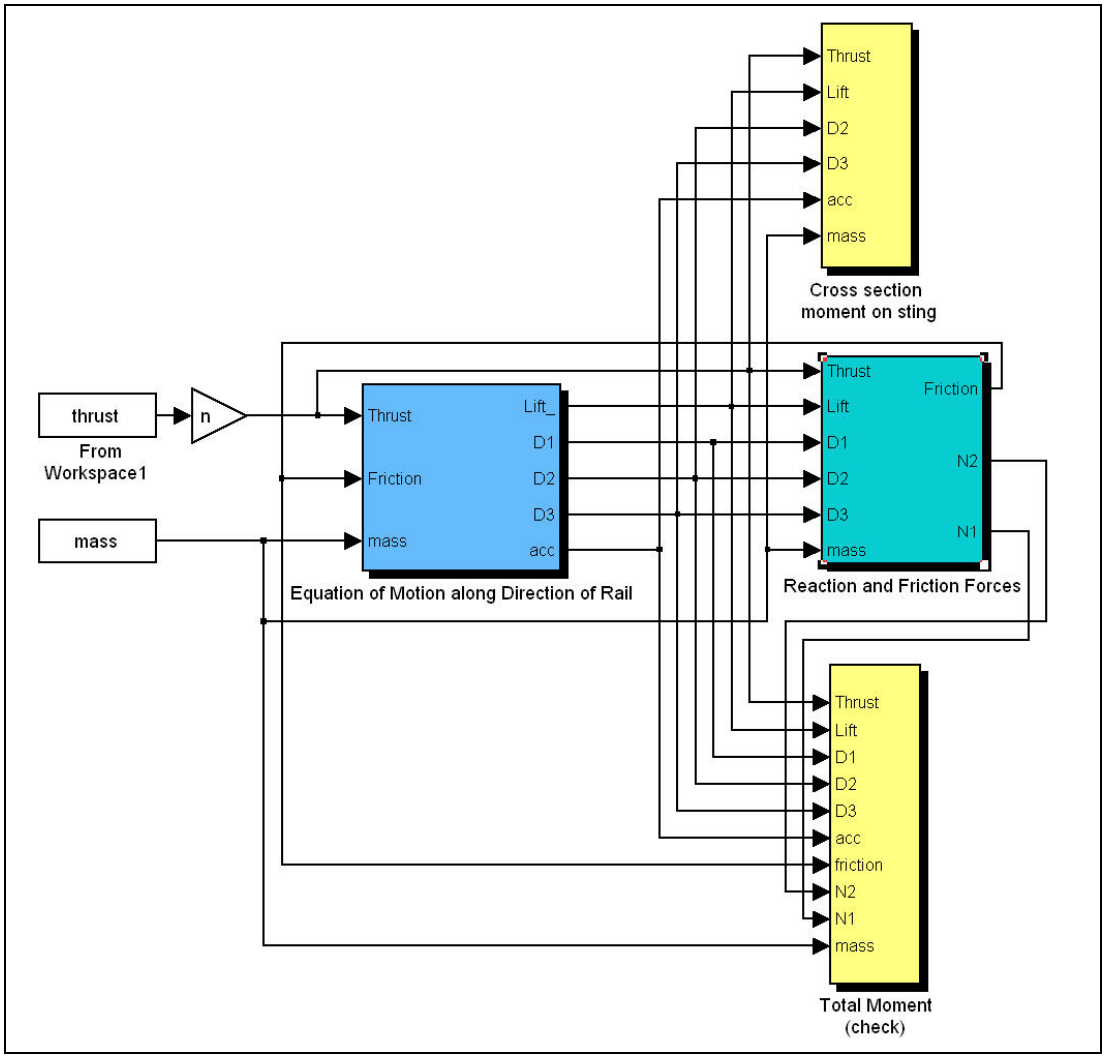

Figure 87 – Simulation Block Diagram (Top Layer)

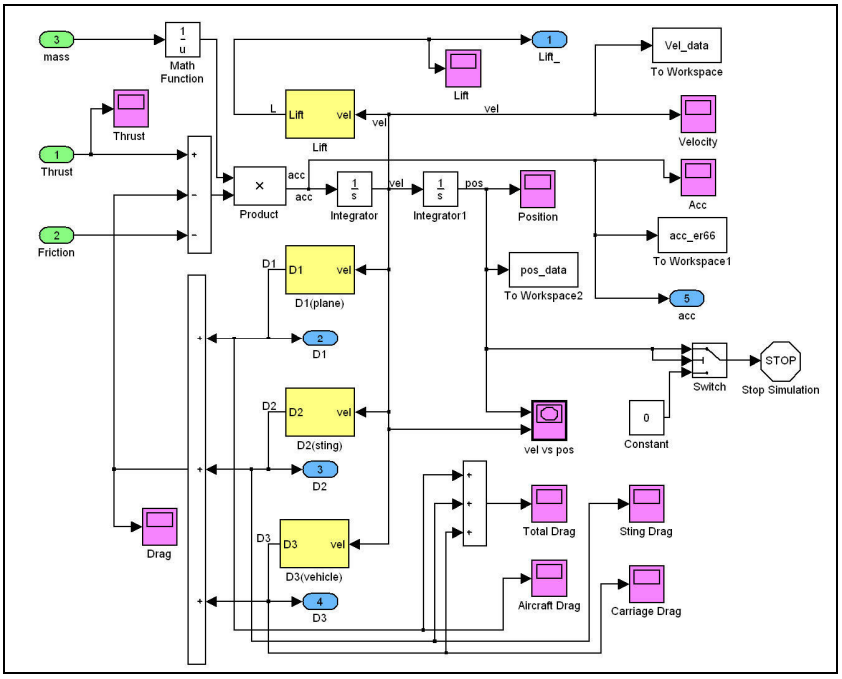

Figure 88 – Equations of Motion Block

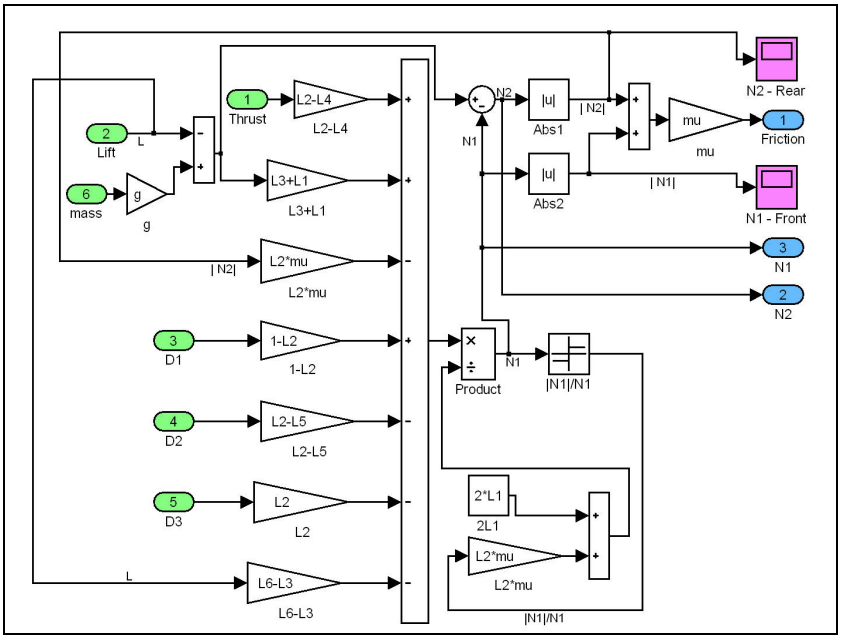

Figure 89 – Reaction Forces Block

APPENDIX B

SEPARATION IMAGES

Figure 90 – Sample Image of TrackEye Analyses

Figure 91 – Combined Frames of Store Separation Images

APPENDIX C

TECHNICAL DRAWINGS

Following figures are the technical drawings of the parts of the pylon model which were used the manufacturing at mechanical production plant in TUBITAK – SAGE. The technical drawings are given for:

- Pylon Model Chassis
- Main Body of Pylon Model
- Link Part of Pylon Model
- Locking Pin of Pylon Model
- Locking Pin Housing
- Sway Brace of Pylon Model
- Pylon Chassis Cover

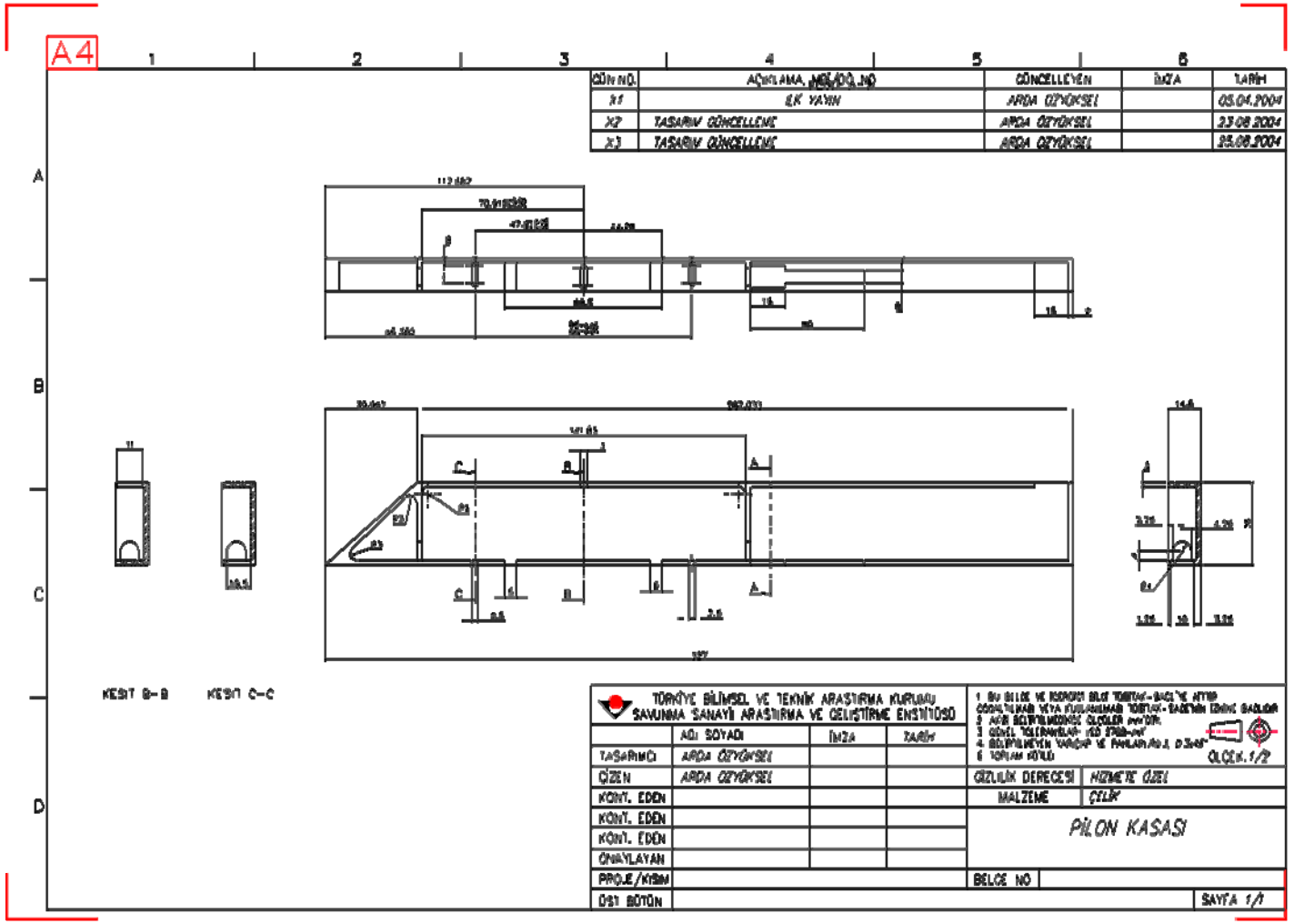

Figure 92 – Technical Drawing of Pylon Model Chassis

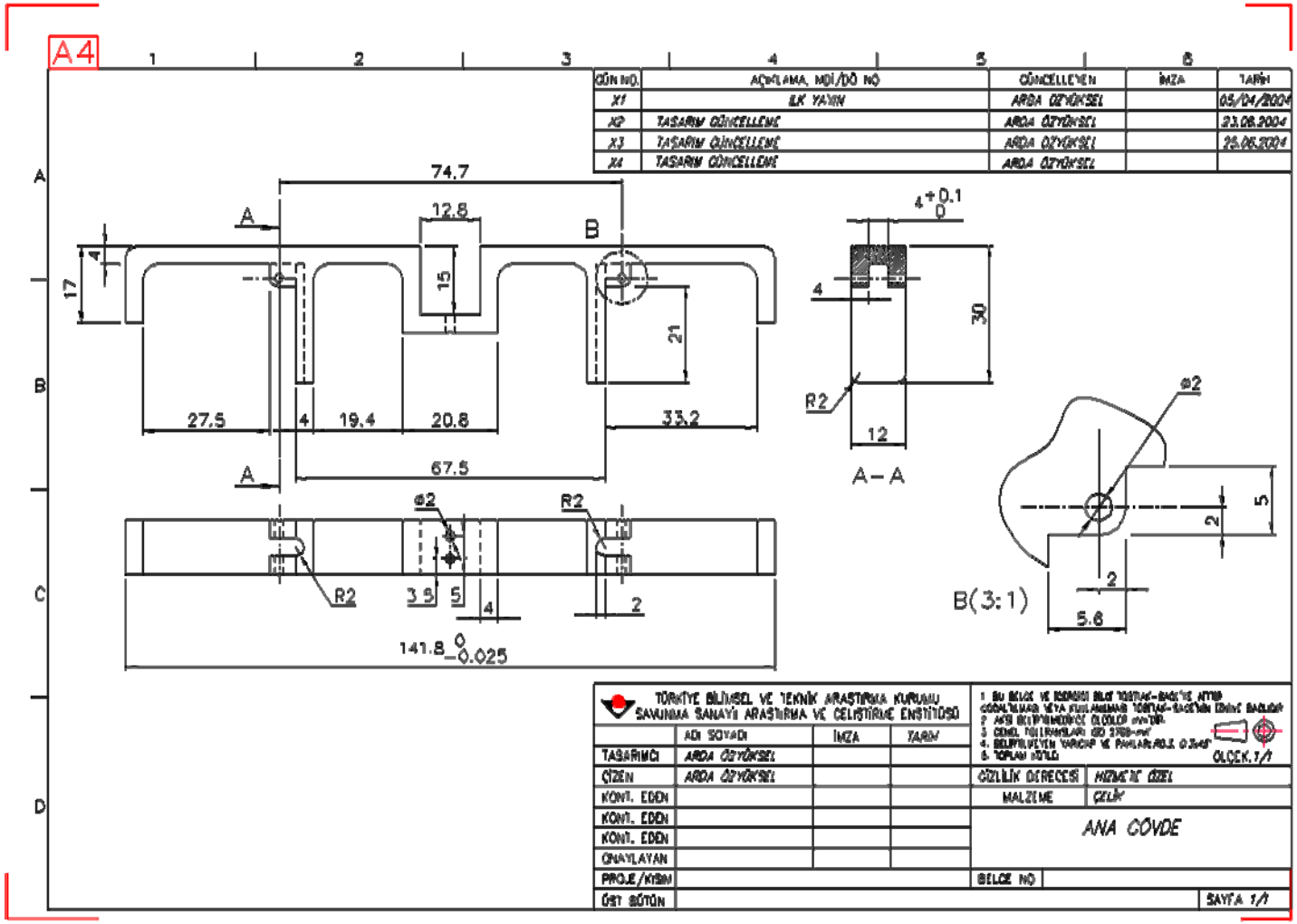

Figure 93 – Technical Drawing of Main Body of Pylon Model

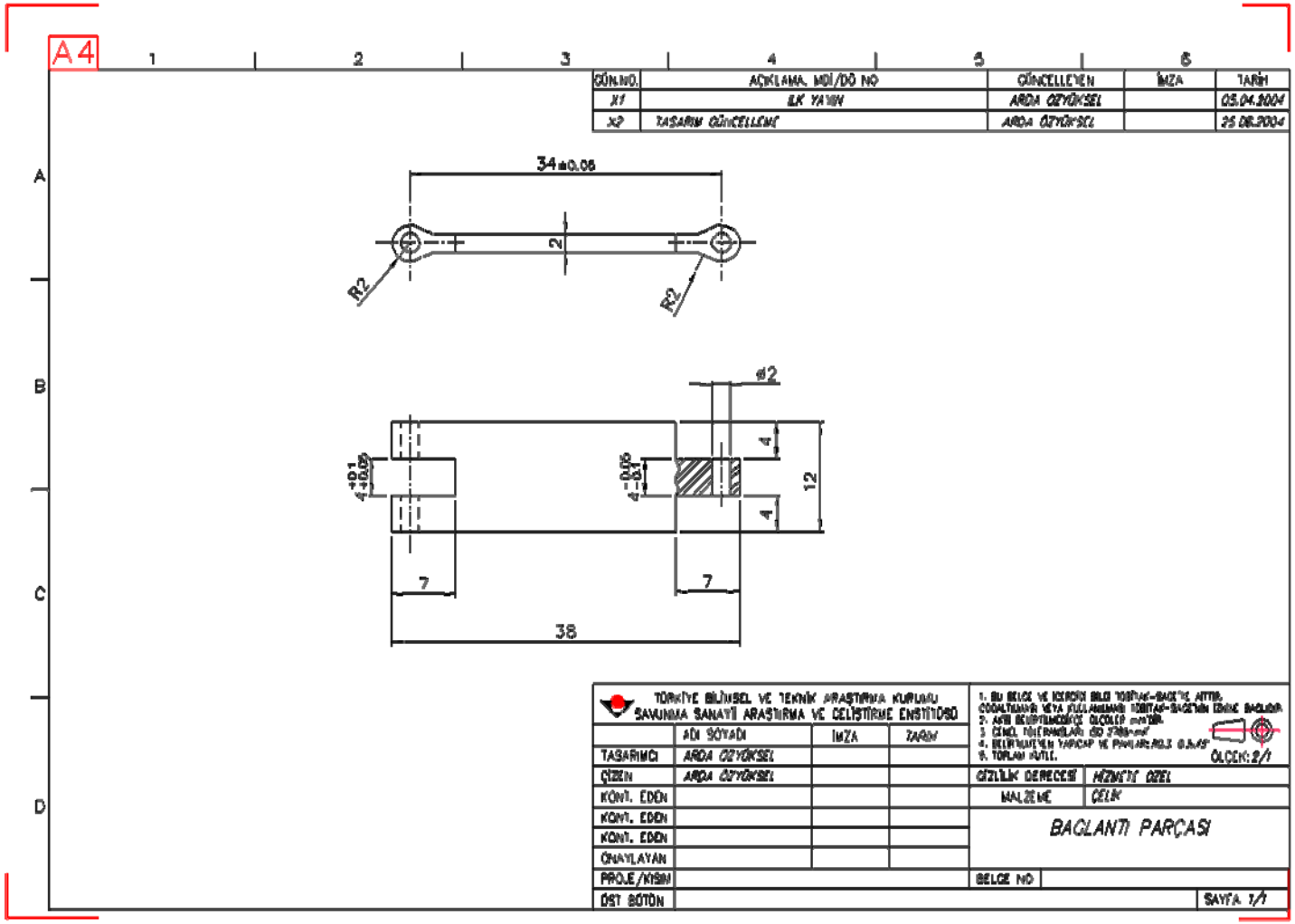

Figure 94 – Technical Drawing of Link Part of Pylon Model

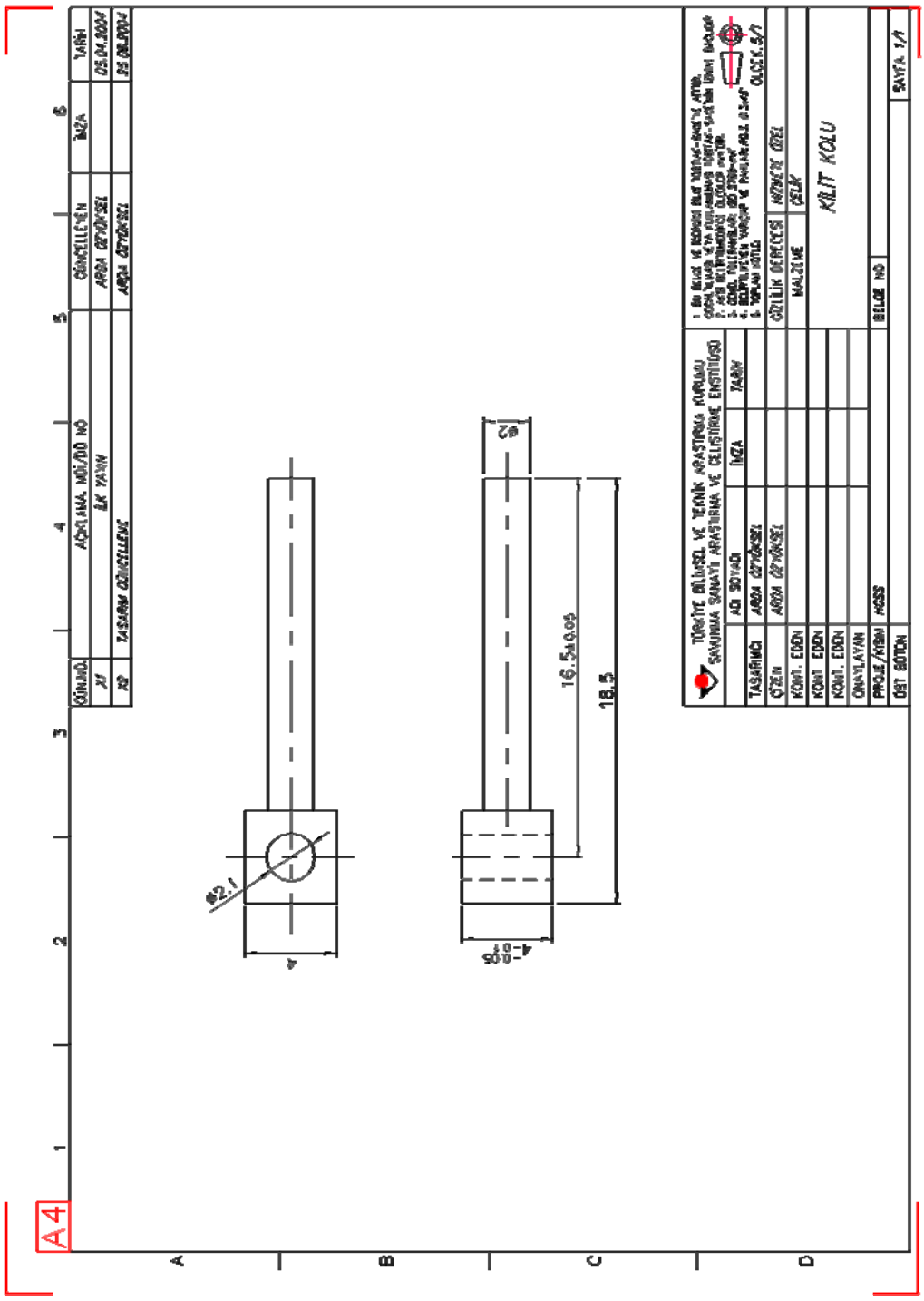

Figure 95 – Technical Drawing of Locking Pin of Pylon Model

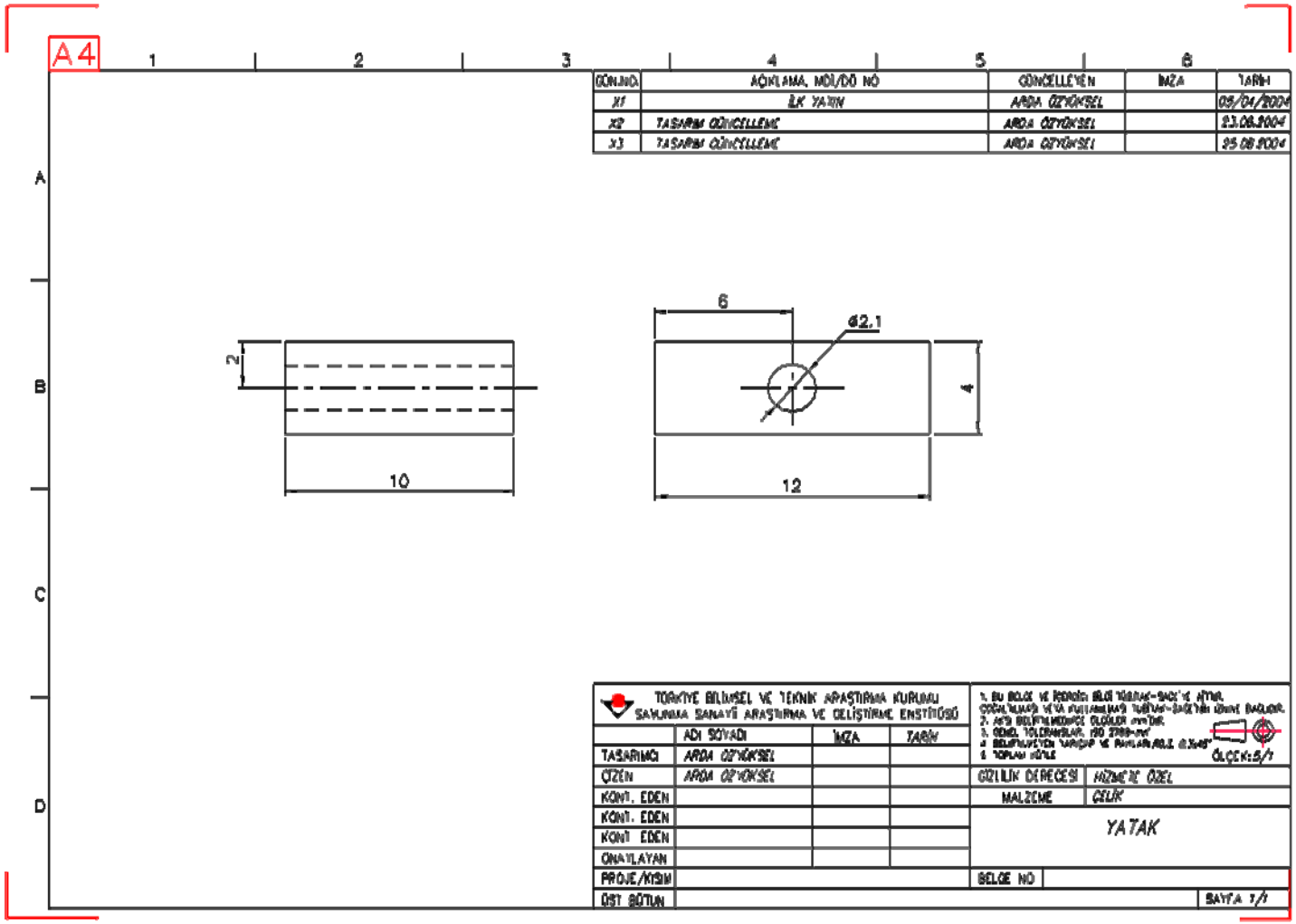

Figure 96 – Technical Drawing of Locking Pin Housing

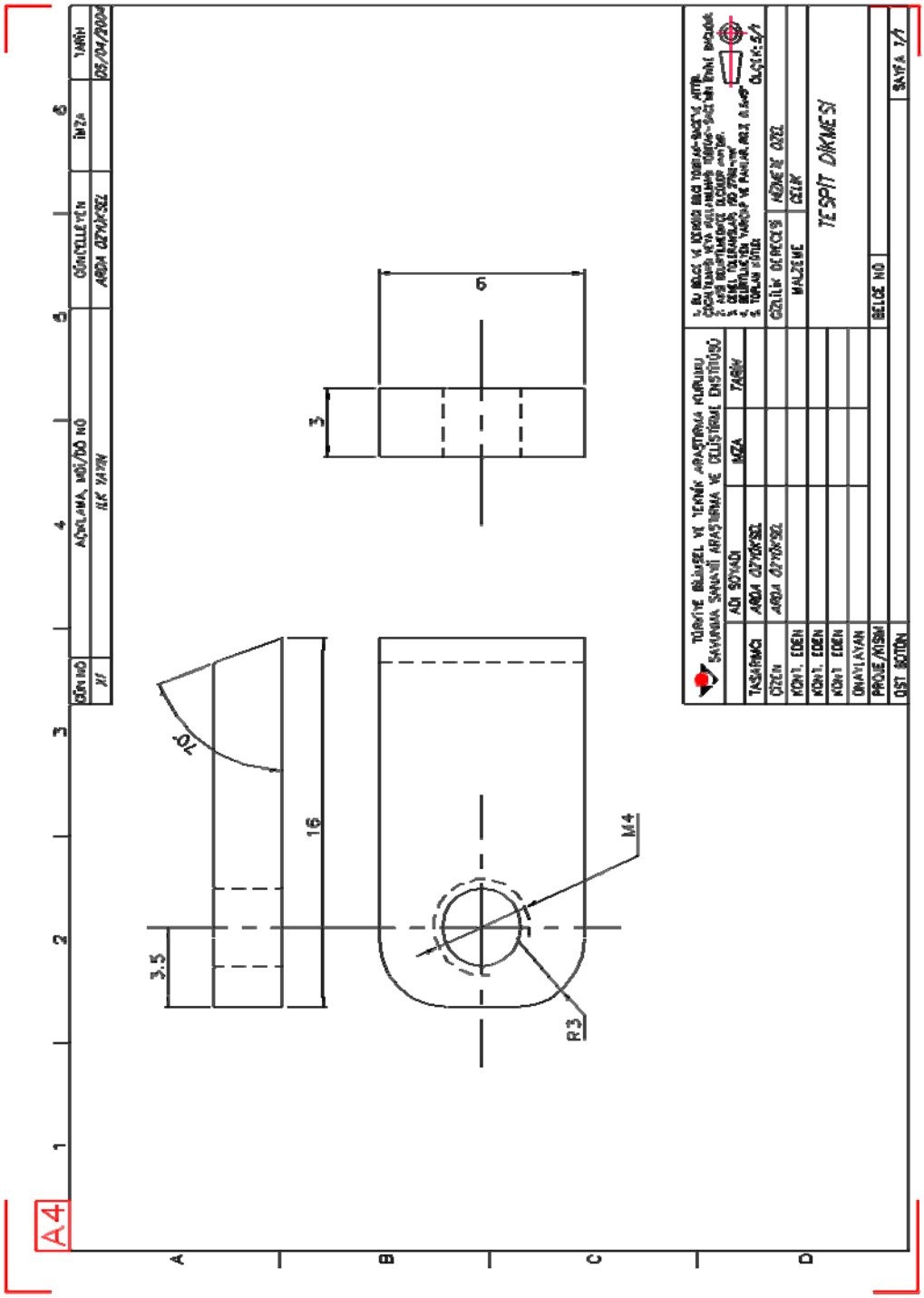

Figure 97 – Technical Drawing of Sway Brace of Pylon Model

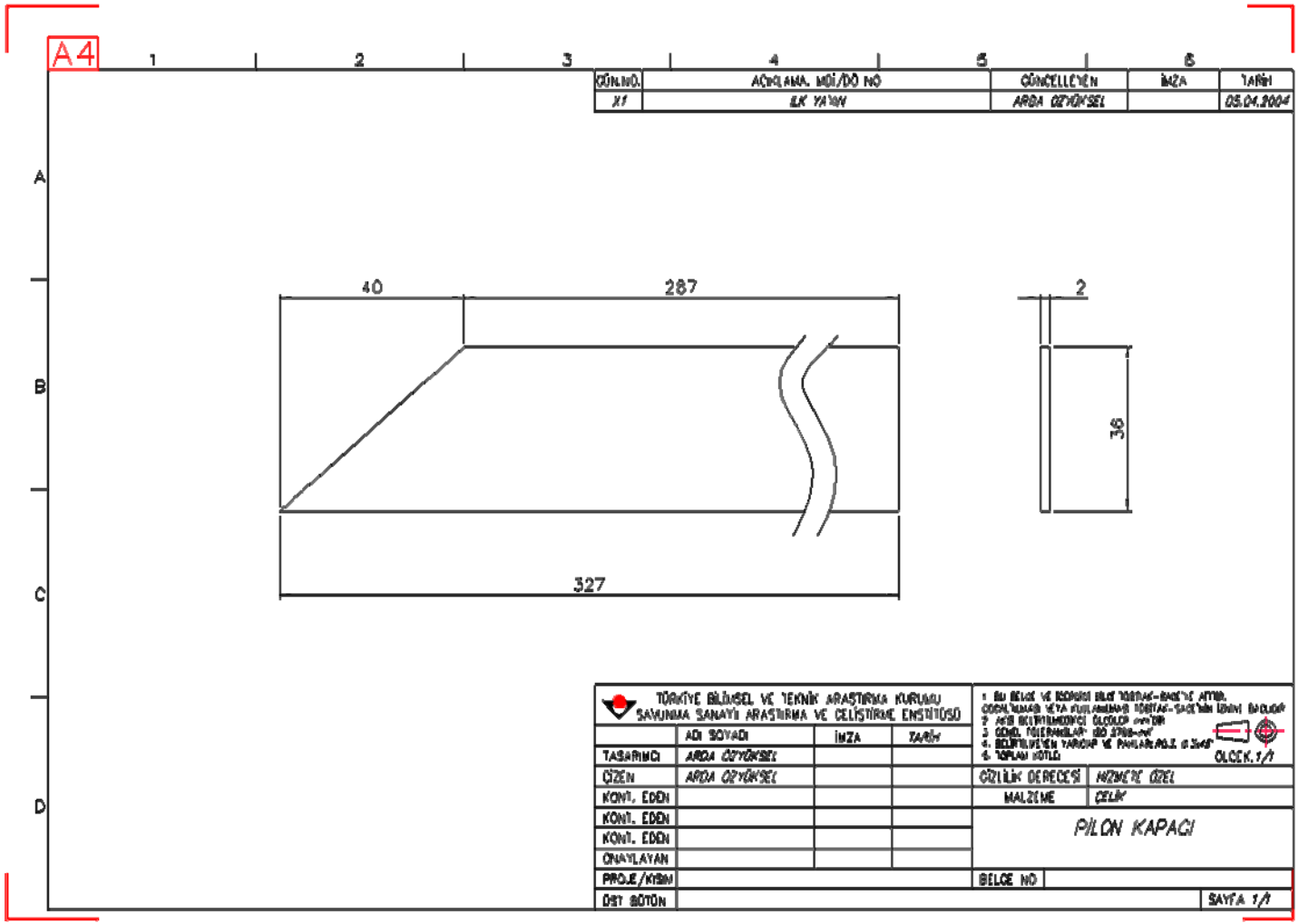

Figure 98 – Technical Drawing of Pylon Chassis Cover